

# APERIODICITY AT THE BOUNDARY OF CHAOS

STEVEN HURDER AND ANA RECHTMAN

**ABSTRACT.** We consider the dynamical properties of  $C^\infty$ -variations of the flow on an aperiodic Kuperberg plug  $\mathbb{K}$ . Our main result is that there exists a smooth 1-parameter family of plugs  $\mathbb{K}_\epsilon$  for  $\epsilon \in (-a, a)$  and  $a < 1$ , such that: (1) The plug  $\mathbb{K}_0 = \mathbb{K}$  is a generic Kuperberg plug; (2) For  $\epsilon < 0$ , the flow in the plug  $\mathbb{K}_\epsilon$  has two periodic orbits that bound an invariant cylinder, all other orbits of the flow are wandering, and the flow has topological entropy zero; (3) For  $\epsilon > 0$ , the flow in the plug  $\mathbb{K}_\epsilon$  has positive topological entropy, and an abundance of periodic orbits.

## 1. INTRODUCTION

In this paper, we analyze the dynamical properties of flows in a  $C^\infty$ -neighborhood of the Kuperberg flows introduced in [9], or to be more precise, of *generic Kuperberg flows* as introduced in [6]. The Kuperberg flows are exceptional for the simplicity of their explicit construction in [9], and this explicitness makes it a straightforward process to construct 1-parameter families of  $C^\infty$ -deformations of a given generic Kuperberg flow. We show in this work that the Kuperberg flows are furthermore remarkable, in that there are  $C^\infty$ -nearby flows with simple dynamics, and that there are  $C^\infty$ -nearby flows with positive topological entropy and an abundance of periodic orbits.

The construction of a Kuperberg flow is based on the construction of an aperiodic plug, which we call a *Kuperberg Plug*, and is noted in this paper by  $\mathbb{K}_0$ . A plug is a manifold with boundary endowed with a flow, that enables the modification of a given flow inside a flow-box, so that after modification, there are orbits that enter the flow-box and never exit. Moreover, Kuperberg's construction does this modification without introducing additional periodic orbits. Expository treatments of Kuperberg's construction were given by Ghys [4] and Matsumoto [11], and in the first chapters of the authors' work [6]. Our work also introduced new concepts for the study of the dynamical properties of the Kuperberg flows, which allows one to investigate many further remarkable aspects of these flows.

As a consequence of Katok's theorem on  $C^2$ -flows on 3-manifolds [8], the topological entropy of a Kuperberg flow is zero. In [6] we developed a technique based on the introduction of an "almost transverse" rectangle inside the plug and a pseudogroup modeling the return map of the flow to the rectangle, to make an explicit computation of the topological entropy. This computation revealed chaotic behavior for the flow, but such that it evolves at a very slow rate, and thus it does not result in positive topological entropy. We proved that, under some extra hypotheses, such generic Kuperberg flows have positive "slow entropy", and that the rates of chaotic behavior grow at a precise subexponential, but non-polynomial rate, as discussed in the proof of [6, Theorem 21.10]. The calculation behind the proof of this result suggests that for some Kuperberg-like flows near to a generic Kuperberg flow, there should be actual chaotic behavior, and also positive entropy.

In this paper we prove the following two theorems which make these remarks more precise.

**THEOREM 1.1.** *There exists a  $C^\infty$  1-parameter family of plugs  $\mathbb{K}_\epsilon$  for  $\epsilon \in (-1, 0]$  such that:*

- (1) *The plug  $\mathbb{K}_0$  is a Kuperberg plug;*
- (2) *For  $\epsilon < 0$ , the flow in the plug  $\mathbb{K}_\epsilon$  has two periodic orbits that bound an invariant cylinder, and every other orbit belongs to the wandering set, and thus the flow has topological entropy zero.*

---

*Key words and phrases.* Kuperberg flows, aperiodic flows, topological entropy.  
 2010 *Mathematics Subject Classification.* Primary 37C10, 37C70, 37B25, 37B40.  
 Preprint date: March 25, 2016; revised September 25.

The proof of Theorem 1.1 uses the same technical tools as developed in the previous works [9, 10, 4, 11, 6] for the study of the dynamics of Kuperberg flows, and the result is notable mainly for its contrast with the following result, that a  $C^\infty$ -neighborhood of a generic Kuperberg flow also contains flows which have exceptionally wild dynamics. In particular, we obtain the following result:

**THEOREM 1.2.** *There exists a  $C^\infty$  1-parameter family of plugs  $\mathbb{K}_\epsilon$  for  $\epsilon \in [0, a)$ ,  $a > 0$ , such that:*

- (1) *The plug  $\mathbb{K}_0$  is a generic Kuperberg plug;*
- (2) *For  $\epsilon > 0$ , the flow in  $\mathbb{K}_\epsilon$  has positive topological entropy, and an abundance of periodic orbits.*

The proof of Theorem 1.2 is based on the understanding of the dynamics of standard Kuperberg flows developed in [6], and in particular uses in a fundamental way the technique of relating the dynamics of a Kuperberg-like flow to the dynamics of its return map to an almost transverse rectangle.

The construction of the plugs  $\mathbb{K}_\epsilon$  in the proofs of both Theorems 1.1 and 1.2 follows closely the original construction by K. Kuperberg in [9], which begins with a modified version of the original Wilson Plug [19], where the modification given in Section 2.2 removes the stable periodic orbits for the flow and replaces them with unstable periodic orbits. The construction of the 1-parameter family of plugs is described in the first part of this work, Section 2.3, and closely follows the construction in [6].

The *Radius Inequality* is the main condition in Kuperberg's construction that is used to prove that the flow is aperiodic. The only change in the requirements of the construction of the flows  $\Phi_t^\epsilon$  which we study, is that the Radius Inequality gets replaced for  $\epsilon \neq 0$  with the *Parametrized Radius Inequality*, as stated in Section 2.3. For  $\epsilon = 0$  we recover the original Radius Inequality for Kuperberg flows.

Section 3 introduces some of the main tools for the study of the dynamics of Kuperberg flows, the radius and level functions, and also gives some of the immediate consequences for the study of the dynamics that are independent of the value of  $\epsilon$  in the Parametrized Radius Inequality.

As we mentioned above, one of the main techniques in [6] is to introduce a pseudogroup modeling the dynamics of the Kuperberg flow. The other main technique is the study of surfaces tangent to the flow, known as propellers, that were used to describe the topological properties of the minimal set of a generic Kuperberg flow. These surfaces are introduced here in Section 4.

The plugs  $\mathbb{K}_\epsilon$  for  $\epsilon < 0$  have rather simple dynamical properties, as stated in Theorem 1.1 and described in Section 5. The study of these flows does not require any extra hypothesis in the constructions.

On the other hand, the study of the dynamical properties of plugs  $\mathbb{K}_\epsilon$  which satisfy the Parametrized Radius Inequality for  $\epsilon \geq 0$  is extraordinarily complicated. The detailed analysis in [6] of the standard Kuperberg flows required the introduction of the *generic hypothesis* in that work (see Hypothesis 6.3 below), in order to deduce a wide range of properties for the flows. For the case when  $\epsilon > 0$ , many of the corresponding results do not hold, so we consider in this work only the question of the existence of compact invariant sets for the flows, such that the restricted dynamics of the flow admits a “horseshoe” in its transversal model. Even with this more restricted goal, it is still necessary to impose geometric hypothesis on the construction as stated in Hypotheses 6.2 and 9.2, in order to obtain the proof of Theorem 1.2.

The construction of the pseudogroup acting on an almost transverse rectangle  $\mathbf{R}_0 \subset \mathbb{K}_\epsilon$  is done in Section 7. Instead of introducing a pseudogroup analogous to the one in Chapter 9 of [6], we introduce the simplest pseudogroup that allows us to prove Theorem 1.2. Section 8 is dedicated to the proof that this pseudogroup contains “horseshoe maps”, and the proof introduces surfaces analogous to the propellers introduced in [6] which are used to define these maps. In Section 9 we describe the situation in which these horseshoe maps can be embedded in the flow  $\Phi_t^\epsilon$ , so that they generate positive entropy for the flow, and not just for the pseudogroup. Then in Section 9.4, we discuss the construction of examples of  $C^\infty$ -deformations of a generic Kuperberg flow, such that the hypotheses of Theorem 9.5 are satisfied, completing the proof of Theorem 1.2.

The results in this paper are inspired by the work in the paper [6], and for the sake of brevity, we are forced to refer occasionally to results in [6]. However, the novel results used in the proof of Theorems 1.1 and 1.2 are explained and proved here. Further questions and open problems concerning the dynamical properties of the many variations of Kuperberg flows are discussed in the paper [7].

## 2. CONSTRUCTION OF PARAMETRIZED FAMILIES

In this section, we present the construction of the 1-parameter family of plugs  $\mathbb{K}_\epsilon$  for  $\epsilon \in (-a, a)$ , and introduce some of the techniques used for the study of their dynamical properties. This follows closely the outline of the construction and study of the usual Kuperberg flows in Chapters 2 and 3 of [6].

In Section 2.2 we give the construction of the modified Wilson plug as introduced by Kuperberg in [9]. The family of plugs is constructed in Section 2.3, and the Parametrized Radius Inequality is introduced.

**2.1. Plugs.** A 3-dimensional plug is a manifold  $P$  endowed with a vector field  $\mathcal{X}$  satisfying the following “plug conditions”. The 3-manifold  $P$  is of the form  $D \times [-2, 2]$ , where  $D$  is a compact 2-manifold with boundary  $\partial D$ . Set

$$\partial_v P = \partial D \times [-2, 2] \quad , \quad \partial_h^- P = D \times \{-2\} \quad , \quad \partial_h^+ P = D \times \{2\} \quad .$$

Then the boundary of  $P$  has a decomposition

$$\partial P = \partial_v P \cup \partial_h P = \partial_v P \cup \partial_h^- P \cup \partial_h^+ P \quad .$$

Let  $\frac{\partial}{\partial z}$  be the *vertical* vector field on  $P$ , where  $z$  is the coordinate of the interval  $[-2, 2]$ .

The vector field  $\mathcal{X}$  must satisfy the conditions:

- (P1) *vertical at the boundary*:  $\mathcal{X} = \frac{\partial}{\partial z}$  in a neighborhood of  $\partial P$ ; thus,  $\partial_h^- P$  and  $\partial_h^+ P$  are the entry and exit regions of  $P$  for the flow of  $\mathcal{X}$ , respectively;
- (P2) *entry-exit condition*: if a point  $(x, -2)$  is in the same trajectory as  $(y, 2)$ , then  $x = y$ . That is, an orbit that traverses  $P$ , exits just in front of its entry point;
- (P3) *trapped orbit*: there is at least one entry point whose entire *forward* orbit is contained in  $P$ ; we will say that its orbit is *trapped* by  $P$ ;
- (P4) *tame*: there is an embedding  $i: P \rightarrow \mathbb{R}^3$  that preserves the vertical direction.

Note that conditions (P2) and (P3) imply that if the forward orbit of a point  $(x, -2)$  is trapped, then the backward orbit of  $(x, 2)$  is also trapped.

A *semi-plug* is a manifold  $P$  endowed with a vector field  $\mathcal{X}$  as above, satisfying conditions (P1), (P3) and (P4), but not necessarily (P2). The concatenation of a semi-plug with an inverted copy of it, that is a copy where the direction of the flow is inverted, is then a plug.

Note that condition (P4) implies that given any open ball  $B(\vec{x}, \epsilon) \subset \mathbb{R}^3$  with  $\epsilon > 0$ , there exists a modified embedding  $i': P \rightarrow B(\vec{x}, \epsilon)$  which preserves the vertical direction again. Thus, a plug can be used to change a vector field  $\mathcal{Z}$  on any 3-manifold  $M$  inside a flowbox, as follows. Let  $\varphi: U_x \rightarrow (-1, 1)^3$  be a coordinate chart which maps the vector field  $\mathcal{Z}$  on  $M$  to the vertical vector field  $\frac{\partial}{\partial z}$ . Choose a modified embedding  $i': P \rightarrow B(\vec{x}, \epsilon) \subset (-1, 1)^3$ , and then replace the flow  $\frac{\partial}{\partial z}$  in the interior of  $i'(P)$  with the image of  $\mathcal{X}$ . This results in a flow  $\mathcal{Z}'$  on  $M$ .

The entry-exit condition implies that a periodic orbit of  $\mathcal{Z}$  which meets  $\partial_h P$  in a non-trapped point, will remain periodic after this modification. An orbit of  $\mathcal{Z}$  which meets  $\partial_h P$  in a trapped point never exits the plug  $P$ , hence after modification, limits to a closed invariant set contained in  $P$ . A closed invariant set contains a minimal set for the flow, and thus, a plug serves as a device to insert a minimal set into a flow.

**2.2. The modified Wilson plug  $\mathbb{W}$ .** We next introduce the “modified Wilson Plug”, which was the starting point of Kuperberg’s construction of her plug. We add to the construction one hypothesis that seems to be implicitly assumed by certain conclusions stated in [4, 11], and that are part of the generic hypothesis used in [6]. This hypothesis is not needed to construct Kuperberg’s aperiodic plug, but it seems necessary in order to prove the results in this paper.

Consider the rectangle, as illustrated in Figure 1,

$$(1) \quad \mathbf{R} = [1, 3] \times [-2, 2] = \{(r, z) \mid 1 \leq r \leq 3 \text{ \& } -2 \leq z \leq 2\} \quad .$$

For a constant  $0 < g_0 \leq 1$ , choose a  $C^\infty$ -function  $g: \mathbf{R} \rightarrow [0, g_0]$  which satisfies the “vertical” symmetry condition  $g(r, z) = g(r, -z)$ . Also, require that  $g(2, -1) = g(2, 1) = 0$ , that  $g(r, z) = g_0$  for  $(r, z)$  near the boundary of  $\mathbf{R}$ , and that  $g(r, z) > 0$  otherwise. We may take  $g_0 = 1/10$  for example.

We make the following additional hypothesis on the function  $g$  in the construction.

**HYPOTHESIS 2.1.** *We require the function  $g$  satisfy the above conditions, and in addition:*

$$(2) \quad g(r, z) = g_0 \quad \text{for} \quad (r-2)^2 + (|z|-1)^2 \geq \epsilon_0^2$$

where  $0 < \epsilon_0 < 1/4$  is sufficiently small, as will be specified later in Section 2.3. In addition, we also require that  $g(r, z)$  is monotone increasing as a function of the distance  $\sqrt{(r-2)^2 + (|z|-1)^2}$  from the special points where it vanishes, and that  $g$  is non-degenerate. Non-degenerate means that the matrix of second partial derivatives at each vanishing point is invertible.

Define the vector field  $\mathcal{W}_v = g \cdot \frac{\partial}{\partial z}$  which has two singularities,  $(2, \pm 1)$ , and is otherwise everywhere vertical. The flow lines of this vector field are illustrated in Figure 1.

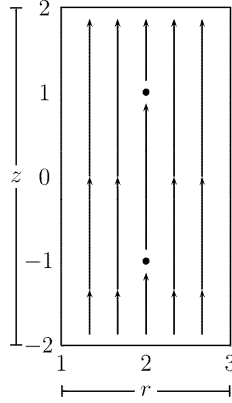


FIGURE 1. Vector field  $\mathcal{W}_v$

Next, choose a  $C^\infty$ -function  $f: \mathbf{R} \rightarrow [-1, 1]$  which satisfies the following conditions:

- (W1)  $f(r, -z) = -f(r, z)$  [anti-symmetry in  $z$ ]
- (W2)  $f(r, z) = 0$  for  $(r, z)$  near the boundary of  $\mathbf{R}$
- (W3)  $f(r, z) \geq 0$  for  $-2 \leq z \leq 0$ .
- (W4)  $f(r, z) \leq 0$  for  $0 \leq z \leq 2$ .
- (W5)  $f(r, z) = 1$  for  $5/4 \leq r \leq 11/4$  and  $-7/4 \leq z \leq -1/4$ .
- (W6)  $f(r, z) = -1$  for  $5/4 \leq r \leq 11/4$  and  $1/4 \leq z \leq 7/4$ .

Condition (W1) implies that  $f(r, 0) = 0$  for all  $1 \leq r \leq 3$ .

Next, define the manifold with boundary

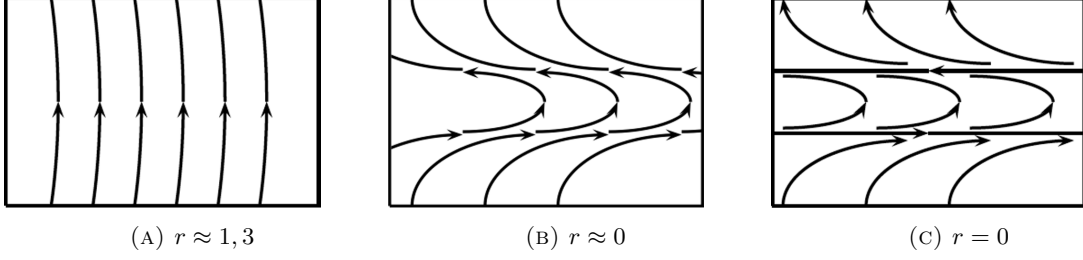
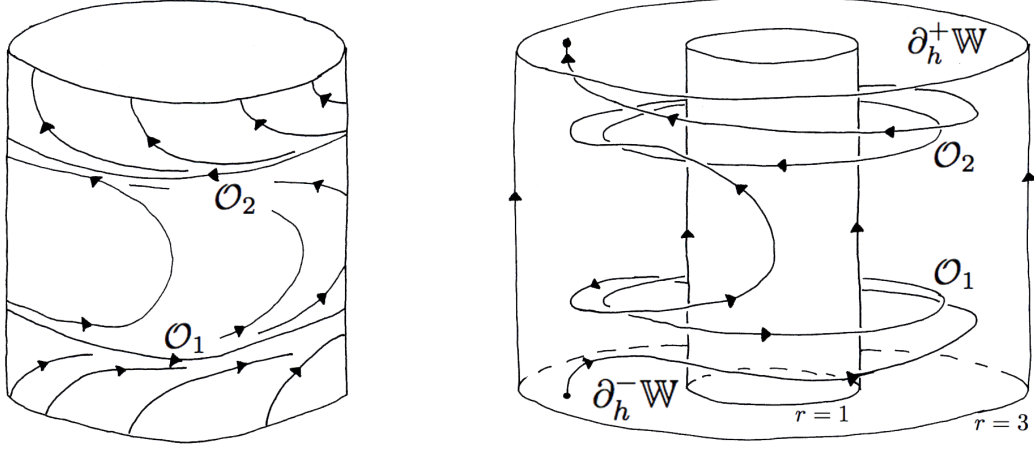
$$(3) \quad \mathbb{W} = [1, 3] \times \mathbb{S}^1 \times [-2, 2] \cong \mathbf{R} \times \mathbb{S}^1$$

with cylindrical coordinates  $x = (r, \theta, z)$ . That is,  $\mathbb{W}$  is a solid cylinder with an open core removed, obtained by rotating the rectangle  $\mathbf{R}$ , considered as embedded in  $\mathbb{R}^3$ , around the  $z$ -axis.

Extend the functions  $f$  and  $g$  above to  $\mathbb{W}$  by setting  $f(r, \theta, z) = f(r, z)$  and  $g(r, \theta, z) = g(r, z)$ , so that they are invariant under rotations around the  $z$ -axes. Define the Wilson vector field on  $\mathbb{W}$  by

$$(4) \quad \mathcal{W} = g(r, \theta, z) \frac{\partial}{\partial z} + f(r, \theta, z) \frac{\partial}{\partial \theta}$$

Let  $\Psi_t$  denote the flow of  $\mathcal{W}$  on  $\mathbb{W}$ . Observe that the vector field  $\mathcal{W}$  is vertical near the boundary of  $\mathbb{W}$  and horizontal in the periodic orbits. Also,  $\mathcal{W}$  is tangent to the cylinders  $\{r = cst\}$ . The flow of  $\Psi_t$  on the cylinders  $\{r = cst\}$  is illustrated (in cylindrical coordinate slices) by the lines in Figures 2 and 3.

FIGURE 2.  $\mathcal{W}$ -orbits on the cylinders  $\{r = \text{const.}\}$ FIGURE 3.  $\mathcal{W}$ -orbits in the cylinder  $\mathcal{C} = \{r = 2\}$  and in  $\mathbb{W}$ 

Define the closed subsets:

$$\begin{aligned}
 \mathcal{C} &\equiv \{r = 2\} \quad [\text{The Full Cylinder}] \\
 \mathcal{R} &\equiv \{(2, \theta, z) \mid -1 \leq z \leq 1\} \quad [\text{The Reeb Cylinder}] \\
 \mathcal{A} &\equiv \{z = 0\} \quad [\text{The Center Annulus}] \\
 \mathcal{O}_i &\equiv \{(2, \theta, (-1)^i)\} \quad [\text{Periodic Orbits, } i=1,2]
 \end{aligned}$$

Note that  $\mathcal{O}_1$  is the lower boundary circle of the Reeb cylinder  $\mathcal{R}$ , and  $\mathcal{O}_2$  is the upper boundary circle.

We give some of the basic properties of the Wilson flow. Let  $R_\varphi: \mathbb{W} \rightarrow \mathbb{W}$  be rotation by the angle  $\varphi$ . That is,  $R_\varphi(r, \theta, z) = (r, \theta + \varphi, z)$ .

**PROPOSITION 2.2.** *Let  $\Psi_t$  be the flow on  $\mathbb{W}$  defined above, then:*

- (1)  $R_\varphi \circ \Psi_t = \Psi_t \circ R_\varphi$  for all  $\varphi$  and  $t$ .
- (2) The flow  $\Psi_t$  preserves the cylinders  $\{r = \text{const.}\}$  and in particular preserves the cylinders  $\mathcal{R}$  and  $\mathcal{C}$ .
- (3)  $\mathcal{O}_i$  for  $i = 1, 2$  are the periodic orbits for  $\Psi_t$ .
- (4) For  $x = (2, \theta, -2)$ , the forward orbit  $\Psi_t(x)$  for  $t > 0$  is trapped.
- (5) For  $x = (2, \theta, 2)$ , the backward orbit  $\Psi_t(x)$  for  $t < 0$  is trapped.
- (6) For  $x = (r, \theta, z)$  with  $r \neq 2$ , the orbit  $\Psi_t(x)$  terminates in the top face  $\partial_h^+ \mathbb{W}$  for some  $t \geq 0$ , and terminates in  $\partial_h^- \mathbb{W}$  for some  $t \leq 0$ .
- (7) The flow  $\Psi_t$  satisfies the entry-exit condition (P2) for plugs.

*Proof.* The only assertion that needs a comment is the last, which follows by (W1) and the symmetry condition imposed on the functions  $g$  and  $f$ .  $\square$

**2.3. The family of spaces  $\mathbb{K}_\epsilon$ .** The construction of the family of Kuperberg Plugs  $\mathbb{K}_\epsilon$  begins with the modified Wilson Plug  $\mathbb{W}$  with vector field  $\mathcal{W}$  constructed in Section 2.2, and follows the original construction of K. Kuperberg, except for the choices of self-embeddings. The parameter  $\epsilon$  is a real number, and admits negative and positive values, though for  $\epsilon > 0$  we will later assume that  $\epsilon$  is “sufficiently small”. For  $\epsilon = 0$  we recover the original Kuperberg Plug. Moreover, as proved in Sections 5 and 9, this is the only plug in the family that has no periodic orbits.

The construction follows the steps in Chapter 3 of [6]. The first step is to re-embed the manifold  $\mathbb{W}$  in  $\mathbb{R}^3$  as a *folded figure-eight*, as shown in Figure 4, preserving the vertical direction.

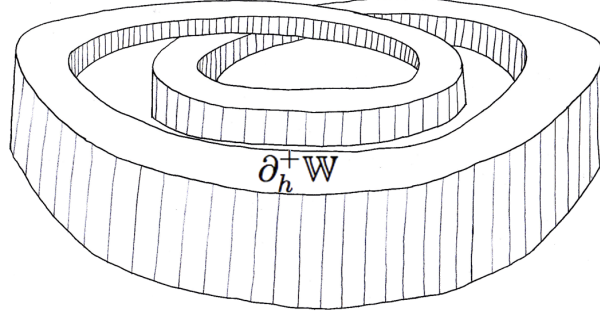


FIGURE 4. Embedding of Wilson Plug  $\mathbb{W}$  as a *folded figure-eight*

The fundamental idea of the Kuperberg Plug is to construct two insertions of  $\mathbb{W}$  in itself. The subtlety of the original construction arises in the precise requirements on this insertion, which were chosen so that the periodic orbits of the flow are “cut open” by a non-periodic orbit for the inserted plug. Here, we modify this construction so that for values of  $\epsilon \neq 0$ , the self-insertion again intercepts the periodic orbits, but the resulting variation of the radius inequality results in a family of plugs with much different characteristics than Kuperberg’s original construction. Finally, in Section 9, we impose further restrictions on the insertion maps for  $\epsilon > 0$ , so that the entropies of the resulting Kuperberg flows can be more readily calculated.

Consider in the annulus  $[1, 3] \times \mathbb{S}^1$  two topological closed disks  $L_i$ , for  $i = 1, 2$ , whose boundaries are composed of two arcs:  $\alpha'_i$  in the interior of  $[1, 3] \times \mathbb{S}^1$ , and  $\alpha_i$  in the outer boundary circle  $\{r = 3\}$ , as depicted in Figure 5. To be precise, let  $\zeta_1 = \pi/4$  and  $\zeta_2 = -\pi/4$ , then let  $\alpha_i$  be the arcs defined by

$$\alpha_1 = \{(3, \theta) \mid |\theta - \zeta_1| \leq 1/10\} \quad , \quad \alpha_2 = \{(3, \theta) \mid |\theta - \zeta_2| \leq 1/10\}$$

We let  $\alpha'_i$  be the curves which in polar coordinates  $(r, \theta)$  are parabolas with minimum values  $r = 3/2$  and base the line segment  $\alpha_i$ , as depicted in Figure 5. We choose an explicit form for the embedded curves, for example, given by  $\alpha'_i \equiv \{r = 3/2 + 300/2 \cdot (\theta - \zeta_i)^2\}$ .

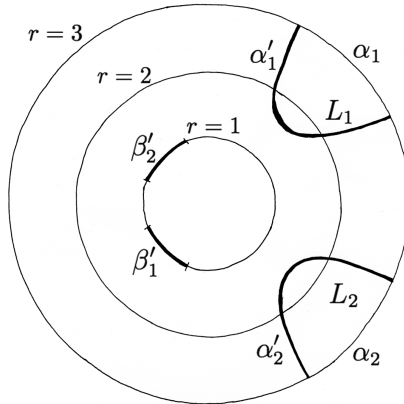


FIGURE 5. The disks  $L_1$  and  $L_2$

Consider the closed sets  $D_i \equiv L_i \times [-2, 2] \subset \mathbb{W}$ , for  $i = 1, 2$ . Note that each  $D_i$  is homeomorphic to a closed 3-ball, that  $D_1 \cap D_2 = \emptyset$ , and each  $D_i$  intersects the cylinder  $\mathcal{C} = \{r = 2\}$  in a rectangle. We label also the top and bottom faces of these regions

$$(5) \quad L_1^\pm = L_1 \times \{\pm 2\}, \quad L_2^\pm = L_2 \times \{\pm 2\}.$$

The next step is to define families of insertion maps  $\sigma_i^\epsilon: D_i \rightarrow \mathbb{W}$ , for  $i = 1, 2$ , in such a way that for  $\epsilon = 0$  the periodic orbits  $\mathcal{O}_1$  and  $\mathcal{O}_2$  for the  $\mathcal{W}$ -flow intersect  $\sigma_i^\epsilon(L_i^-)$  in points corresponding to  $\mathcal{W}$ -trapped points. Consider the two disjoint arcs  $\beta'_i$  in the inner boundary circle  $\{r = 1\}$ ,

$$\begin{aligned} \beta'_1 &= \{(1, \theta) \mid |\theta - (\zeta_1 + \pi)| \leq 1/10\} \\ \beta'_2 &= \{(1, \theta) \mid |\theta - (\zeta_2 + \pi)| \leq 1/10\} \end{aligned}$$

Now choose a smooth family of orientation preserving diffeomorphisms  $\sigma_i^\epsilon: \alpha'_i \rightarrow \beta'_i$ ,  $i = 1, 2$ , for  $-a \leq \epsilon \leq a$ , where  $a < \epsilon_0$  is sufficiently small. Extend these maps to smooth embeddings  $\sigma_i^\epsilon: D_i \rightarrow \mathbb{W}$ , for  $i = 1, 2$ , as illustrated in Figure 6. We require the following conditions for all  $\epsilon$  and for  $i = 1, 2$ :

- (K1)  $\sigma_i^\epsilon(\alpha'_i \times z) = \beta'_i \times z$  for all  $z \in [-2, 2]$ , the interior arc  $\alpha'_i$  is mapped to a boundary arc  $\beta'_i$ .
- (K2)  $\mathcal{D}_i^\epsilon = \sigma_i^\epsilon(D_i)$  then  $\mathcal{D}_1^\epsilon \cap \mathcal{D}_2^\epsilon = \emptyset$ ;
- (K3) For every  $x \in L_i$ , the image  $\mathcal{I}_{i,x}^\epsilon \equiv \sigma_i^\epsilon(x \times [-2, 2])$  is an arc contained in a trajectory of  $\mathcal{W}$ ;
- (K4) We have  $\sigma_1^\epsilon(L_1 \times \{-2\}) \subset \{z < 0\}$  and  $\sigma_2^\epsilon(L_2 \times \{2\}) \subset \{z > 0\}$ ;
- (K5) Each slice  $\sigma_i^\epsilon(L_i \times \{z\})$  is transverse to the vector field  $\mathcal{W}$ , for all  $-2 \leq z \leq 2$ .
- (K6)  $\mathcal{D}_i^\epsilon$  intersects the periodic orbit  $\mathcal{O}_i$  and not  $\mathcal{O}_j$ , for  $i \neq j$ .

The “horizontal faces” of the embedded regions  $\mathcal{D}_i^\epsilon \subset \mathbb{W}$  are labeled by

$$(6) \quad \mathcal{L}_1^{\epsilon\pm} = \sigma_1^\epsilon(L_1 \times \{\pm 2\}), \quad \mathcal{L}_2^{\epsilon\pm} = \sigma_2^\epsilon(L_2 \times \{\pm 2\}).$$

Note that the arcs  $\mathcal{I}_{i,x}^\epsilon$  are line segments from  $\sigma_i^\epsilon(x \times \{-2\})$  to  $\sigma_i^\epsilon(x \times \{2\})$  which follow the  $\mathcal{W}$ -trajectory, and traverse the insertion from one face to another. Since  $\mathcal{W}$  is vertical near the boundary of  $\mathbb{W}$  and horizontal at the two periodic orbits, (K3-K6) imply that the arcs  $\mathcal{I}_{i,x}^\epsilon$  are vertical near the inserted curve  $\sigma_i^\epsilon(\alpha'_i)$  and horizontal at the intersection of the insertion with the periodic orbit  $\mathcal{O}_i$ . Thus, the embeddings of the surfaces  $\sigma_i^\epsilon(L_i \times \{z\})$  make a *half turn* upon insertion, for each  $-2 \leq z \leq 2$ , as depicted in Figure 6. The turning is clockwise for the bottom insertion  $i = 1$  as in Figure 6, and counter-clockwise for the upper insertion  $i = 2$ .

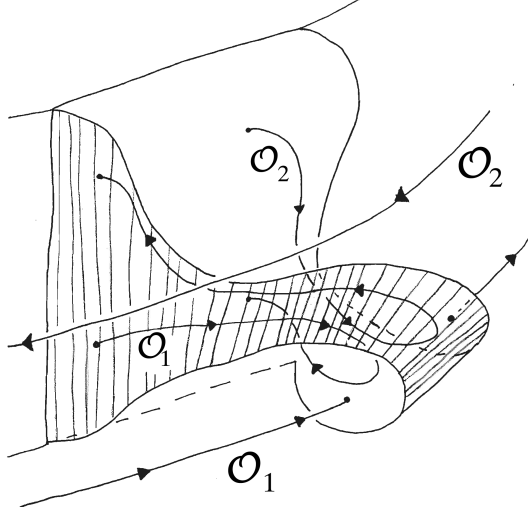


FIGURE 6. The image of  $L_1 \times [-2, 2]$  in  $\mathbb{W}$  under  $\sigma_1$

The first insertion  $\sigma_1^\epsilon(D_1)$  in Figure 6 intersects the first periodic orbit of  $\mathcal{W}$  and is disjoint of the second periodic orbit. The picture of the second insertion  $\sigma_2^\epsilon(D_2)$  is disjoint from the first insertion and the first periodic orbit, and it intersects the second periodic orbit.

The embeddings  $\sigma_i^\epsilon$  are also required to satisfy two further conditions:

(K7) For  $i = 1, 2$ , the disk  $L_i$  contains a point  $(2, \theta_i)$  such that the image under  $\sigma_i^\epsilon$  of the vertical segment  $(2, \theta_i) \times [-2, 2] \subset D_i \subset \mathbb{W}$  is contained in  $\{r = 2 + \epsilon\} \cap \{\theta_i^- \leq \theta \leq \theta_i^+\}$ , and for  $\epsilon = 0$  it is contained in  $\{r = 2\} \cap \{\theta_i^- \leq \theta \leq \theta_i^+\} \cap \{z = (-1)^i\}$ .

(K8) *Parametrized Radius Inequality*: For all  $x' = (r', \theta', -2) \in L_i^-$ , let  $x = (r, \theta, z) = \sigma_i^\epsilon(r', \theta', -2) \in \mathcal{L}_i^{\epsilon-}$ , then  $r < r' + \epsilon$  unless  $x' = (2, \theta_i, -2)$  and then  $r = 2 + \epsilon$ .

Note that by (K3) we have  $r(\sigma_i^\epsilon(r', \theta', z')) = r(\sigma_i^\epsilon(r', \theta', -2))$  for all  $-2 \leq z' \leq 2$ , so that (K8) holds for all points  $x' = (r', \theta', z') \in L_i \times [-2, 2]$ .

Observe that for  $\epsilon = 0$ , we recover the Radius Inequality of Kuperberg, one of the most fundamental concepts of Kuperberg's construction. Figure 7 represents the radius inequality for  $\epsilon < 0$ ,  $\epsilon = 0$ , and  $\epsilon > 0$ . Note that in the third illustration (c) for the case  $\epsilon > 0$ , the insertion as illustrated has a vertical shift upwards. This is not required by conditions (K7) and (K8), but will be used to prove Theorem 1.2 as explained in Section 8.2. (The vertex points  $\{v_1^\epsilon, v_2^\epsilon\}$  defined in (31) correspond to this vertical offset.)

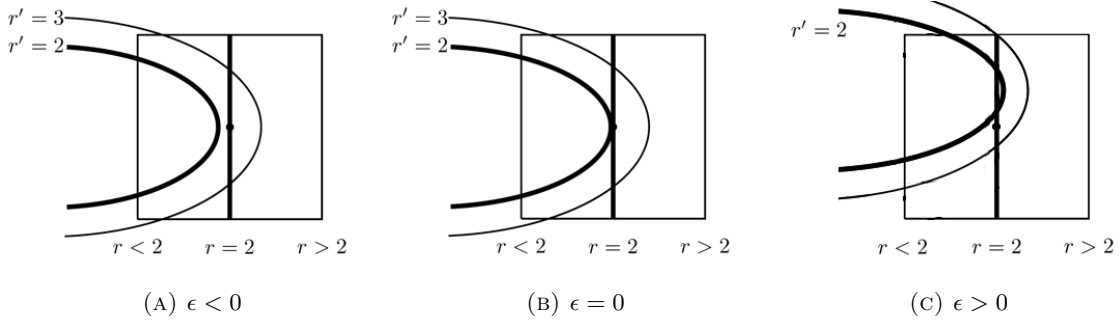


FIGURE 7. The modified radius inequality for the cases  $\epsilon < 0$ ,  $\epsilon = 0$  and  $\epsilon > 0$

**REMARK 2.3.** We add the following hypothesis relating the value of  $\epsilon_0$  in (2) and the insertions: let  $\epsilon_0$  as introduced in Hypothesis 2.1 be sufficiently small so that the  $\epsilon_0$ -neighborhood of the periodic orbits  $\mathcal{O}_i$  intersects the insertion regions  $\mathcal{D}_i^\epsilon$  on the interior of their faces for all  $\epsilon$  considered.

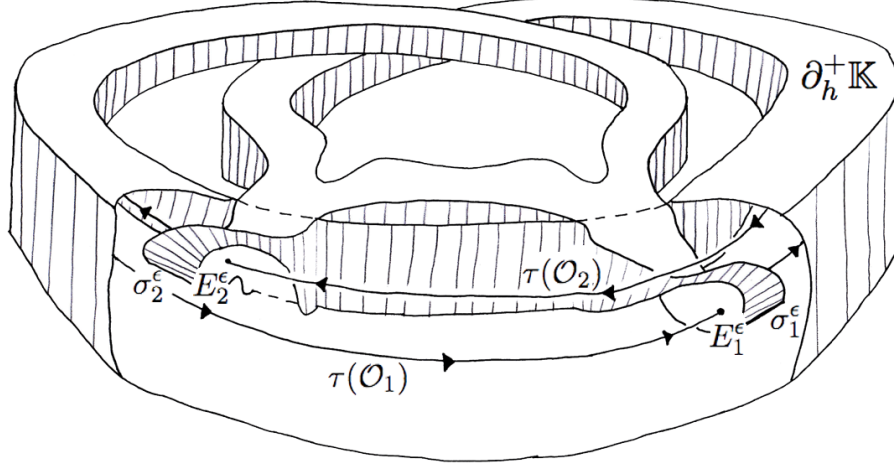
Finally, define  $\mathbb{K}_\epsilon$  to be the quotient manifold obtained from  $\mathbb{W}$  by identifying the sets  $D_i$  with  $\mathcal{D}_i^\epsilon$ . That is, for each point  $x \in D_i$  identify  $x$  with  $\sigma_i^\epsilon(x) \in \mathbb{W}$ , for  $i = 1, 2$ .

The restricted  $\mathcal{W}$ -flow on the inserted disk  $\mathcal{D}_i^\epsilon = \sigma_i^\epsilon(D_i)$  is not compatible with the restricted  $\mathcal{W}$ -flow on  $D_i$ . Thus, to obtain a smooth vector field  $\mathcal{K}_\epsilon$  from this construction, it is necessary to modify  $\mathcal{W}$  on each insertion  $\mathcal{D}_i^\epsilon$ . The idea is to replace the vector field  $\mathcal{W}$  on the interior of each region  $\mathcal{D}_i^\epsilon$  with the image vector field. This requires a minor technical step first.

Smoothly reparametrize the image of  $\mathcal{W}|_{D_i}$  under  $\sigma_i^\epsilon$  on an open neighborhood of the boundary of  $\mathcal{D}_i^\epsilon$  so that it agrees with the restriction of  $\mathcal{W}$  to the same neighborhood. This is possible since the vector field  $\mathcal{W}$  is vertical on a sufficiently small open neighborhood of  $\partial D_i \cap \partial \mathbb{W}$ , so is mapped by  $\sigma_i^\epsilon$  to an orbit segment of  $\mathcal{W}$  by (K3). We obtain a vector field  $\mathcal{W}'_i$  on  $\mathcal{D}_i^\epsilon$  with the same orbits as the image of  $\mathcal{W}|_{D_i}$ .

Then modify  $\mathcal{W}$  on each insertion  $\mathcal{D}_i^\epsilon$ , replacing it with the modified image  $\mathcal{W}'_i$ . Let  $\mathcal{W}'$  denote the vector field on  $\mathbb{W}$  after these modifications, and note that  $\mathcal{W}'$  is smooth. By the modifications made above, the vector field  $\mathcal{W}'$  descends to a smooth vector field on  $\mathbb{K}_\epsilon$  denoted by  $\mathcal{K}_\epsilon$ . Let  $\Phi_t^\epsilon$  denote the flow of the vector field  $\mathcal{K}_\epsilon$  on  $\mathbb{K}_\epsilon$ . The resulting space  $\mathbb{K}_\epsilon \subset \mathbb{R}^3$  is illustrated in Figure 8. Note that the flow of  $\mathcal{K}_\epsilon$  on  $\mathbb{K}_\epsilon$  clearly satisfies the plug conditions (P1) and (P4) of Section 2, while Proposition 3.3 below will show that the condition (P2) is also satisfied. For the cases  $\epsilon < 0$ , the trapped orbit condition (P3) is shown by Corollary 3.4, so that the flow of  $\mathcal{K}_\epsilon$  on  $\mathbb{K}_\epsilon$  is a plug in the sense of Section 2.



FIGURE 8. The Kuperberg Plug  $\mathbb{K}_\epsilon$ 

### 3. LEVEL AND RADIUS FUNCTIONS

In this section we recover some of the results on the orbit behaviors of the flows  $\mathbb{K}_\epsilon$  that are independent of  $\epsilon$  and that will be useful for the study of their dynamics in the plugs  $\mathbb{K}_\epsilon$ . As with the study of the Kuperberg flow  $\mathcal{K}_0$ , an orbit in  $\mathbb{K}_\epsilon$  is formed by concatenating pieces of orbits of the Wilson plug, where these orbit segments are the result of the construction of  $\mathbb{K}_\epsilon$  via the insertion maps  $\sigma_i^\epsilon$ . Thus, understanding the way these arcs concatenate is a fundamental aspect of understanding the dynamics of the flow in  $\mathbb{K}_\epsilon$ .

We start by introducing notations that will be used throughout this work, and also some basic concepts which are fundamental for relating the dynamics of the two vector fields  $\mathcal{W}$  and  $\mathcal{K}_\epsilon$ . These results are contained in the literature [4, 6, 9, 10, 11], though in a variety of differing notations and presentations. We adopt the notation of [6], and parts of the following text is also adapted from this work.

Recall that  $\mathcal{D}_i^\epsilon = \sigma_i^\epsilon(D_i)$  for  $i = 1, 2$  are solid 3-disks embedded in  $\mathbb{W}$ . Introduce the sets:

$$(7) \quad \mathbb{W}'_\epsilon \equiv \mathbb{W} - \{\mathcal{D}_1^\epsilon \cup \mathcal{D}_2^\epsilon\} \quad , \quad \widehat{\mathbb{W}}_\epsilon \equiv \overline{\mathbb{W} - \{\mathcal{D}_1^\epsilon \cup \mathcal{D}_2^\epsilon\}} .$$

The closure  $\widehat{\mathbb{W}}_\epsilon$  of  $\mathbb{W}'_\epsilon$  is the *piège de Wilson creusé* as defined in [4, page 292]. The compact space  $\widehat{\mathbb{W}}_\epsilon \subset \mathbb{W}$  is the result of “drilling out” the interiors of  $\mathcal{D}_1^\epsilon$  and  $\mathcal{D}_2^\epsilon$ , as the terminology *creusé* suggests.

For  $x, y \in \mathbb{K}_\epsilon$ , we say that  $x \prec_{\mathcal{K}_\epsilon} y$  if there exists  $t \geq 0$  such that  $\Phi_t^\epsilon(x) = y$ . Likewise, for  $x', y' \in \mathbb{W}$ , we say that  $x' \prec_{\mathcal{W}} y'$  if there exists  $t \geq 0$  such that  $\Psi_t(x') = y'$ .

Let  $\tau: \mathbb{W} \rightarrow \mathbb{K}_\epsilon$  denote the quotient map, which for  $i = 1, 2$ , identifies a point  $x \in D_i$  with its image  $\sigma_i^\epsilon(x) \in \mathcal{D}_i^\epsilon$ . Even if  $\tau$  depends on  $\epsilon$ , we will denote it simply by  $\tau$ . Then the restriction  $\tau': \mathbb{W}'_\epsilon \rightarrow \mathbb{K}_\epsilon$  is injective and onto. Let  $(\tau')^{-1}: \mathbb{K}_\epsilon \rightarrow \mathbb{W}'_\epsilon$  denote the inverse map, which followed by the inclusion  $\mathbb{W}'_\epsilon \subset \mathbb{W}$ , yields the (discontinuous) map  $\tau^{-1}: \mathbb{K}_\epsilon \rightarrow \mathbb{W}$ , where  $i = 1, 2$ , we have:

$$(8) \quad \tau^{-1}(\tau(x)) = x \text{ for } x \in D_i \text{ , and } \sigma_i^\epsilon(\tau^{-1}(\tau(x))) = x \text{ for } x \in \mathcal{D}_i^\epsilon .$$

For  $x \in \mathbb{K}_\epsilon$ , let  $x = (r, \theta, z)$  be defined as the  $\mathbb{W}$ -coordinates of  $\tau^{-1}(x) \subset \mathbb{W}'_\epsilon$ . In this way, we obtain (discontinuous) coordinates  $(r, \theta, z)$  on  $\mathbb{K}_\epsilon$ .

In particular, let  $r: \mathbb{W}'_\epsilon \rightarrow [1, 3]$  be the restriction of the radius coordinate on  $\mathbb{W}$ , then the function is extended to the *radius function* of  $\mathbb{K}_\epsilon$ , again denoted by  $r$ , where for  $x \in \mathbb{K}_\epsilon$  set  $r(x) = r(\tau^{-1}(x))$ . The flow of the vector field  $\mathcal{W}$  on  $\mathbb{W}$  preserves the radius function on  $\mathbb{W}$ , so  $x' \prec_{\mathcal{W}} y'$  implies that  $r(x') = r(y')$ . However,  $x \prec_{\mathcal{K}_\epsilon} y$  need not imply that  $r(x) = r(y)$ , and the points of discontinuity are the transition points defined below.

Let  $\partial_h^- \mathbb{K}_\epsilon \equiv \tau(\partial_h^- \mathbb{W} \setminus (L_1^- \cup L_2^-))$  and  $\partial_h^+ \mathbb{K}_\epsilon \equiv \tau(\partial_h^+ \mathbb{W} \setminus (L_1^+ \cup L_2^+))$  denote the bottom and top horizontal faces of  $\mathbb{K}_\epsilon$ , respectively. Note that the vertical boundary component  $\partial_v \mathbb{K}_\epsilon \equiv \tau(\widehat{\mathbb{W}}_\epsilon \cap \partial_v \mathbb{W})$  is tangent to the flow.

Points  $x' \in \partial_h^- \mathbb{W}$  and  $y' \in \partial_h^+ \mathbb{W}$  are said to be *facing*, and we write  $x' \equiv y'$ , if  $x' = (r, \theta, -2)$  and  $y' = (r, \theta, 2)$  for some  $r$  and  $\theta$ . There is also a notion of facing points for  $x, y \in \mathbb{K}_\epsilon$ , if either of two cases are satisfied:

- For  $x = \tau(x') \in \partial_h^- \mathbb{K}_\epsilon$  and  $y = \tau(y') \in \partial_h^+ \mathbb{K}_\epsilon$ , if  $x' \equiv y'$  then  $x \equiv y$ .
- For  $i = 1, 2$ , for  $x', y' \in \partial^\pm \mathbb{W}$  and  $x = \sigma_i^\epsilon(x')$  and  $y = \sigma_i^\epsilon(y')$ , if  $x' \equiv y'$  then  $x \equiv y$ .

The context in which the notation  $x \equiv y$  is used dictates which usage applies.

Consider the embedded disks  $\mathcal{L}_i^{\pm} \subset \mathbb{W}$  defined by (6), which appear as the faces of the insertions in  $\mathbb{W}$ . Their images in the quotient manifold  $\mathbb{K}_\epsilon$  are denoted by:

$$(9) \quad E_1^\epsilon = \tau(\mathcal{L}_1^{\epsilon-}), \quad S_1^\epsilon = \tau(\mathcal{L}_1^{\epsilon+}), \quad E_2^\epsilon = \tau(\mathcal{L}_2^{\epsilon-}), \quad S_2^\epsilon = \tau(\mathcal{L}_2^{\epsilon+}).$$

Note that  $\tau^{-1}(E_i^\epsilon) = L_i^-$ , while  $\tau^{-1}(S_i^\epsilon) = L_i^+$ . The *transition points* of an orbit of  $\mathcal{K}_\epsilon$  are those points which meet the  $E_i^\epsilon$ ,  $S_i^\epsilon$ ,  $\partial_h^- \mathbb{K}_\epsilon$  or  $\partial_h^+ \mathbb{K}_\epsilon$ , for  $i = 1, 2$ . They are then either *primary* or *secondary* transition points, where  $x \in \mathbb{K}_\epsilon$  is:

- a *primary entry point* if  $x \in \partial_h^- \mathbb{K}_\epsilon$ ;
- a *primary exit point* if  $x \in \partial_h^+ \mathbb{K}_\epsilon$ ;
- a *secondary entry point* if  $x \in E_1^\epsilon \cup E_2^\epsilon$ ;
- a *secondary exit point* if  $x \in S_1^\epsilon \cup S_2^\epsilon$ .

If a  $\mathcal{K}_\epsilon$ -orbit contains no transition points, then it lifts to a  $\mathcal{W}$ -orbit in  $\mathbb{W}$  which flows from  $\partial_h^- \mathbb{W}$  to  $\partial_h^+ \mathbb{W}$ .

A  $\mathcal{W}$ -arc is a closed segment  $[x, y]_{\mathcal{K}_\epsilon} \subset \mathbb{K}_\epsilon$  of the flow of  $\mathcal{K}_\epsilon$  whose endpoints  $\{x, y\}$  are the only transition points in  $[x, y]_{\mathcal{K}_\epsilon}$ . The open interval  $(x, y)_{\mathcal{K}_\epsilon}$  is then the image under  $\tau$  of a unique  $\mathcal{W}$ -orbit segment in  $\mathbb{W}'_\epsilon$ , denoted by  $(x', y')_{\mathcal{W}}$  (see Figure 9.) Let  $[x', y']_{\mathcal{W}}$  denote the closure of  $(x', y')_{\mathcal{W}}$  in  $\widehat{\mathbb{W}}_\epsilon$ , then we say that  $[x', y']_{\mathcal{W}}$  is the *lift* of  $[x, y]_{\mathcal{K}_\epsilon}$ . Note that the radius function  $r$  is constant along  $[x', y']_{\mathcal{W}}$ .

The properties of the Wilson flow  $\mathcal{W}$  on  $\widehat{\mathbb{W}}_\epsilon$  determine the endpoints of lifts  $[x', y']_{\mathcal{W}}$ . We state the six cases which arise explicitly, as they will be cited in later arguments. For a proof we refer to Lemma 4.1 of [6]. Figure 9 helps in visualizing these cases.

**LEMMA 3.1.** *Let  $[x, y]_{\mathcal{K}_\epsilon} \subset \mathbb{K}_\epsilon$  be a  $\mathcal{W}$ -arc, and let  $[x', y']_{\mathcal{W}} \subset \widehat{\mathbb{W}}_\epsilon$  denote its lift.*

- (1) **(p-entry/entry)** *If  $x$  is a primary entry point, then  $x' \in \partial_h^- \mathbb{W} \setminus (L_1^- \cup L_2^-)$ , and if  $y$  is an entry point, then  $y$  is a secondary entry point and  $y' \in \mathcal{L}_i^{\epsilon-}$  for  $i = 1$  or  $2$ .*
- (2) **(p-entry/exit)** *If  $x$  is a primary entry point, then  $x' \in \partial_h^- \mathbb{W} \setminus (L_1^- \cup L_2^-)$ , and if  $y$  is an exit point, then  $y' \in \partial_h^+ \mathbb{W} \setminus (L_1^+ \cup L_2^+)$  is a primary exit point, and by the entry/exit condition on  $\mathbb{W}$  we have  $x \equiv y$ .*
- (3) **(s-entry/entry)** *If  $x$  is a secondary entry point, then  $x' \in L_i^-$ , for  $i = 1$  or  $2$ , and if  $y$  is an entry point, then we have  $y' \in \mathcal{L}_j^{\epsilon-}$  where  $j = 1, 2$  is not necessarily equal to  $i$ .*
- (4) **(s-entry/exit)** *If  $x$  is a secondary entry point, then  $x' \in L_i^-$ , for  $i = 1$  or  $2$ , and if  $y$  is an exit point, then  $y$  is a secondary exit point,  $y' \in L_i^+$  and  $x \equiv y$  by the entry/exit condition of  $\mathbb{W}$ .*
- (5) **(s-exit/entry)** *If  $x$  is a secondary exit point, then  $x' \in \mathcal{L}_i^{\epsilon+}$ , for  $i = 1$  or  $2$ , and if  $y$  is an entry point, so that  $y' \in \mathcal{L}_j^{\epsilon-}$  then  $j = 2$  if  $i = 2$ , and  $j = 1, 2$  if  $i = 1$ .*
- (6) **(s-exit/exit)** *If  $x$  is a secondary exit point, then  $x' \in \mathcal{L}_i^{\epsilon+}$ , for  $i = 1$  or  $2$ , and if  $y$  is a primary exit point,  $y' \in \{\partial_h^+ \mathbb{W} \setminus (L_1^+ \cup L_2^+)\}$ . If  $y$  is a secondary exit point, then  $y' \in L_j^+$ , where  $j = 1$  or  $2$  is not necessarily equal to  $i$ .*

Figure 9 illustrates some of the notions discussed in this section. The disks  $L_1^-$  and  $L_2^-$  contained in  $\partial_h^- \mathbb{W}$  are drawn in the bottom face, though they are partially obscured by the inner cylindrical boundary  $\{r = 1\}$ . The image of  $L_1^-$  under  $\sigma_1^\epsilon$  is the entry face of the insertion region in the lower half of the cylinder, while the image of  $L_2^-$  under  $\sigma_2^\epsilon$  is the entry face of the insertion region in the upper half of the core cylinder.

Analogously, the disks  $L_1^+$  and  $L_2^+$  in  $\partial_h^+ \mathbb{W}$  are mapped to the exit region of the insertion regions. The intersection of the  $\mathcal{W}$ -periodic orbits  $\mathcal{O}_i$  with the insertions in  $\mathbb{W}$  are illustrated, as well as two  $\mathcal{W}$ -arcs in  $\mathbb{W}'_\epsilon$  that belong to the same orbit. One  $\mathcal{W}$ -arc goes from  $\partial_h^- \mathbb{W}$  to  $\mathcal{L}_1^{\epsilon-}$ , hence from a principal entry point to a secondary entry point (as in Lemma 3.1(1)). The second  $\mathcal{W}$ -arc goes from  $\mathcal{L}_1^{\epsilon+}$  to  $\mathcal{L}_1^{\epsilon-}$ , thus from a secondary exit point to a secondary entry point (as in Lemma 3.1(5)).

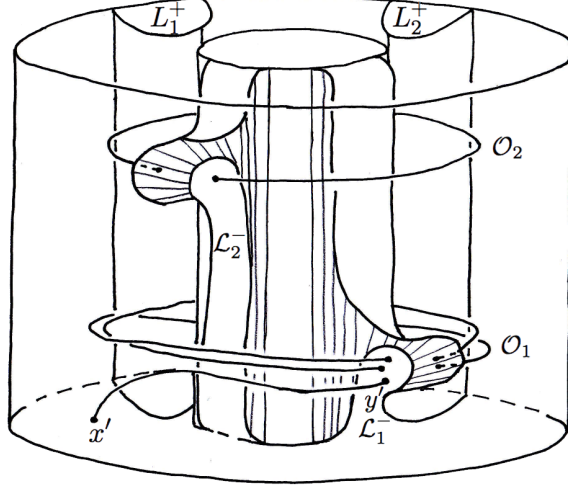


FIGURE 9.  $\mathcal{W}$ -arcs lifted to  $\mathbb{W}'_\epsilon$

Introduce the radius coordinate function along  $\mathcal{K}_\epsilon$ -orbits, where for  $x \in \mathbb{K}_\epsilon$ , set  $\rho_x^\epsilon(t) \equiv r(\Phi_t^\epsilon(x))$ . Note that if  $\Phi_t^\epsilon(x)$  is not a transition point then the function  $\rho_x^\epsilon(t)$  is locally constant at  $t$ , and thus if a  $\mathcal{K}_\epsilon$ -arc  $\{\Phi_t^\epsilon(x) \mid t_0 \leq t \leq t_1\}$  contains no transition point, then  $\rho_x^\epsilon(t) = \rho_x^\epsilon(t_0)$  for all  $t_0 \leq t \leq t_1$ .

The *level function* along an orbit indexes the discontinuities of the radius function. Given  $x \in \mathbb{K}_\epsilon$ , set  $n_x(0) = 0$ , and for  $t > 0$ , define

$$(10) \quad n_x(t) = \# \{(E_1^\epsilon \cup E_2^\epsilon) \cap \Phi_s^\epsilon(x) \mid 0 < s \leq t\} - \# \{(S_1^\epsilon \cup S_2^\epsilon) \cap \Phi_s^\epsilon(x) \mid 0 < s \leq t\}.$$

That is,  $n_x(t)$  is the total number of secondary entry points, minus the total number of secondary exit points, traversed by the flow of  $x$  over the interval  $0 < s \leq t$ .

The function can be extended to negative time by setting, for  $t < 0$ ,

$$(11) \quad n_x(t) = \# \{(S_1^\epsilon \cup S_2^\epsilon) \cap \Phi_s^\epsilon(x) \mid t < s \leq 0\} - \# \{(E_1^\epsilon \cup E_2^\epsilon) \cap \Phi_s^\epsilon(x) \mid t < s \leq 0\}.$$

We use throughout this work a Riemannian metric on the tangent bundle to  $\mathbb{K}_\epsilon$ . The Wilson plug  $\mathbb{W}$  has a natural product Riemannian metric, where the rectangle  $\mathbf{R}$  in (1) has the product euclidean metric, and the circle factor  $\mathbb{S}^1$  has length  $2\pi$ . Then modify this metric along the insertions  $\sigma_i^\epsilon$  to smooth them out, and so obtain a Riemannian metric on  $\mathbb{K}_\epsilon$ .

For  $x' \prec_{\mathcal{W}} y'$  in  $\mathbb{W}$ , let  $d_{\mathbb{W}}(x', y')$  denote the path length of the  $\mathcal{W}$ -orbit segment  $[x', y']_{\mathcal{W}}$  between them. Similarly, for  $x \prec_{\mathcal{K}_\epsilon} y$  in  $\mathbb{K}_\epsilon$ , let  $d_{\mathbb{K}_\epsilon}(x, y)$  denote the path length of the  $\mathcal{K}_\epsilon$ -orbit segment  $[x, y]_{\mathcal{K}_\epsilon}$ . Note that if  $[x, y]_{\mathcal{K}_\epsilon}$  is a  $\mathcal{W}$ -arc with lift  $[x', y']_{\mathcal{W}}$  then we have  $d_{\mathbb{K}_\epsilon}(x, y) = d_{\mathbb{W}}(x', y')$  by the choice of the metric on  $\mathbb{W}$ .

In Chapter 4 of [6] (Lemmas 4.3 and 4.4 and Corollary 4.5) the following basic length estimates are established for the Kuperberg Plug  $\mathbb{K}_0$ , and the proofs for this case carry over directly to the flows on the plugs  $\mathbb{K}_\epsilon$ :

- (1) Let  $0 < \delta < 1$ . There exists  $L(\delta) > 0$  such that for any  $\xi \in \mathbb{W}$  with  $|r(\xi) - 2| \geq \delta$ , the total  $\mathcal{W}$ -orbit segment  $[x', y']_{\mathcal{W}}$  through  $\xi$  has length bounded above by  $L(\delta)$ .
- (2) There exists  $0 < d_{\min} < d_{\max}$  such that if  $[x', y']_{\mathcal{W}} \subset \mathbb{W}'_\epsilon$  is the lift of a  $\mathcal{W}$ -arc  $[x, y]_{\mathcal{K}_\epsilon}$ , then we have the uniform estimate

$$(12) \quad d_{\min} \leq d_{\mathbb{W}}(x', y') \leq d_{\max}.$$

Thus for  $[x, y]_{\mathcal{K}_\epsilon} \subset \mathbb{K}_\epsilon$  a  $\mathcal{W}$ -arc, there is a uniform length estimate

$$(13) \quad d_{\min} \leq d_{\mathbb{K}_\epsilon}(x, y) \leq d_{\max}.$$

We end this section by recalling some technical results, which are key to analyzing the orbits of the flows  $\Phi_t^\epsilon$  on  $\mathbb{K}_\epsilon$ . For a proof of the first of these, we refer to [6, Proposition 5.5], whose proof carries over directly to the case of the flow  $\Phi_t^\epsilon$  on  $\mathbb{K}_\epsilon$ .

**PROPOSITION 3.2.** *Let  $x \in \mathbb{K}_\epsilon$ . For  $n \geq 3$ , assume that we are given successive transition points  $x_\ell = \Phi_{t_\ell}^\epsilon(x)$  for  $0 = t_0 < t_1 < \dots < t_{n-1} < t_n$ . Let  $[x'_\ell, y'_{\ell+1}]_{\mathbb{W}}$  be the lift of the  $\mathcal{W}$ -arc  $[x_\ell, x_{\ell+1}]_{\mathbb{K}}$  for all  $0 \leq \ell \leq n-1$ . Suppose that  $n_{x_0}(t) \geq 0$  for all  $0 \leq t < t_n$ , and that  $n_{x_0}(t_{n-1}) = 0$ . Then  $x'_0 \prec_{\mathcal{W}} y'_n$ , and hence  $r(x'_0) = r(y'_n)$ . Moreover, if  $x_0$  is an entry point and  $x_n$  is an exit point, then  $x_0 \equiv x_n$ .*

For a proof of the next result, we refer to the proof of [6, Proposition 5.6].

**PROPOSITION 3.3.** *Let  $x \in \partial_h^- \mathbb{K}_\epsilon$  be a primary entry point, and label the successive transition points by  $x_\ell = \Phi_{t_\ell}^\epsilon(x)$  for  $0 = t_0 < t_1 < \dots < t_{n-1} < t_n$ . If  $x_n$  is a primary exit point, then  $x \prec_{\mathcal{W}} x_n$  and hence  $x \equiv x_n$ . Moreover,  $n_x(t) \geq 0$  for  $0 \leq t < t_n$ .*

Note that this implies the flow of  $\mathcal{K}_\epsilon$  on  $\mathbb{K}_\epsilon$  satisfies condition (P2) of Section 2. The following result proves that  $\mathbb{K}_\epsilon$  satisfies condition (P3) for all  $\epsilon$ , implying that  $\mathbb{K}_\epsilon$  is a plug.

**COROLLARY 3.4.** *Let  $x \in \partial_h^- \mathbb{K}_\epsilon$  be a primary entry point with  $r(x) = 2$ . Then the forward  $\mathcal{K}_\epsilon$ -orbit of  $x$  is trapped.*

*Proof.* Assume that the forward  $\mathcal{K}_\epsilon$ -orbit of  $x$  is not trapped, and let  $x_\ell = \Phi_{t_\ell}^\epsilon(x)$  for  $0 = t_0 < t_1 < \dots < t_{n-1} < t_n$  be the transition points. Then  $x_n$  is a primary exit point and by Proposition 3.3,  $x \prec_{\mathcal{W}} x_n$ , which is impossible since  $r(x) = 2$ .  $\square$

#### 4. PROPELLERS AND DOUBLE PROPELLERS IN $\mathbb{W}$

Propellers, simple and double, as defined in Chapters 11, 12 and 13 of [6], are obtained from the Wilson flow of selected arcs in  $\partial_h^- \mathbb{W}$ . Double propellers are formed by the union of two (simple) propellers, as described below. These geometric structures associated to the Kuperberg flows  $\Phi_t^\epsilon$  are an essential tool for analyzing their dynamical properties.

Consider a curve in the entry region,  $\gamma \subset \partial_h^- \mathbb{W}$ , with a parametrization  $\gamma(s) = (r(s), \theta(s), -2)$  for  $0 \leq s \leq 1$ , and assume that the map  $\gamma: [0, 1] \rightarrow \partial_h^- \mathbb{W}$  is a homeomorphism onto its image. We use the notation  $\gamma_s = \gamma(s)$  when convenient, so that  $\gamma_0 = \gamma(0)$  denotes the initial point and  $\gamma_1 = \gamma(1)$  denotes the terminal point of  $\gamma$ . For  $\delta > 0$ , assume that  $r(\gamma_0) = 3$ ,  $r(\gamma_1) = 2 + \delta$ , and  $2 + \delta < r(\gamma_s) < 3$  for  $0 < s < 1$ .

The  $\mathcal{W}$ -orbits of the points in  $\gamma$  traverse  $\mathbb{W}$  from  $\partial_h^- \mathbb{W}$  to  $\partial_h^+ \mathbb{W}$ , and hence the flow of  $\gamma$  generates a compact invariant surface  $P_\gamma \subset \mathbb{W}$ . The surface  $P_\gamma$  is parametrized by  $(s, t) \mapsto \Psi_t(\gamma(s))$  for  $0 \leq s \leq 1$  and  $0 \leq t \leq T_s$ , where  $T_s$  is the exit time for the  $\mathcal{W}$ -flow of  $\gamma(s)$ . Observe that as  $s \rightarrow 1$  and  $\delta \rightarrow 0$ , the exit time  $T_s \rightarrow \infty$ .

The surface  $P_\gamma$  is called a *propeller*, due to the nature of its shape in  $\mathbb{R}^3$ . It takes the form of a “tongue” wrapping around the core cylinder  $\mathcal{C}(2 + \delta)$  which contains the orbit of  $\gamma_1$ . To visualize the shape of this surface, consider the case where  $\gamma$  is topologically transverse to the cylinders  $\mathcal{C}(r_0) = \{r = r_0\}$  for  $2 + \delta \leq r_0 \leq 3$ . The transversality assumption implies that the radius  $r(\gamma_s)$  is *monotone decreasing* as  $s$  increases. Figure 10 illustrates the surface  $P_\gamma$  as a “flattened” propeller on the right, and its embedding in  $\mathbb{W}$  on the left. As  $\delta \rightarrow 0$  the surface approaches the cylinder  $\mathcal{C} = \{r = 2\}$  in an infinite spiraling manner.

We comment on the details in Figure 10. The horizontal boundary  $\partial_h P_\gamma$  is composed of the initial curve  $\gamma \subset \partial_h^- \mathbb{W}$ , and its mirror image  $\bar{\gamma} \subset \partial_h^+ \mathbb{W}$  via the entry/exit condition on the Wilson Plug. The vertical boundary  $\partial_v P_\gamma$  is composed of the vertical segment  $\gamma_0 \times [-2, 2]$  in  $\partial_v \mathbb{W}$ , and the orbit  $\{\Psi_t(\gamma_1) \mid 0 \leq t \leq T_1\}$  which is the inner (or long) edge in the interior of  $\mathbb{W}$ . One way to visualize the surface, is to consider the product surface  $\gamma \times [-2, 2]$ , and then start deforming it by an isotopy which follows the flow lines of  $\mathcal{W}$ , as

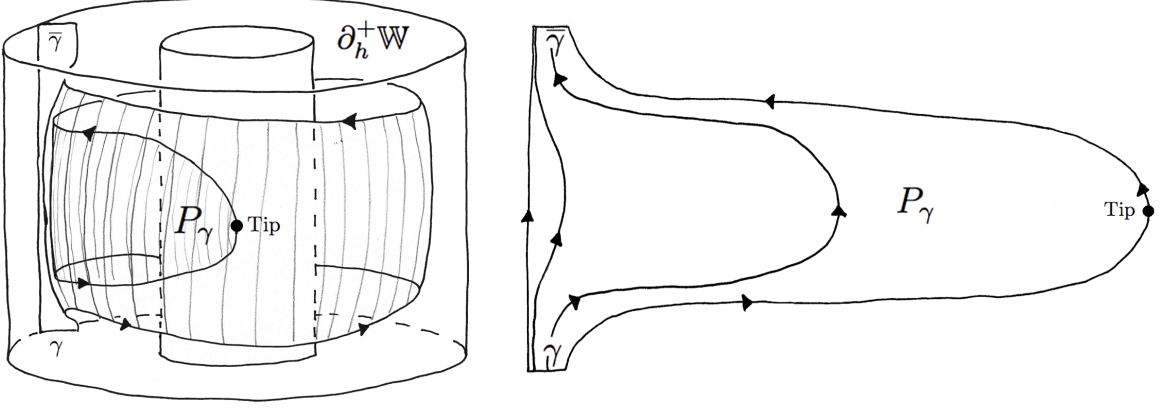


FIGURE 10. Embedded and flattened finite propeller

illustrated in Figure 10. In the right hand side of the figure, some of the orbits in the propeller are illustrated, while in the left hand side, just the boundary orbit is illustrated.

Consider the orbit  $\{\Psi_t(\gamma_1) \mid 0 \leq t \leq T_1\}$  of the endpoint  $\gamma_1$  with  $r(\gamma_1) = 2 + \delta$ . The path  $t \mapsto \Psi_t(\gamma_1)$  makes a certain number of turns in the positive  $\mathbb{S}^1$ -direction before reaching the core annulus  $\mathcal{A}$  at  $z = 0$ . The Wilson vector field  $\mathcal{W}$  is vertical on the plane  $\mathcal{A}$ , so the flow of  $\gamma_1$  then crosses  $\mathcal{A}$ , after which the orbit  $\Psi_t(\gamma_1)$  starts turning in the negative direction and ascending until it reaches  $\partial_h^+ \mathbb{W}$ . The point where the flow  $\Psi_t(\gamma_1)$  intersects  $\mathcal{A}$  is called the *tip* of the propeller  $P_\gamma$ .

The anti-symmetry of the vector field  $\mathcal{W}$  implies that the number of turns in one direction (considered as a real number) equals the number of turns in the opposite direction. To be precise, for  $\gamma_1 = (r_1, \theta_1, -2)$  in coordinates, let  $\Psi_t(\gamma_1) = (r_1(t), \theta_1(t), z_1(t))$  in coordinates. The function  $z_1(t)$  is monotone increasing, and by the symmetry, we have  $z_1(T_1/2) = 0$ . Thus, the tip is the point  $\Psi_{T_1/2}(\gamma_1)$ .

Next, for fixed  $0 \leq a < 2\pi$ , consider the intersection of  $P_\gamma$  with a slice

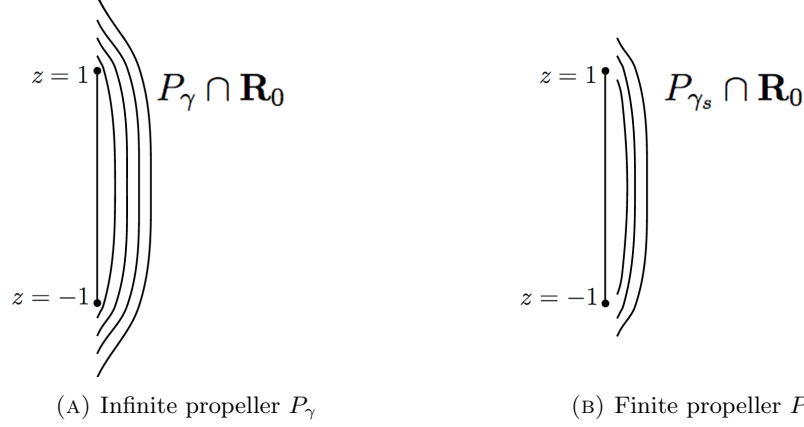
$$(14) \quad \mathbf{R}_a \equiv \{\xi = (r, a, z) \mid 1 \leq r \leq 3, -2 \leq z \leq 2\}.$$

Each rectangle  $\mathbf{R}_a$  is tangent to the Wilson flow along the annulus  $\mathcal{A}$ , and also near the boundaries of  $\mathbb{W}$ , but is transverse to the flow at all other points. The case when  $a = \theta_1(T_1/2)$  is special, as the tip of the propeller is tangent to  $\mathbf{R}_a$ .

Assume that  $a \neq \theta_1(T_1/2)$ , then the orbit  $\Psi_t(\gamma_1)$  intersects  $\mathbf{R}_a$  in a series of points on the line  $\mathcal{C}(2 + \delta) \cap \mathbf{R}_a$  that are paired, as illustrated in the right hand side of Figure 11. Moreover, the intersection  $P_\gamma \cap \mathbf{R}_a$  consists of a finite sequence of arcs between the symmetrically paired points of  $\Psi_t(\gamma_1) \cap \mathbf{R}_a$ . The number of such arcs is equal to, plus or minus one, the number of times the curve  $\Psi_t(\gamma_1)$  makes a complete turn around the cylinder  $\mathcal{C}(2 + \delta)$ .

We comment on the details of Figure 11, which illustrates the case of  $\mathbf{R}_0$  where  $a = \theta_0$ . The vertical line between the points  $(2, \theta_0, -1)$  and  $(2, \theta_0, 1)$  (marked in the figure simply by  $z = -1$  and  $z = 1$ , respectively) is the trace of the Reeb cylinder in  $\mathbf{R}_0$ . The trace of a propeller in  $\mathbf{R}_0$  is a collection of arcs that have their endpoints in the vertical line  $\{r = 2 + \delta\}$ . In the left hand figure,  $r(\gamma_1) = 2$  and the propeller in consideration is infinite, as defined below. The curves form an infinite family, here just four arcs are shown, accumulating on the vertical line. The right hand figure illustrates the case  $r(\gamma_1) > 2$ , and the propeller is finite.

Finally, consider the case where  $\delta \rightarrow 0$ , so that the endpoint  $\gamma_1$  of  $\gamma$  lies in the cylinder  $\mathcal{C}$ . Then for  $0 \leq s < 1$ , we have  $r(\gamma(s)) > 2$ , so the  $\Psi_t$ -flow of  $\gamma_s \in \partial_h^- \mathbb{W}$  escapes from  $\mathbb{W}$ . Define the curve  $\bar{\gamma}$  in  $\partial_h^+ \mathbb{W}$  to be the trace of these facing endpoints in  $\partial_h^+ \mathbb{W}$ , parametrized by  $\bar{\gamma}(s)$  for  $0 \leq s < 1$ , where  $\gamma(s) \equiv \bar{\gamma}(s)$ . Define  $\bar{\gamma}_1 = \lim_{s \rightarrow 1} \bar{\gamma}(s)$  so that  $\bar{\gamma}_1 \equiv \gamma_1$  also.

FIGURE 11. Trace of propellers in  $\mathbf{R}_0$ 

Note that the forward  $\Psi_t$ -orbit of  $\gamma_1$  is asymptotic to the periodic orbit  $\mathcal{O}_1$ , while the backward  $\Psi_t$ -orbit of  $\bar{\gamma}_1$  is asymptotic to the periodic orbit  $\mathcal{O}_2$ . Introduce their “pseudo-orbit”,

$$(15) \quad \mathcal{Z}_\gamma = \mathcal{Z}_\gamma^- \cup \mathcal{Z}_\gamma^+, \quad \mathcal{Z}_\gamma^- = \{\Psi_t(\gamma_1) \mid t \geq 0\} \text{ and } \mathcal{Z}_\gamma^+ = \{\Psi_t(\bar{\gamma}_1) \mid t \leq 0\}$$

Each curve  $\mathcal{Z}_\gamma^\pm$  traces out a semi-infinite ray in  $\mathcal{C}$  which spirals from the bottom or top face to a periodic orbit, and thus  $\mathcal{Z}_\gamma$  traces out two semi-infinite curves in  $\mathcal{C}$  spiraling to the periodic orbits  $\mathcal{O}_1 \cup \mathcal{O}_2$ .

For  $0 < \delta \leq 1$ , denote by  $\gamma^\delta$  the curve with image  $\gamma([0, \delta])$ , parametrized by

$$(16) \quad \gamma^\delta(s) = \gamma(\delta \cdot s).$$

**DEFINITION 4.1.** Let  $\gamma$  be a curve parametrized by  $\gamma: [0, 1] \rightarrow \mathbb{W}$  as above, with  $r(\gamma_0) = 3$  and  $r(\gamma_1) = 2$ . Introduce the infinite propeller and its closure in  $\mathbb{W}$ :

$$(17) \quad P_\gamma \equiv \mathcal{Z}_\gamma \cup \bigcup_{\delta > 0} P_{\gamma^\delta} \quad , \quad \bar{P}_\gamma \equiv \overline{\bigcup_{\delta > 0} P_{\gamma^\delta}}$$

As observed in [6], the closure  $\bar{P}_\gamma$  of an infinite propeller contains the Reeb cylinder  $\mathcal{R}$ , with  $\bar{P}_\gamma = P_\gamma \cup \mathcal{R}$ .

We now introduce the notion of double propellers in  $\mathbb{W}$ . Consider a smooth curve  $\Gamma \subset \partial_h^- \mathbb{W}$  parametrized by  $\Gamma: [0, 2] \rightarrow \partial_h^- \mathbb{W}$ , with the notation  $\Gamma_s = \Gamma(s)$ , such that:

- (1)  $r(\Gamma_s) \geq 2$  for all  $0 \leq s \leq 2$ ;
- (2)  $r(\Gamma_0) = r(\Gamma_2) = 3$ , so that both endpoints lie in the boundary  $\partial_h^- \mathbb{W} \cap \partial_v \mathbb{W}$ ;
- (3)  $\Gamma$  is topologically transverse to the cylinders  $\mathcal{C}(r)$  for  $2 \leq r \leq 3$ , except at the midpoint  $\Gamma_1$ .

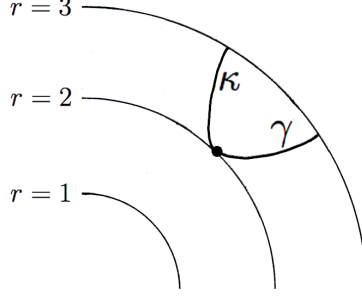
It then follows that  $r(\Gamma_s) \geq r(\Gamma_1) = 2 + \delta$  for all  $0 \leq s \leq 2$ , and some  $\delta \geq 0$ . See Figure 12 for an illustration in the case when  $\delta = 0$ .

Assume that  $\delta > 0$ , so that  $r(\Gamma_s) > 2$  for all  $0 \leq s \leq 2$ , then the  $\mathcal{W}$ -orbit of each  $\Gamma_s$  traverses  $\mathbb{W}$ . The  $\Psi_t$ -flow of the points in  $\Gamma$  form a compact surface embedded in  $\mathbb{W}$ , whose boundary is contained in the boundary of  $\mathbb{W}$ , and thus the surface separates  $\mathbb{W}$  into two connected components. This surface is denoted  $P_\Gamma$  and called the *double propeller* defined by the  $\Psi_t$ -flow of  $\Gamma$ .

Consider the curves  $\gamma, \kappa \subset \partial_h^- \mathbb{W}$  obtained by dividing the curve  $\Gamma$  into two segments at the midpoint  $s = 1$ . Parametrize these curves as follows:

$$\begin{aligned} \gamma &= \Gamma \mid [0, 1] & , & \quad \Gamma(s) \text{ for } 0 \leq s \leq 1 \\ \kappa &= \Gamma \mid [1, 2] & , & \quad \Gamma(2-s) \text{ for } 0 \leq s \leq 1 \end{aligned}$$

The orbit  $\{\Psi_t(\Gamma_1) \mid 0 \leq t \leq T_1\}$  forms the *long boundary* of the propellers  $P_\gamma$  and  $P_\kappa$  generated by the  $\mathcal{W}$ -flow of these curves. Then  $P_\Gamma$  is viewed as the gluing of  $P_\gamma$  and  $P_\kappa$  along the long boundary, hence the notation “double propeller” for  $P_\Gamma$ .

FIGURE 12. A curve  $\Gamma = \gamma \cup \kappa$  in  $\partial_h^- \mathbb{W}$ 

If  $\delta = 0$ , define two infinite propellers  $P_\gamma$  and  $P_\kappa$  as in Definition 4.1, and then define  $P_\Gamma = P_\gamma \cup P_\kappa$ , where the  $\Psi_t$ -orbit  $\mathcal{Z}_\gamma$  of the midpoint  $\Gamma_1$ , defined as in (15), is again common to both  $P_\gamma$  and  $P_\kappa$ , and  $P_\Gamma$  is viewed as the gluing of the two propellers along an “infinite zipper”.

**DEFINITION 4.2.** *Let  $\Gamma$  be as above with  $r(\Gamma_1) = 2$ . Let  $\gamma^\delta$  and  $\kappa^\delta$  for  $0 < \delta \leq 1$  be the curves as defined in (16). The infinite double propeller is the union:*

$$(18) \quad P_\Gamma \equiv \mathcal{Z}_\gamma \cup \bigcup_{\delta > 0} \{P_{\gamma^\delta} \cup P_{\kappa^\delta}\}$$

## 5. GLOBAL DYNAMICS FOR $\epsilon < 0$

We now analyze the global dynamics of the flows  $\Phi_t^\epsilon$  on  $\mathbb{K}_\epsilon$  for the case when  $\epsilon < 0$ . Recall that the assumption  $\epsilon < 0$  means that the self-insertion maps  $\sigma_i^\epsilon$  for  $i = 1, 2$  of the Wilson Plug  $\mathbb{W}$  do not penetrate far enough into  $\mathbb{W}$  to break the two periodic orbits of the Wilson flow  $\Psi_t$  by trapping them with the attracting orbits to these periodic orbits, as is the case when  $\epsilon = 0$ . As a consequence, we show that the flow  $\Phi_t^\epsilon$  has simple dynamics: there is an invariant set that is a cylinder whose boundary components are the two periodic orbits, and these are the only periodic orbits of the flow in the plug  $\mathbb{K}_\epsilon$ .

On the technical level, by the Parametrized Radius Inequality condition (K8), we have the strict inequality  $r' < r$ , as illustrated in Figure 7(A). That is, the radius coordinate is strictly increasing at a secondary entry point and strictly decreasing at a secondary exit point. Thus, there exists some  $\Delta > 0$ , depending on  $\epsilon$ , such that whenever an orbit hits an entry point, the radius increases by at least  $\Delta$ . The main consequence of this fact is that, unless an orbit hits the cylinder  $\tau(\mathcal{C})$  where  $\mathcal{C}$  is the cylinder of radius 2 in  $\mathbb{W}$ , its behavior is the same as in the Wilson plug. In spite of the simplicity of this portrait of the dynamics of the flow  $\Phi_t^\epsilon$ , the proofs of these claims uses key aspects on the analysis of the flow  $\Phi_t^0$  that were developed in [6].

Note that as  $\epsilon < 0$  tends to 0, the constant  $\Delta$  also tends to zero, and as a consequence the length of a given non-trapped orbit in  $\mathbb{K}_\epsilon$  grows increasingly long, as the number of possible reinsertions of the orbit through the faces of the insertions increases to infinity. The geometry of the parametrized flow  $\Phi_t^\epsilon$  as a function of  $\epsilon < 0$  is reminiscent of the Moving Leaf Lemma in [2] which is the key to analyzing the dynamics of flows in counter-examples to the Periodic Orbit Conjecture, as constructed in [3, 17].

**5.1. Orbit lifting property.** The first step in the analysis the dynamics of the flow  $\Phi_t^\epsilon$  is to establish the following key technical result, which should be compared with Propositions 6.5 and 6.7 of [6]. Recall that we defined  $\rho_x^\epsilon(t) \equiv r(\Phi_t^\epsilon(x))$ .

**PROPOSITION 5.1.** *Let  $x$  be a primary or secondary entry point of  $\mathbb{K}_\epsilon$  and  $y$  an exit point with  $x \equiv y$ . Assume that either:*

- (1)  $r(x) > 2$ ,
- (2)  $r(x) < 2$  and  $\rho_x^\epsilon(t) \neq 2$  for all  $t \geq 0$ ,

then  $x \prec_{\mathcal{K}_\epsilon} y$ . Moreover, the collection of lifts of the  $\mathcal{W}$ -arcs in  $[x, y]_{\mathcal{K}_\epsilon}$  contains all the  $\mathcal{W}$ -arcs of the  $\mathcal{W}$ -orbit of  $x'$  that are in  $\widehat{\mathbb{W}}_\epsilon$ , where  $\tau(x') = x$ .

*Proof.* Let  $x = x_0$  and  $0 = t_0 < t_1 < \dots < t_n < \dots$  with  $x_\ell = \Phi_{t_\ell}^\epsilon(x)$  be the transition points for the positive  $\mathcal{K}_\epsilon$ -orbit of  $x = x_0$ . Note that if the forward orbit of  $x_0$  is finite, meaning that there exists  $t > 0$  such that  $\Phi_t^\epsilon(x_0)$  is a primary exit point, then there are a finite number of transitions points. For  $\ell \geq 0$ , let  $[x'_\ell, y'_{\ell+1}]_{\mathcal{W}} \subset \widehat{\mathbb{W}}_\epsilon$  be the lift of the  $\mathcal{K}_\epsilon$ -arc  $[x_\ell, x_{\ell+1}]_{\mathcal{K}_\epsilon} \subset \mathbb{K}_\epsilon$ .

Assume that  $y$  is not in the  $\mathcal{K}_\epsilon$ -orbit of  $x_0$ . We prove that this implies that there exists  $s > 0$  such that for every  $t \geq s$  we have  $n_{x_0}(t) > 0$  and deduce a contradiction from this.

If  $x_1$  is an exit point, then  $[x'_0, y'_1]_{\mathcal{W}}$  is a complete  $\mathcal{W}$ -orbit traveling from  $\partial_h^- \mathbb{W}$  to  $\partial_h^+ \mathbb{W}$ . Thus, by definition we have  $x'_0 \equiv y'_1$ , or equivalently that  $x_0 \equiv x_1 = y$  and we obtain a contradiction to our assumption. Thus, we can assume that  $x_1$  is a secondary entry point and  $n_{x_0}(t_1) = 1$ .

Next, we prove that  $n_{x_0}(t) \geq 0$  for all  $t > 0$ . Suppose not, then there exists  $t > 0$  such that  $n_{x_0}(t) < 0$ . Let  $\ell > 1$  be the first index such that  $n_{x_0}(t_\ell) = 0$  and  $n_{x_0}(t_{\ell+1}) = -1$ . Then  $x_\ell$  and  $x_{\ell+1}$  are both exit points, so by Proposition 3.2 we obtain that  $x'_0 \prec_{\mathcal{W}} y'_\ell$  and  $x_0 \equiv x_{\ell+1}$ , implying that  $x_{\ell+1} = y$  which contradicts the assumption that  $y$  is not in the  $\mathcal{K}_\epsilon$ -orbit of  $x_0$ . Thus  $n_{x_0}(t) \geq 0$  for all  $t > 0$ .

Next, suppose there exists  $\ell > 1$  such that  $n_{x_0}(t_\ell) = 0$ , then let  $\ell > 1$  be the least such index. If  $x_\ell$  is a primary exit point, then by Proposition 3.3, the claim of the Proposition follows. Otherwise,  $x_{\ell+1}$  is defined, and both  $x_{\ell-1}$  and  $x_\ell$  are exit points, so by Proposition 3.2 we obtain that  $x'_0 \prec_{\mathcal{W}} y'_{\ell+1}$ . Then by Proposition 3.2  $x_1 \equiv x_{\ell-1}$ , and it follows that the  $\mathcal{W}$ -arc  $[x'_\ell, y'_{\ell+1}]_{\mathcal{W}}$  is the  $\mathcal{W}$ -arc following  $[x'_0, y'_1]_{\mathcal{W}}$  in the intersection of the  $\mathcal{W}$ -orbit of  $x'_0$  with  $\widehat{\mathbb{W}}_\epsilon$ .

We then apply this argument repeatedly to every  $\mathcal{K}_\epsilon$ -arc  $[x_\ell, x_{\ell+1}]_{\mathcal{K}_\epsilon}$  for which  $n_{x_0}(s) = 0$  for  $t_\ell \leq s < t_{\ell+1}$ , to conclude that  $[x_\ell, x_{\ell+1}]_{\mathcal{K}_\epsilon}$  lifts to an arc  $[x'_\ell, y'_{\ell+1}]_{\mathcal{W}} \subset \widehat{\mathbb{W}}_\epsilon$ . Note that for each such  $\ell$ , the  $\mathcal{W}$ -arc  $[x'_\ell, y'_{\ell+1}]_{\mathcal{W}}$  is contained in the  $\mathcal{W}$ -orbit of  $x'_0$ , and for distinct  $\ell > 0$  these  $\mathcal{W}$ -arcs are disjoint. On the other hand, the  $\mathcal{W}$ -orbit of  $x'_0$  is finite as  $r(x'_0) \neq 2$  by assumption. We conclude that there is at most a finite number of indices  $\ell$  such that  $n_{x_0}(t_\ell) = 0$ . Thus, there exists  $s_0 > 0$  such that  $n_{x_0}(t) > 0$  for all  $t \geq s_0$ .

There are now two possible cases to analyze: either the  $\mathcal{K}_\epsilon$ -orbit of  $x_0$  is finite and thus exits  $\mathbb{K}_\epsilon$  at a primary exit point, or the  $\mathcal{K}_\epsilon$ -orbit of  $x_0$  is infinite.

Assume first that the  $\mathcal{K}_\epsilon$ -orbit of  $x_0$  is finite. Then there exists  $\ell > 1$  such that  $x_\ell$  is a primary exit point. Let  $n = n_{x_0}(t_{\ell-1}) \geq 0$ . Since  $n_{x_0}(t) > 0$  for  $t \geq s_0$  we can assume that  $n > 0$ . Then  $x_{\ell-1}$  must be a secondary exit point. Otherwise, the  $\mathcal{W}$ -arc  $[x'_{\ell-1}, y'_\ell]_{\mathcal{W}}$  goes from an entry to an exit point in  $\mathbb{W}$ , which must then be facing. This would imply that  $x_{\ell-1}$  is a primary entry point, contrary to assumptions.

Thus,  $x_{\ell-1}$  is a secondary exit point and therefore  $n_{x_0}(t_{\ell-2}) = n+1$ . Then there exists  $k > 0$ , chosen to be the smallest index such that  $n_{x_0}(t_k) = n$  and  $n_{x_0}(t) \geq n$  for every  $t_k \leq t < t_\ell$ , implying that  $n_{x_0}(t_{k-1}) = n-1$ . Then  $x_k$  is an entry point and Proposition 3.2 applied to the  $\mathcal{K}_\epsilon$ -arc  $[x_k, x_\ell]_{\mathcal{K}_\epsilon}$  implies that  $x_k \equiv x_\ell$ . But then  $x_k$  is a primary entry point and thus  $x_k = x_0$ , which is again a contradiction as we assumed that  $n_{x_0}(t_k) = n > 0$ .

Finally, consider the case where the  $\mathcal{K}_\epsilon$ -orbit of  $x_0$  is infinite. Recall that we may assume that  $n_{x_0}(t) > 0$  for all  $t \geq s_0$ . We then have to consider the two following situations: either the level function  $n_{x_0}(t)$  admits an upper bound for  $t \geq 0$ , or the function  $n_{x_0}(t)$  is unbounded.

Assume that  $n_{x_0}(t)$  grows without bound. We show that this leads to a contradiction. Let  $\ell_i$  be the first index such that  $n_{x_0}(t_{\ell_i}) = i$ , thus  $\ell_0 = 0$ ,  $\ell_1 = 1$  and all the points  $x_{\ell_i}$  are secondary entry points. We claim that

$$(19) \quad \rho_{x_0}^\epsilon(t_{\ell_i}) \geq r(x) + n_{x_0}(t_{\ell_i}) \cdot \Delta = r(x) + i \cdot \Delta.$$

Let us prove the claim by recurrence on  $i$ . For  $i = 1$  condition (K8) in the construction of  $\mathbb{K}_\epsilon$  implies that  $\rho_{x_0}^\epsilon(t_1) \geq r(x) + \Delta$ . Assume that for  $i = k-1$  the inequality is satisfied. If  $\ell_k = \ell_{k-1} + 1$  the claim follows from (K8). If not, observe that  $n_{x_0}(t_{\ell_k-1}) = k-1$ , thus by Proposition 3.2 we have that  $x'_{\ell_k-1} \prec_{\mathcal{W}} y'_{\ell_k-1}$  and



$\rho_{x_0}^\epsilon(t_{\ell_{k-1}}) = \rho_{x_0}^\epsilon(t_{\ell_k-1})$ . Since  $x_{\ell_k}$  is a secondary entry point we have that  $\rho_{x_0}^\epsilon(t_{\ell_k}) \geq r(x) + k \cdot \Delta$  proving the claim. Since  $\Delta > 0$  and the function  $\rho_{x_0}^\epsilon(t)$  is bounded above by 3, this is impossible, and thus the level function  $n_{x_0}(t)$  must be bounded.

It remains to consider the case where there exists some  $N > 0$  such that  $n_{x_0}(t) \leq N$  for all  $t \geq 0$ . Then there exists  $0 \leq n_0 \leq N$  which is the least integer such that there exists  $0 < \ell_0 < \ell_1 < \dots < \ell_k < \dots$  such that  $n_{x_0}(t_{\ell_j}) = n_0$ . That is,  $n_0 = \liminf_{\ell > 0} n_{x_0}(t_\ell) \leq N$ . Since  $n_0$  is the least such integer, there exists  $k \geq 0$  such that  $n_{x_0}(t) \geq n_0$  for all  $t \geq t_{\ell_k}$ . Then the segment  $[x_{\ell_k}, x_{\ell_{k+1}+1}]_{\mathcal{K}_\epsilon}$  satisfies the hypotheses of Proposition 3.2, so we have  $x'_{\ell_k} \prec_{\mathcal{W}} y'_{\ell_{k+1}+1}$ . Thus the lifted  $\mathcal{W}$ -arcs  $[x'_{\ell_m}, y'_{\ell_{m+1}+1}]_{\mathcal{W}}$  for  $m \geq k$  belong to the  $\mathcal{W}$ -orbit of  $x'_{\ell_k}$ . Then by the estimates (12) and (13) above, considering the lengths of the lifted  $\mathcal{W}$ -orbit segments  $[x'_{\ell_m}, y'_{\ell_{m+1}+1}]_{\mathcal{W}}$  yields the estimate  $d_{\min} \cdot (m - k) \leq L(2 - r(x'_{\ell_k}))$  for all  $m \geq k$ . However, we can choose  $m$  arbitrarily large, and so also  $(m - k)$ , which yields a contradiction.

We proved so far that  $x \prec_{\mathcal{K}_\epsilon} y$ . Observe that  $x_1$  is a secondary entry point and assume  $y = x_n$ , for some  $n > 0$ . Let  $\ell_i$  be all the indices  $1 \leq \ell_i \leq n$  such that  $n_{x_0}(t_{\ell_i}) = 0$ . Then  $n_{x_0}(t_{\ell_i-1}) = 1$  and Proposition 3.2 implies  $x_1 \equiv x_{\ell_i-1}$ . Thus the  $\mathcal{W}$ -arc  $[x'_{\ell_i}, y'_{\ell_{i+1}+1}]_{\mathcal{W}}$  is the second arc in the  $\mathcal{W}$ -orbit of  $x'$  that belongs to  $\widehat{\mathbb{W}}_\epsilon$ . The same argument proves that  $x_{\ell_{i+1}} \equiv x_{\ell_i-1}$  and  $[x'_{\ell_{i+1}}, y'_{\ell_{i+2}+1}]_{\mathcal{W}}$  is the third arc in the  $\mathcal{W}$ -orbit of  $x'$  that belongs to  $\widehat{\mathbb{W}}_\epsilon$ . We conclude that the arcs  $[x'_{\ell_i}, y'_{\ell_{i+1}+1}]_{\mathcal{W}}$ , for all  $i$ , are all the arcs in the  $\mathcal{W}$ -orbit of  $x'$  that belong to  $\widehat{\mathbb{W}}_\epsilon$ .  $\square$

We point out two important corollaries of Proposition 5.1 and its proof.

**COROLLARY 5.2.** *Let  $x \in \mathbb{K}_\epsilon$  be such that  $\rho_x^\epsilon(t) \neq 2$  for every  $t \geq 0$ . If  $x$  is not a transition point, then the forward  $\mathcal{K}_\epsilon$ -orbit of  $x$  exits  $\mathbb{K}_\epsilon$ .*

*Proof.* Let  $x \in \mathbb{K}_\epsilon$  be such that  $\rho_x^\epsilon(t) \neq 2$  for every  $t \geq 0$ , and assume that the forward orbit never exits  $\mathbb{K}_\epsilon$ . Since for every  $t \geq 0$  the  $\mathcal{W}$ -orbit of  $\tau^{-1}(\Phi_t^\epsilon(x))$  is finite, the assumption implies that the forward  $\mathcal{K}_\epsilon$ -orbit of  $x$  has infinitely many transition points. Then either the level function  $n_{x_0}(t)$  is upper and lower bounded, or is not. The proof of Proposition 5.1 gives a contradiction in both cases.  $\square$

**COROLLARY 5.3.** *The  $\mathcal{K}_\epsilon$ -orbit  $\mathcal{O}_i^\epsilon$  containing  $\tau(\mathcal{O}_i)$ , for  $i = 1, 2$ , is periodic.*

*Proof.* The arc  $\tau(\mathcal{O}_i)$ , for  $i = 1, 2$ , intersects the entry region  $E_i^\epsilon$  at a point  $p_i^- \in E_i^\epsilon$  whose radius coordinate satisfies  $r(p_i^-) > 2$ , as illustrated in Figure 7(A). Then by the proof of Proposition 5.1, the  $\mathcal{K}_\epsilon$ -orbit of  $x_i$  contains the facing point  $y_i \in S_i^\epsilon$ , which is by construction the other endpoint of the arc  $\tau(\mathcal{O}_i)$ .  $\square$

We end this section with a brief discussion of the trapped set of  $\mathbb{K}_\epsilon$  for  $\epsilon < 0$ . Corollary 3.4 states that for  $x \in \partial_h^- \mathbb{K}_\epsilon$  with  $r(x) = 2$  the  $\mathcal{K}_\epsilon$ -orbit of  $x$  is trapped. The same argument can be applied to secondary entry points with radius 2. Thus if  $x$  is a primary entry point with  $r(x) \neq 2$  and such that there exists  $t > 0$  with  $\rho_x^\epsilon(t) = 2$ , the orbit of  $x$  is trapped. Thus the trapped set changes with  $\epsilon$ : it is composed of the curve

$$\{\tau(x') \in \partial_h^- \mathbb{K}_\epsilon \mid x' = (2, \theta, -1)\},$$

and the curve of primary entry points  $x \in \partial_h^- \mathbb{K}_\epsilon$  such that the  $\mathcal{K}_\epsilon$ -orbit of  $x$  hits  $E_i^\epsilon$  in a point with radius 2. Observe that these conclusions hold for negative orbits also.

**5.2. Existence of exactly two periodic orbits.** Corollary 5.3 implies that the plugs  $\mathbb{K}_\epsilon$  have at least two periodic orbits, corresponding to the periodic orbits of the Wilson plug  $\mathbb{W}$ . We next show that these are the only periodic orbits of the flow  $\Phi_t^\epsilon$ . Moreover, these orbits form the boundary of an invariant cylinder  $\mathfrak{M}_\epsilon \subset \mathbb{K}_\epsilon$ , whose limit as  $\epsilon \rightarrow 0$  is the invariant open set  $\mathfrak{M}_0 \subset \mathbb{K}_0$ , introduced in [6] and discussed in further detail below.

The proof of the following result is based in spirit, and also in many details, on the proof of the aperiodicity of the plug  $\mathbb{K}_0$  as given in [6, Theorem 8.1].

**THEOREM 5.4.** *For  $\epsilon < 0$ , the flow  $\Phi_t^\epsilon$  has exactly two periodic orbits,  $\mathcal{O}_1^\epsilon$  and  $\mathcal{O}_2^\epsilon$ .*

*Proof.* Suppose there exist a periodic orbit inside  $\mathbb{K}_\epsilon$  and let  $x$  be a point on it. Let  $0 \leq t_0 < t_1 < \dots < t_n < \dots$  with  $x_\ell = \Phi_{t_\ell}^\epsilon(x)$  be the transition points for the  $\mathcal{K}_\epsilon$ -orbit  $\{\Phi_t^\epsilon(x) \mid t \geq 0\}$ , and suppose that  $t_n > 0$  is the first subsequent transition point with  $x_n = \Phi_{t_n}^\epsilon(x_0) = x_0$ , so that  $\Phi_{t+t_n}^\epsilon(x) = \Phi_t^\epsilon(x)$  for all  $t$ .

Let  $[x'_\ell, y'_{\ell+1}]_{\mathcal{W}} \subset \widehat{\mathbb{W}}_\epsilon$  be the lift of the  $\mathcal{K}_\epsilon$ -arc  $[x_\ell, x_{\ell+1}]_{\mathcal{K}_\epsilon} \subset \mathbb{K}_\epsilon$ , for  $0 \leq \ell \leq n$  and let  $r_\ell$  be the radius coordinate of the arc  $[x'_\ell, y'_{\ell+1}]_{\mathcal{W}}$ . Periodicity of the orbit implies that  $[x'_0, y'_1]_{\mathcal{W}} = [x'_n, y'_{n+1}]_{\mathcal{W}}$ . Moreover, the  $r$ -coordinate is constant on each  $\mathcal{W}$ -arc  $[x'_\ell, y'_{\ell+1}]_{\mathcal{W}}$ , so it has a minimal value  $r_0$ . Without loss, assume this minimum occurs for  $[x'_0, y'_1]_{\mathcal{W}}$ .

Observe that since the radius is minimum on  $[x'_0, y'_1]_{\mathcal{W}}$  and the radius strictly increases at secondary entry points,  $x_0$  is a secondary exit point and  $x_1$  is a secondary entry point. Assume that  $n_{x_0}(t_{n-1}) = k$  for some integer  $k$ , we next analyze the different situations depending on the value of  $k$ .

If  $k < 0$ , let  $\ell > 1$  be the first index such that  $n_{x_0}(t_\ell) = -1$ , then  $n_{x_0}(t_{\ell-1}) = 0$  and Proposition 3.2 implies that  $x'_0 \prec_{\mathcal{W}} y'_\ell$ . Thus  $r_{\ell-1} = r_0$  and  $r_\ell < r_0$ , contradicting the fact that  $r_0$  is minimum. Thus  $n_{x_0}(t) \geq 0$  for all  $t \geq 0$ .

If  $k = 0$ , Proposition 3.2 implies that  $x'_0 \prec_{\mathcal{W}} y'_n$ , and thus  $r_{n-1} = r_0 = r_n$ , that is a contradiction because the orbit cannot pass a transition point with the radius coordinate staying constant.

If  $k > 0$ , let us consider the toy case where the level is strictly increasing, or in other words, the case where all the transition points  $x_\ell$  for  $1 \leq \ell \leq n-1$  are secondary entry points. Since  $x_0 = x_n$  is a secondary exit point, Proposition 3.2 implies that  $x_{n-1} \equiv x_n$  and  $x'_{n-2} \prec_{\mathcal{W}} y'_{n+1} = y'_1$ . Thus  $r_{n-3} < r_{n-2} = r_n = r_0$ , contradicting the minimality of  $r_0$ .

If the level is not strictly increasing, consider first the case when  $k > 1$ . We use a technique introduced by Ghys in [4, page 299], which defines a monotone increasing function  $i(a)$  derived from the level function  $n_{x_0}(t)$ . For  $0 \leq a \leq k-1$ , set  $i(a)$  such that  $n_{x_0}(t_{\ell_{i(a)}}) = a$  and  $n_{x_0}(t) \geq a$  for all  $t \geq t_{\ell_{i(a)}}$ . Then  $0 = i(0) < i(1) < \dots < i(k-1) < n-1$  and  $x_{\ell_{i(a)}}$  is a secondary entry point for all  $a$ . Moreover,  $x_{\ell_{i(k-1)}} \prec_{\mathcal{W}} x_n$ , by Proposition 3.2, and thus  $r_{\ell_{i(k-1)}} = r_n = r_0$ . Then  $r_0 = r_{\ell_{i(0)}} < r_{\ell_{i(1)}} < \dots < r_{\ell_{i(k-1)}} = r_0$ , a contradiction.

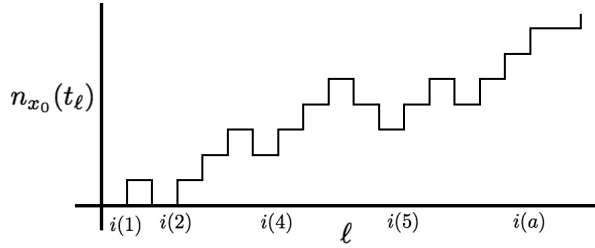


FIGURE 13. The functions  $n_{x_0}$  and  $i(a)$

We are left with the case  $k = 1$  and  $n_{x_0}(t_n) = 0$ . Thus  $1 = n_{x_0}(t_1) = n_{x_0}(t_{n-1})$  and  $x'_1 \prec_{\mathcal{W}} y'_n$ . Moreover, since  $x_1$  is a secondary entry point and  $x_n$  is a secondary exit point, then  $x_1 \equiv x_n = x_0$ . This implies that the in  $\mathbb{W}$ ,  $x'_0 \prec_{\mathcal{W}} x'_1 \prec_{\mathcal{W}} x'_0$  and hence the arc  $[x'_0, y'_1]_{\mathcal{W}}$  is one of the arcs  $\mathcal{O}_i \cap \mathbb{W}_\epsilon$  for  $i = 1, 2$ .

Thus the only periodic orbits are the  $\mathcal{K}_\epsilon$ -orbits of  $\tau(\mathcal{O}_i)$  for  $i = 1, 2$ .  $\square$

The discussion of the trapped set at the end of Section 5.1 and Theorem 5.4, yields the following assertion in Theorem 1.1.

**COROLLARY 5.5.** *All orbits of the flow  $\Phi_t^\epsilon$  are wandering, except for the periodic orbits  $\tau(\mathcal{O}_i)$  for  $i = 1, 2$ .*

**5.3. Invariant sets.** The flow  $\Psi_t$  on the modified Wilson Plug  $\mathbb{W}$  preserves the Reeb cylinder  $\mathcal{R} \subset \mathbb{W}$  introduced in Section 2.2. The restriction of the flow to this invariant set consists of the two periodic orbits  $\mathcal{O}_i$ ,  $i = 1, 2$ , for the flow, along with orbits asymptotic to these orbits, as illustrated by the restriction of the flow to the central band in Figure 2(C).

Consider the intersection  $\mathcal{R}'_\epsilon = \mathcal{R} \cap \widehat{\mathbb{W}}_\epsilon$ , where  $\widehat{\mathbb{W}}_\epsilon$  is the closure of  $\mathbb{W}'_\epsilon$  as defined in (7). Then  $\mathcal{R}'_\epsilon$  is a compact submanifold of  $\mathcal{R}$  with boundary, which is the union of the two arcs  $\mathcal{O}_i \cap \mathbb{W}'_\epsilon$  which are contained in the  $\mathcal{W}$ -periodic orbits, and the boundary of the “notches”, that is the intersections of  $\mathcal{R}$  with  $\mathcal{D}_i^\epsilon$  for  $i = 1, 2$ . This set is illustrated in Figure 14. We consider in this section the image of  $\tau(\mathcal{R}'_\epsilon)$  under the flow  $\Phi_t^\epsilon$ .

First, recall that for  $\epsilon = 0$ , the images  $\tau(\mathcal{O}_i \cap \widehat{\mathbb{W}}_\epsilon) \subset \mathbb{K}_0$  of these orbits are not periodic. One of the main results in [6] is that under some generic assumptions, the unique minimal set for the flow  $\Phi_t^0$  equals the closure of the  $\mathcal{K}_0$ -flow of the image of the Reeb cylinder  $\tau(\mathcal{R}'_0)$ , and has the structure of a *zippered lamination*. For a precise definition of a zippered lamination we refer to [6, Chapter 19].

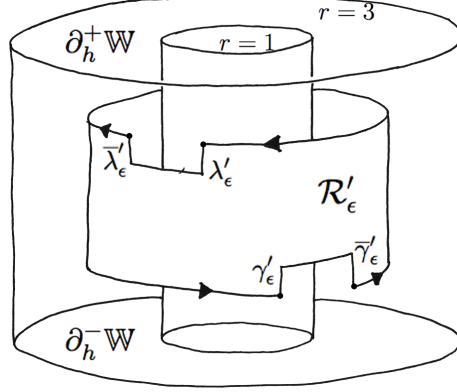


FIGURE 14. The notched cylinder  $\mathcal{R}'$  embedded in  $\mathbb{W}$

Observe that the set  $\tau(\mathcal{R}'_\epsilon) \subset \mathbb{K}_\epsilon$  is not invariant under the flow  $\Phi_t^\epsilon$  since the Reeb cylinder  $\mathcal{R}$  intersects the inserted regions  $\mathcal{D}_i^\epsilon$  for  $i = 1, 2$ . Instead, we must consider the submanifold  $\mathfrak{M}_\epsilon$  obtained by applying the flow  $\Phi_t^\epsilon$  to the image  $\tau(\mathcal{R}'_\epsilon)$ :

$$(20) \quad \mathfrak{M}_\epsilon \equiv \{\Phi_t^\epsilon(\tau(\mathcal{R}'_\epsilon)) \mid -\infty < t < \infty\} \subset \mathbb{K}_\epsilon.$$

For  $\epsilon < 0$ , Corollary 5.3 implies that  $\mathcal{K}_\epsilon$ -orbits of the boundary segments  $\tau(\mathcal{O}_i \cap \mathbb{W}'_\epsilon)$  are periodic orbits. In fact, a much stronger statement is true.

**PROPOSITION 5.6.** *For  $\epsilon < 0$ , the set  $\mathfrak{M}_\epsilon$  is homeomorphic to a cylinder.*

*Proof.* Consider the intersections of  $\mathcal{R}$  with  $\mathcal{D}_i^\epsilon$  for  $i = 1, 2$ . The notches formed by deleting the intersection  $\mathcal{D}_1^\epsilon$  contains 3 boundary curves: label the curve in  $\mathcal{L}_1^{\epsilon-}$  by  $\gamma'_\epsilon$ . The facing curve transverse to the flow is labeled by  $\bar{\gamma}'_\epsilon$ . Analogously, the notches formed by deleting the intersection  $\mathcal{D}_2^\epsilon$  contains 3 boundary curves, where  $\lambda'_\epsilon$  labels the curve transverse to the flow in  $\mathcal{L}_2^{\epsilon-}$ , and  $\bar{\lambda}'_\epsilon$  is the facing curve. These curves are illustrated in Figure 14.

The projections of the curves  $\gamma'_\epsilon$  and  $\lambda'_\epsilon$  to  $\mathbb{K}_\epsilon$  are denoted by  $\gamma_\epsilon = \tau(\gamma'_\epsilon)$  and  $\lambda_\epsilon = \tau(\lambda'_\epsilon)$ . These are curves in the entry regions  $E_1^\epsilon$  and  $E_2^\epsilon$ , respectively. In the same way consider the curves  $\bar{\gamma}_\epsilon = \tau(\bar{\gamma}'_\epsilon)$  and  $\bar{\lambda}_\epsilon = \tau(\bar{\lambda}'_\epsilon)$  which are contained in the exit regions  $S_1^\epsilon$  and  $S_2^\epsilon$ .

The Parametrized Radius Inequality for  $\epsilon < 0$  implies that each point on these four curves lies in the region  $\{r > 2\}$ . Thus, by Proposition 5.1 the  $\mathcal{K}_\epsilon$ -orbit of each point  $x \in \gamma_\epsilon$  passes through the facing point  $y \in \bar{\gamma}_\epsilon$ . Thus, the  $\Phi_t^\epsilon$ -flow of the curve  $\gamma_\epsilon$  generates a compact surface denoted by  $\Sigma_{\gamma_\epsilon} \subset \mathbb{K}_\epsilon$  that “fills the notch” created by deleting the rectangular region  $\mathcal{R} \cap \mathcal{D}_1^\epsilon$ . Analogously, the  $\Phi_t^\epsilon$ -flow of the curve  $\lambda_\epsilon$  generates a compact surface denoted by  $\Sigma_{\lambda_\epsilon} \subset \mathbb{K}_\epsilon$  that “fills the notch” created by deleting the rectangular region  $\mathcal{R} \cap \mathcal{D}_2^\epsilon$ . Both of these surfaces with boundary are diffeomorphic to a rectangular region, but the embeddings of this region in  $\mathbb{K}_\epsilon$  becomes increasingly “twisted” as  $\epsilon \rightarrow 0$ . In any case, the surface  $\mathfrak{M}_\epsilon$  obtained by attaching these surfaces  $\Sigma_{\gamma_\epsilon}$  and  $\Sigma_{\lambda_\epsilon}$  along their boundary to the boundary of the notches in the image  $\tau(\mathcal{R}'_\epsilon)$  is homeomorphic to a cylinder whose boundary components are the periodic orbits  $\mathcal{O}_i^\epsilon$  for  $i = 1, 2$ .  $\square$

Let us describe the surfaces  $\Sigma_{\gamma_\epsilon}$  and  $\Sigma_{\lambda_\epsilon}$ . The description below proceeds analogously to the surface  $\mathfrak{M}_0$  obtained from the  $\Phi_t^0$ -flow of the Reeb cylinder  $\mathcal{R}'_0 \subset \mathbb{K}_0$  which is described in complete detail in Chapter 12 of [6]. We describe the surface  $\Sigma_{\gamma_\epsilon}$  below, and the description of the surface  $\Sigma_{\lambda_\epsilon}$  is exactly analogous.

Consider the curve  $\gamma_\epsilon \in E_1^\epsilon$  and the corresponding curve  $\gamma''_\epsilon = \tau^{-1}(\gamma_\epsilon) \in L_1^-$ . Note that the curves  $\gamma'_\epsilon$  and  $\gamma''_\epsilon$  satisfy  $\tau(\gamma'_\epsilon) = \tau(\gamma''_\epsilon) = \gamma_\epsilon$ , but the curve  $\gamma'_\epsilon$  lies in the cylinder of points  $r = 2$  in  $\mathbb{W}$ , while the curve  $\gamma''_\epsilon$  is contained in the bottom face of  $\mathbb{W}$ . In particular, the radius coordinate along  $\gamma''_\epsilon$  is strictly greater than 2. Let  $r_1 \geq 2 + \Delta$  be the minimum radius attained along the curve. Then the  $\Psi_t$ -flow of  $\gamma''_\epsilon$  generates a finite propeller  $P_{\gamma_\epsilon}$  as described in Section 4. Consider the notched propeller  $P'_{\gamma_\epsilon} = P_{\gamma_\epsilon} \cap \mathbb{W}'_\epsilon$ . Thus  $\tau(P'_{\gamma_\epsilon}) \subset \mathfrak{M}_\epsilon$  and is attached to  $\tau(\mathcal{R}'_\epsilon)$  via the insertion map  $\sigma_1^\epsilon$ .

Since this propeller is finite, its intersection with  $E_1^\epsilon$  and  $E_2^\epsilon$  is along a finite number of curves, whose radius coordinate is bounded below by  $r_1 + \Delta$ . Each of these curves generates a finite propeller, simple or double, that is attached to  $\tau(P'_{\gamma_\epsilon})$  via the map  $\sigma_i^\epsilon$ , for  $i = 1$  or  $2$ . Iterating this process a finite number of steps, we construct the compact surface  $\Sigma_{\gamma_\epsilon}$ . Analogously, we obtain the surface  $\Sigma_{\lambda_\epsilon}$ . We conclude that  $\mathfrak{M}_\epsilon$  is formed from the union of  $\tau(\mathcal{R}')$  with a finite number of finite propellers. An important observation is that the points in  $\mathfrak{M}_\epsilon$  with radius coordinate equal to 2 are exactly those in  $\tau(\mathcal{R}'_\epsilon)$ .

**REMARK 5.7.** *The propellers in the construction might have “bubbles” formed by double propellers, as described in Chapters 15 and 18 of [6]. These are compact surfaces that are attached to internal notches, which are notches in a propeller that do not intersect the boundary of the propeller.*

Observe that as  $\epsilon \rightarrow 0$ , the first propeller attached to  $\tau(\mathcal{R}'_\epsilon)$  becomes arbitrarily long, and when  $\epsilon = 0$  we obtain an infinite propeller. The set  $\mathfrak{M}_0$  is no longer a cylinder, and has a very complicated structure. We can thus see  $\mathfrak{M}_0$  as the limit of the embedded cylinders  $\mathfrak{M}_\epsilon$ . This phenomenon is analogous to the behavior of the leaves for a compact foliation as they approach its bad set, as described in [2].

To complete the proof of Theorem 1.1, choose a  $C^\infty$ -family of embeddings  $\sigma_i^\epsilon$  which satisfy the Parametrized Radius inequality, for  $-1 \leq \epsilon \leq 0$ . Let  $\Phi_t^\epsilon$  be the resulting flows on the plug  $\mathbb{K}_\epsilon$ . Then the results of Section 5 show that these flows satisfy the assertions of Theorem 1.1.

## 6. GEOMETRIC HYPOTHESES FOR $\epsilon \geq 0$

The dynamical properties of the Kuperberg flows  $\Phi_t^\epsilon$  when  $\epsilon \geq 0$  are far more subtle than when  $\epsilon < 0$ , and to obtain our results on the global dynamics of  $\Phi_t^\epsilon$  when  $\epsilon \geq 0$  requires that we impose a variety of additional hypotheses on the construction of  $\Phi_t^\epsilon$ . In this section, we formulate some basic additional geometric assumptions for the insertion maps  $\sigma_i^\epsilon$  beyond what we specified in Section 2.3. The basic point is to require that they have the geometric shape which is intuitively implicit in Figures 5, 6 and 7(C).

First, we note a straightforward consequence of the Parametrized Radius Inequality (K8) in Section 2.3. Recall that  $\theta_i$  is the radian angle coordinate specified in (K8) such that for  $x' = (2, \theta_i, -2) \in L_i$  we have  $r(\sigma_i^\epsilon(2, \theta_i, -2)) = 2 + \epsilon$ .

**LEMMA 6.1.** *For  $\epsilon > 0$  there exists  $2 + \epsilon < r_\epsilon < 3$  such that  $r(\sigma_i^\epsilon(r_\epsilon, \theta_i, -2)) = r_\epsilon$ .*

*Proof.* Since  $r(\sigma_i^\epsilon(2, \theta_i, -2)) = 2 + \epsilon$  and  $r(\sigma_i^\epsilon(3, \theta_i, -2)) < 3$ , by the continuity in  $r$  of the function  $r(\sigma_i^\epsilon(r, \theta_i, -2))$  we conclude that there exists  $2 + \epsilon < r_\epsilon < 3$  such that  $r(\sigma_i^\epsilon(r_\epsilon, \theta_i, -2)) = r_\epsilon$ .  $\square$

We then add an additional assumption on the insertion maps  $\sigma_i^\epsilon$  for  $i = 1, 2$  that the radius is *decreasing* under the insertion map, for  $r \geq r_\epsilon$ .

**HYPOTHESIS 6.2.** *If  $r_\epsilon$  is the smallest  $2 + \epsilon < r_\epsilon < 3$  such that  $r(\sigma_i^\epsilon(r_\epsilon, \theta_i, -2)) = r_\epsilon$ , then assume that  $r(\sigma_i^\epsilon(r, \theta_i, -2)) < r$  for  $r > r_\epsilon$ .*

Next, we introduce an hypothesis on the insertion maps  $\sigma_i^\epsilon$  for  $i = 1, 2$  which, in essence, guarantees that the images of the level curves for  $r' = c$  are “quadratic” for  $c$  near the value  $r = 2$ , as pictured in Figure 7. Recall our notational conventions. For  $i = 1, 2$ , let  $x' = (r', \theta', -2) \in L_i^-$  denote a point in the domain of  $\sigma_i^\epsilon$  and denote its image by  $(r, \theta, z) = \sigma_i^\epsilon(x') \in \mathcal{L}_i^\epsilon \subset \mathbb{W}$ .

Let  $\pi_z: \mathbb{W} \rightarrow \partial_h^- \mathbb{W}$  denote the projection along the  $z$ -coordinate, so  $\pi_z(r, \theta, z) = (r, \theta, -2)$ .

We first assume that  $\sigma_i^\epsilon$  restricted to the bottom face,  $\sigma_i^\epsilon: L_i^- \rightarrow \mathcal{L}_i^{\epsilon-} \subset \mathbb{W}$ , has image transverse to the vertical fibers of  $\pi_z$ . Then  $\pi_z \circ \sigma_i^\epsilon: L_i^- \rightarrow \mathbb{W}$  is a diffeomorphism into the face  $\partial_h^- \mathbb{W}$ . Denote the image set of this map by  $\mathfrak{D}_i \subset \partial_h^- \mathbb{W}$ . Then we can define the inverse map

$$(21) \quad \Upsilon_i^\epsilon = (\pi_z \circ \sigma_i^\epsilon)^{-1}: \mathfrak{D}_i \rightarrow L_i^- .$$

In particular, express the inverse map  $x' = \Upsilon_i^\epsilon(x)$  in polar coordinates as:

$$(22) \quad x' = (r', \theta', -2) = \Upsilon_i^\epsilon(r, \theta, -2) = (r(\Upsilon_i^\epsilon(r, \theta, -2)), \theta(\Upsilon_i^\epsilon(r, \theta, -2)), -2) = (R_{i,r}^\epsilon(\theta), \Theta_{i,r}^\epsilon(\theta), -2) .$$

In the following hypothesis, we impose uniform conditions on the derivatives of the maps  $\Upsilon_i^\epsilon$ . Recall that  $0 < \epsilon_0 < 1/4$  was specified in Hypothesis 2.1, and we assume that  $0 < \epsilon < \epsilon_0$ .

**HYPOTHESIS 6.3** (*Strong Radius Inequality*). *For  $i = 1, 2$ , assume that:*

- (1)  $\sigma_i^\epsilon: L_i^- \rightarrow \mathbb{W}$  is transverse to the fibers of  $\pi_z$ ;
- (2)  $r = r(\sigma_i^\epsilon(r', \theta', -2)) < r + \epsilon$ , except for  $x' = (2, \theta_i, -2)$  and then  $r = 2 + \epsilon$ ;
- (3)  $\Theta_{i,r}^\epsilon(\theta)$  is an increasing function of  $\theta$  for each fixed  $r$ ;
- (4) For  $2 - \epsilon_0 \leq r \leq 2 + \epsilon_0$  and  $i = 1, 2$ , assume that  $R_{i,r}^\epsilon(\theta)$  has non-vanishing derivative, except when  $\theta = \bar{\theta}_i$  as defined by  $\Upsilon_i^\epsilon(2 + \epsilon, \bar{\theta}_i, -2) = (2, \theta_i, -2)$ ;
- (5) For  $2 - \epsilon_0 \leq r \leq 2 + \epsilon_0$  and  $\theta_i - \epsilon_0 \leq \theta \leq \theta_i + \epsilon_0$  for  $i = 1, 2$ , assume that

$$(23) \quad \frac{d}{d\theta} \Theta_{i,s}(\theta) > 0 \quad , \quad \frac{d^2}{d\theta^2} R_{i,s}(\theta) > 0 .$$

Thus for  $2 - \epsilon_0 \leq r \leq 2 + \epsilon_0$ , the graph of  $R_{i,r}(\theta)$  is parabolic with vertex  $\theta = \bar{\theta}_i$ .

Consequently, each surface  $\mathcal{L}_i^{\epsilon-}$  is transverse to the coordinate vector fields  $\partial/\partial\theta$  and  $\partial/\partial z$  on  $\mathbb{W}$ .

**REMARK 6.4.** *Hypotheses 6.2 and 6.3 combined, imply that  $r_\epsilon$  is the unique value of  $2 + \epsilon < r_\epsilon < 3$  for which  $r(\sigma_i^\epsilon(r_\epsilon, \theta_i, -2)) = r_\epsilon$ . It follows that the radius function  $\rho_x^\epsilon$  at a secondary entry point  $x$  with  $r(x) > r_\epsilon$  is strictly increasing.*

## 7. A PSEUDOGROUP MODEL

The analysis of the dynamical properties of the standard Kuperberg flow  $\Phi_t$ , as made in [6], was based on the introduction of an “almost transverse” rectangle  $\mathbf{R}_0 \subset \mathbb{K}$ , and a detailed study of the dynamics of the induced pseudogroup for the return map  $\widehat{\Phi}$  of the flow to  $\mathbf{R}_0$ . Our analysis of the dynamics of the flows  $\Phi_t^\epsilon$  for the case when  $\epsilon > 0$  follows a similar approach. We utilize the same rectangle  $\mathbf{R}_0$  as defined in (24) below, which is the same as in [6], but we use a simplified model for the pseudogroup, which incorporates the induced return maps to  $\mathbf{R}_0$  for both of the flows  $\Psi_t$  and  $\Phi_t^\epsilon$ . The dynamics for the induced map  $\widehat{\Psi}$  from the Wilson flow is fairly straightforward to analyze, while that of the induced map  $\widehat{\Phi}^\epsilon$  from the Kuperberg flow is extraordinarily complicated, so we restrict to analyzing the dynamics of selected maps defined by  $\widehat{\Phi}^\epsilon$ , and the task is then more manageable.

The goal is to show that for  $\epsilon > 0$ , the dynamics of the return map  $\widehat{\Phi}^\epsilon$  contains disjoint families of “horseshoes”, as will be proved in Section 8, which then yields the conclusions of Theorem 1.2. The first step is to introduce the pseudogroup  $\widehat{\mathcal{G}}_\epsilon$  and the pseudo $\star$ group  $\widehat{\mathcal{G}}_\epsilon^*$  in this section, as Definitions 7.2 and 7.3 below. In the next Section 8, we show that the action of  $\widehat{\mathcal{G}}_\epsilon^* \subset \widehat{\mathcal{G}}_\epsilon$  contains invariant horseshoe dynamical subsystems.

**7.1. A good rectangle.** We introduce the “almost transversal” rectangle to the flows  $\Psi_t$  and  $\Phi_t^\epsilon$  which is used for the study of the return dynamics of their flows, and for the construction of associated pseudogroups.

Choose a value of  $\theta_0$  such that the rectangle  $\mathbf{R}_0$  as defined in cylindrical coordinates,

$$(24) \quad \mathbf{R}_0 \equiv \{\xi = (r, \theta_0, z) \mid 1 \leq r \leq 3, -2 \leq z \leq 2\} \subset \mathbb{W}'_\epsilon ,$$

is disjoint from both the regions  $D_i$  and their insertions  $\mathcal{D}_i^\epsilon$  for  $i = 1, 2$ , as defined in Section 2.3. For example, for the curves  $\alpha_i$  and  $\beta'_i$  defined in Section 2.3, we take  $\theta_0 = \pi$  so that  $\mathbf{R}_0$  is between the embedded regions  $\mathcal{D}_i^\epsilon$  for  $i = 1, 2$  as illustrated in Figure 15.

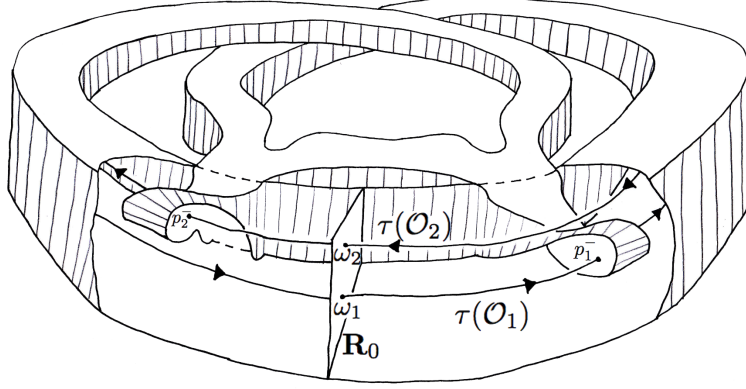


FIGURE 15. The rectangle  $\mathbf{R}_0$  in the Kuperberg plug  $\mathbb{K}_\epsilon$

As  $\mathbf{R}_0 \subset \mathbb{W}'_\epsilon$ , the quotient map  $\tau: \mathbb{W} \rightarrow \mathbb{K}_\epsilon$  is injective on  $\mathbf{R}_0$ . We use a slight abuse of notation, and also denote the image  $\tau(\mathbf{R}_0) \subset \mathbb{K}_\epsilon$  by  $\mathbf{R}_0$  with coordinates  $r = r(\xi)$  and  $z = z(\xi)$  for  $\xi \in \mathbf{R}_0$ .

The periodic points in  $\mathbf{R}_0$  for the Wilson flow are denoted by

$$(25) \quad \omega_1 = \mathcal{O}_1 \cap \mathbf{R}_0 = (2, \theta_0, -1) \quad , \quad \omega_2 = \mathcal{O}_2 \cap \mathbf{R}_0 = (2, \theta_0, 1) \quad .$$

For  $i = 1, 2$ , the first transition point for the forward orbit of  $\omega_i$  is denoted by  $p_i^- = \tau(\mathcal{L}_i^{\epsilon-} \cap \mathcal{O}_i)$ , and for the backward orbit the first transition point is the special exit point  $p_i^+ = \tau(\mathcal{L}_i^{\epsilon+} \cap \mathcal{O}_i)$ .

Define a metric on  $\mathbf{R}_0$  by  $d_{\mathbf{R}_0}(\xi, \xi') = \sqrt{(r' - r)^2 + (z' - z)^2}$ , for  $\xi = (r, \theta_0, z)$  and  $\xi' = (r', \theta_0, z')$ .

We next introduce the first return map  $\widehat{\Psi}$  on  $\mathbf{R}_0$  for the Wilson flow  $\Psi_t$ . The map  $\widehat{\Psi}$  is defined at  $\xi \in \mathbf{R}_0$  if there is a  $\mathcal{W}$ -orbit segment  $[\xi, \eta]_{\mathcal{W}}$  with  $\eta \in \mathbf{R}_0$  and its interior  $(\xi, \eta)_{\mathcal{W}}$  is disjoint from  $\mathbf{R}_0$ . We then set  $\widehat{\Psi}(\xi) = \eta$ . Thus, the domain of  $\widehat{\Psi}$  is the set:

$$(26) \quad \text{Dom}(\widehat{\Psi}) \equiv \{\xi \in \mathbf{R}_0 \mid \exists t > 0 \text{ such that } \Psi_t(\xi) \in \mathbf{R}_0 \text{ and } \Psi_s(\xi) \notin \mathbf{R}_0 \text{ for } 0 < s < t\} \quad .$$

The radius function is constant along the orbits of the Wilson flow, so that  $r(\widehat{\Psi}(\xi)) = r(\xi)$  for all  $\xi \in \text{Dom}(\widehat{\Psi})$ . Also, note that the points  $\omega_i$  for  $i = 1, 2$  defined in (25) are fixed-points for  $\widehat{\Psi}$ . For all other points  $\xi \in \mathbf{R}_0$  with  $\xi \neq \omega_i$ , it was assumed in Section 2.2 that the function  $g(r, \theta, z) > 0$ , so the  $\mathcal{W}$ -orbit of  $\xi$  has a “vertical drift” arising from the term  $g(r, \theta, z) \frac{\partial}{\partial z}$  in the formula (4) for  $\mathcal{W}$ .

The precise description of the domain  $\text{Dom}(\widehat{\Psi})$  is discussed in detail in Chapter 9 of [6], to which we refer the reader for further details. For our applications here, it suffices to note that the domain  $\text{Dom}(\widehat{\Psi})$  contains an open neighborhood of the vertical line segment  $\mathcal{R} \cap \mathbf{R}_0$ . The dynamical properties of  $\Psi_t$  on  $\text{Dom}(\widehat{\Psi})$  are described in Proposition 2.2, and illustrated in Figures 2 and 3.

Next, let  $\widehat{\Phi}^\epsilon$  denote the first return map on  $\mathbf{R}_0$  for the Kuperberg flow  $\Phi_t^\epsilon$ . The domain of  $\widehat{\Phi}^\epsilon$  is the set:

$$(27) \quad \text{Dom}(\widehat{\Phi}^\epsilon) \equiv \{\xi \in \mathbf{R}_0 \mid \exists t > 0 \text{ such that } \Phi_t^\epsilon(\xi) \in \mathbf{R}_0 \text{ and } \Phi_s^\epsilon(\xi) \notin \mathbf{R}_0 \text{ for } 0 < s < t\} \quad .$$

The precise description of the domain  $\text{Dom}(\widehat{\Phi}^\epsilon)$  is very complicated, due to the nature of the orbits of  $\Phi_t^\epsilon$  as the union of  $\mathcal{W}$ -arcs for the Wilson flow. Moreover, the map  $\widehat{\Phi}^\epsilon: \text{Dom}(\widehat{\Phi}^\epsilon) \rightarrow \mathbf{R}_0$  has many points of discontinuity, which arise when an orbit is tangent to section  $\mathbf{R}_0$  along the line  $\mathbf{R}_0 \cap \mathcal{A}$ . An extensive discussion of the properties of the return map  $\widehat{\Phi}^\epsilon$  for the case  $\epsilon = 0$  is discussed in detail in Chapter 9 of [6]. We adapt these results as required, for the case  $\epsilon > 0$ .

**7.2. The pseudogroup  $\widehat{\mathcal{G}}_\epsilon$ .** A key idea, introduced in the work [6], is to associate a pseudogroup  $\mathcal{G}_K$  to the return map  $\widehat{\Phi}$  and study the dynamics of this pseudogroup. This approach allows a more careful analysis of the interaction of the return maps  $\widehat{\Psi}$  and  $\widehat{\Phi}$  in determining the dynamics of  $\Phi_t^\epsilon$ . In this paper, we work with a pseudogroup  $\widehat{\mathcal{G}}_\epsilon$  generated by the return maps *for both flows*, and then show that under the proper hypotheses, the orbits of  $\widehat{\mathcal{G}}_\epsilon$  in an invariant “horseshoe” subset of  $\mathbf{R}_0$  agrees with the orbits of  $\widehat{\Phi}^\epsilon$ .

First, we recall the formal definition of a pseudogroup modeled on a space  $X$ .

**DEFINITION 7.1.** *A pseudogroup  $\mathcal{G}$  modeled on a topological space  $X$  is a collection of homeomorphisms between open subsets of  $X$  satisfying the following properties:*

- (1) *For every open set  $U \subset X$ , the identity  $Id_U: U \rightarrow U$  is in  $\mathcal{G}$ .*
- (2) *For every  $\varphi \in \mathcal{G}$  with  $\varphi: U_\varphi \rightarrow V_\varphi$  where  $U_\varphi, V_\varphi \subset X$  are open subsets of  $X$ , then also  $\varphi^{-1}: V_\varphi \rightarrow U_\varphi$  is in  $\mathcal{G}$ .*
- (3) *For every  $\varphi \in \mathcal{G}$  with  $\varphi: U_\varphi \rightarrow V_\varphi$  and each open subset  $U' \subset U_\varphi$ , then the restriction  $\varphi|_{U'}$  is in  $\mathcal{G}$ .*
- (4) *For every  $\varphi \in \mathcal{G}$  with  $\varphi: U_\varphi \rightarrow V_\varphi$  and every  $\varphi' \in \mathcal{G}$  with  $\varphi': U_{\varphi'} \rightarrow V_{\varphi'}$ , if  $V_\varphi \subset U_{\varphi'}$  then the composition  $\varphi' \circ \varphi$  is in  $\mathcal{G}$ .*
- (5) *If  $U \subset X$  is an open set,  $\{U_\alpha \subset X \mid \alpha \in \mathcal{A}\}$  are open sets whose union is  $U$ ,  $\varphi: U \rightarrow V$  is a homeomorphism to an open set  $V \subset X$  and for each  $\alpha \in \mathcal{A}$  we have  $\varphi_\alpha = \varphi|_{U_\alpha}: U_\alpha \rightarrow V_\alpha$  is in  $\mathcal{G}$ , then  $\varphi$  is in  $\mathcal{G}$ .*

We first introduce a map which encodes a part of the insertion dynamics of the return map  $\widehat{\Phi}^\epsilon$ . The reader interested in more more complete development of these ideas can consult Chapter 9 of [6].

Let  $U_{\phi_1^+} \subset \text{Dom}(\widehat{\Phi}^\epsilon)$  be the subset of  $\mathbf{R}_0$  consisting of points  $\xi \in \text{Dom}(\widehat{\Phi}^\epsilon)$  with  $\eta = \widehat{\Phi}^\epsilon(\xi)$ , such that the  $\mathcal{K}_\epsilon$ -arc  $[\xi, \eta]_{\mathcal{K}_\epsilon}$  contains a single transition point  $x$ , with  $x \in E_1^\epsilon$ .

Note that for such  $\xi$ , we see from Figures 9 and 15, that its  $\mathcal{K}_\epsilon$ -orbit exits the surface  $E_1^\epsilon$  as the  $\mathcal{W}$ -orbit of a point  $x' \in L_1^-$  with  $\tau(x') = x$ , flowing upwards from  $\partial_h^- \mathbb{W}$  until it intersects  $\mathbf{R}_0$  again. If the  $\mathcal{K}_\epsilon$ -orbit of  $\xi$  enters  $E_1^\epsilon$  but exits through  $S_1^\epsilon$  before crossing  $\mathbf{R}_0$ , then it is not considered to be in the domain  $U_{\phi_1^+}$  as it contains more than one transition point between  $\xi$  and  $\eta$ .

Let  $\phi_1^+: U_{\phi_1^+} \rightarrow V_{\phi_1^+}$  denote the map defined by the restriction of  $\widehat{\Phi}^\epsilon$ . As the  $\mathcal{K}_\epsilon$ -arcs  $[\xi, \eta]_{\mathcal{K}_\epsilon}$  defining  $\phi_1^+$  do not intersect  $\mathcal{A}$ , the restricted map  $\phi_1^+$  is continuous. Observe that the action of the map  $\phi_1^+$  corresponds to a flow through a transition point which increases the level function  $n_x(t)$  by  $+1$ .

We can now define the pseudogroup  $\widehat{\mathcal{G}}_\epsilon$  acting on  $\mathbf{R}_0$  associated to the return maps  $\widehat{\Psi}$  and  $\widehat{\Phi}^\epsilon$ .

**DEFINITION 7.2.** *Let  $\widehat{\mathcal{G}}_\epsilon$  denote the pseudogroup generated by the collection of all maps formed by compositions of the maps*

$$(28) \quad \{Id, \phi_1^+, \widehat{\Psi}|U \mid U \subset \text{Dom}(\widehat{\Psi}) \text{ is open and } \widehat{\Psi}|U \text{ is continuous}\}$$

*and their restrictions to open subsets in their domains.*

The notion of a pseudo\*group was introduced by Matsumoto in [12], which is a subset of the maps in a pseudogroup that satisfy conditions (1) to (4) of Definition 7.1, but need not satisfy the condition (5) on unions of maps.

**DEFINITION 7.3.** *Let  $\widehat{\mathcal{G}}_\epsilon^*$  denote the collection of all maps formed by compositions of the maps in (28) above, and their restrictions to open subsets in their domains.*

Note that  $\widehat{\mathcal{G}}_\epsilon^*$  is a pseudo\*group contained in  $\widehat{\mathcal{G}}_\epsilon$  but is not a pseudogroup itself. A key point in the proof of Proposition 8.2 later in this work, is that for appropriately chosen  $k \geq \ell(\epsilon)$ , there is a well-defined non-trivial element  $\varphi_k = \widehat{\Psi}^k \circ \phi_1^+ \in \widehat{\mathcal{G}}_\epsilon^*$  which is a concatenation of a power of the Wilson return map  $\widehat{\Psi}$  with the first return map  $\phi_1^+$  of the flow  $\Phi_t^\epsilon$ .

We conclude with an observation and a fundamental technical result which relates the orbits of the map  $\widehat{\Psi}$  with those of the map  $\widehat{\Phi}^\epsilon$ , that encodes the existence of “shortcuts” as given in Proposition 3.2. We require

the following result, which is analogous to Proposition 5.1. Recall that the constant  $r_\epsilon > 2$  was introduced in Lemma 6.1, and that we assume that Hypothesis 6.2 is satisfied.

**PROPOSITION 7.4.** *Let  $x$  be a primary or secondary entry point of  $\mathbb{K}_\epsilon$  and  $y$  the exit point with  $x \equiv y$ . Assume that  $r(x) \geq r_\epsilon$ , then  $x \prec_{\mathcal{K}_\epsilon} y$ , and the collection of lifts of the  $\mathcal{W}$ -arcs in  $[x, y]_{\mathcal{K}_\epsilon}$  contains all the  $\mathcal{W}$ -arcs of the  $\mathcal{W}$ -orbit of  $x'$  that are in  $\widehat{\mathbb{W}}_\epsilon$ , where  $\tau(x') = x$ .*

*Proof.* The proof follows in the same way as that of Proposition 5.1, where we note that for  $r > r_\epsilon$  the radius strictly grows along any orbit of  $\Phi_t^\epsilon$  when entering a face of one of the insertions.  $\square$

Introduce the local coordinate function  $\tilde{r}(\xi)$  which is defined for points in  $\mathbf{R}_0$  whose forward orbit hits  $E_i^\epsilon$ , for  $i = 1, 2$ , before reaching any other transition point or returning to  $\mathbf{R}_0$ . Let  $x \in E_i^\epsilon$  be the first secondary entry point in the forward orbit  $\xi$ , set  $\tilde{r}(\xi) = r(x)$ . Then, for  $\xi$  in the domain  $U_{\phi_1^+} \subset \mathbf{R}_0$  of the map  $\phi_1^+ \in \widehat{\mathcal{G}}_\epsilon$ , we have  $\tilde{r}(\xi) = r(\phi_1^+(\xi))$ . Recall that  $\xi \in U_{\phi_1^+}$  if the forward  $\mathcal{K}_\epsilon$ -orbit of  $\xi$  hits  $E_1^\epsilon$  before returning to  $\mathbf{R}_0$ , so in particular  $U_{\phi_1^+}$  contains an open neighborhood of the set  $\{\tilde{r} = 2\} \subset \mathbf{R}_0$ . Next, define the subset

$$(29) \quad U_{r_\epsilon} = \{\xi \in D(\widehat{\Phi}^\epsilon) \mid \tilde{r}(\xi) > r_\epsilon\} \subset \mathbf{R}_0.$$

**COROLLARY 7.5.** *Let  $\xi \in U_{r_\epsilon}$  be such that  $\eta$  is contained in the forward  $\mathcal{W}$ -orbit of  $\xi$ . Then there exists some  $\ell > 0$  such that  $\eta = (\widehat{\Phi}^\epsilon)^\ell(\xi)$ .*

*Proof.* If the  $\mathcal{W}$ -arc  $[\xi, \eta]_{\mathcal{W}}$  does not intersect an entry region  $\mathcal{L}_i^{\epsilon-}$  then it is also a  $\mathcal{K}$ -arc, and so the result follows. Otherwise, let  $x \in \mathcal{L}_i^{\epsilon-}$  be the first transition point along  $[\xi, \eta]_{\mathcal{W}}$  and let  $y \in \mathcal{L}_j^{\epsilon+}$  be the last exit point. Then  $x \equiv y$ , and  $\xi \in U_{r_\epsilon}$  implies that  $r(x) > r_\epsilon$ , so by Proposition 7.4 we have that  $y$  and  $\eta$  are in the forward  $\mathcal{K}_\epsilon$ -orbit of  $\xi$ . Thus, there exists some  $\ell > 0$  such that  $\eta = (\widehat{\Phi}^\epsilon)^\ell(\xi)$ .  $\square$

## 8. HORSESHOES FOR THE PSEUDOGROUP DYNAMICS

In this section, we show that for  $0 < \epsilon < \epsilon_0$  sufficiently small, the pseudo $\star$ group  $\widehat{\mathcal{G}}_\epsilon^*$  contains a map  $\varphi$  with “horseshoe dynamics”. In fact, the precise statement, Theorem 8.6 below, gives an even stronger conclusion, showing that there exists a countable collection of such maps, each with an invariant Cantor set for which the action is coded by a shift map, and each disjoint from the others. The proof of Theorem 8.6 will be via a construction, which uses the relations between the action of the maps  $\widehat{\Psi}$  and  $\phi_1^+$  on  $\mathbf{R}_0$ , and the geometry of the traces of propellers and double propellers in  $\mathbf{R}_0$ .

**8.1. Traces of propellers.** We describe the surfaces in the Wilson plug  $\mathbb{W}$  that are generated by the Wilson flow of curves in the bottom face  $\partial_h^- \mathbb{W}$ , and especially those curves which cross the circle  $\{r = 2\} \subset \partial_h^- \mathbb{W}$ . These surfaces are similar to the double propellers introduced in Definition 4.2.

Let  $\Gamma : [0, 2] \rightarrow L_1^- \subset \partial_h^- \mathbb{W}$  be a curve such that:

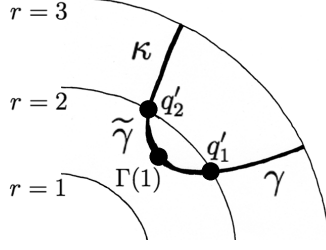
- $r(\Gamma(0)) = r(\Gamma(2)) = 3$ ;
- $r(\Gamma(t)) > r(\Gamma(1))$  for all  $t \neq 1$  and  $r(\Gamma(1)) < 2$ ;
- $\Gamma$  is transverse to the circle  $\{r = 2\}$ .

We will call such a curve a *traversing curve*. Let  $t_1 < t_2$  be such that  $r(\Gamma(t_1)) = r(\Gamma(t_2)) = 2$ . We can divide  $\Gamma$  in three overlapping parts, as illustrated in Figure 16:

- $\gamma$  the curve  $\Gamma([0, t_1])$ ;
- $\tilde{\gamma}$  the curve  $\Gamma([t_1, t_2])$ ;
- $\kappa$  the curve  $\Gamma([t_2, 2])$ .

Label the interior endpoints of these curves as  $q'_1 = \Gamma(t_1) \in \gamma \cap \tilde{\gamma}$  and  $q'_2 = \Gamma(t_2) \in \tilde{\gamma} \cap \kappa$ . Note that the forward orbits of the points  $\{q'_1, q'_2\} \subset \partial_h^- \mathbb{W}$  by the flow  $\Psi_t$  spiral upward to the periodic orbit  $\mathcal{O}_1$ , and so are trapped in the Wilson plug  $\mathbb{W}$ .



FIGURE 16. The curve  $\Gamma = \gamma \cup \tilde{\gamma} \cup \kappa$  in  $\partial_h^- \mathbb{W}$ 

Recall from Section 3 that we say points  $x' \in \partial_h^- \mathbb{W}$  and  $y' \in \partial_h^+ \mathbb{W}$  are *facing*, and we write  $x' \equiv y'$ , if  $x' = (r, \theta, -2)$  and  $y' = (r, \theta, 2)$  for some  $r$  and  $\theta$ . Let  $\bar{\Gamma} \subset \partial_h^+ \mathbb{W}$  be the facing curve to  $\Gamma$ , and denote by  $\bar{\gamma}$ ,  $\bar{\kappa}$  and  $\bar{\tilde{\gamma}}$  the corresponding segments of  $\bar{\Gamma}$  facing to the curves  $\gamma$ ,  $\kappa$  and  $\tilde{\gamma}$ . Then also define  $\bar{q}'_1 = \bar{\Gamma}(t_1) \in \bar{\gamma} \cap \bar{\tilde{\gamma}}$  and  $\bar{q}'_2 = \bar{\Gamma}(t_2) \in \bar{\tilde{\gamma}} \cap \bar{\kappa}$ . The antisymmetry assumption on the vector field  $\mathcal{W}$  implies that the forward  $\Psi_t$  flow of a point  $\Gamma(t) \in \partial_h^- \mathbb{W}$  terminates in the facing point  $\bar{\Gamma}(t) \in \partial_h^+ \mathbb{W}$ , except for the cases when  $t = t_1, t_2$ .

Now consider the surface  $P_\Gamma \subset \mathbb{W}$  generated by the  $\Psi_t$ -flow of a traversing curve  $\Gamma$ . The flows of the points  $q'_1, q'_2 \in \Gamma$  are trapped in  $\mathbb{W}$ , hence the surface  $P_\Gamma$  is non-compact. On the other hand, by the conditions (W1) to (W6) on the function  $f$  in the definition of the Wilson flow  $\mathcal{W}$  in Section 2.2, the vector field  $\mathcal{W}$  is transverse to  $\mathbf{R}_0$  away from the boundary cylinders  $r = 1$  and  $r = 3$ , and the annulus  $\{z = 0\} = \mathcal{A}$ . It follows that each connected component of  $P_\Gamma \cap \mathbf{R}_0$  is a closed embedded curve in  $\mathbf{R}_0$ . We next analyze the properties of these curves.

Observe that the  $\Psi_t$ -flows of the curve segments  $\gamma$  and  $\kappa$  generate infinite propellers  $P_\gamma$  and  $P_\kappa$  as in Definition 4.1, and illustrated in Figure 10, whose trace on  $\mathbf{R}_0$  is pictured in Figure 11(A). We denote the curves in  $P_\gamma \cap \mathbf{R}_0$  by  $\gamma_0(\ell)$ , for  $\ell > 0$  and unbounded. Recall that these are simple arcs whose endpoints lie on the vertical line  $\{r = 2\} \cap \mathbf{R}_0$ . The lower endpoint  $p_1^-(1)$  of  $\gamma_0(1)$  is the first intersection of the forward  $\mathcal{W}$ -orbit of  $q'_1$  with  $\mathbf{R}_0$ . Then for  $\ell > 1$ , the lower endpoint  $p_1^-(\ell)$  of  $\gamma_0(\ell)$  is  $\hat{\Psi}^{\ell-1}(p_1^-(1))$ . Likewise, the upper endpoint  $p_1^+(1)$  of  $\gamma_0(1)$  is the first intersection of the backward  $\mathcal{W}$ -orbit of  $\bar{q}'_1$  with  $\mathbf{R}_0$ , and for  $\ell > 1$  the upper endpoint of  $\gamma_0(\ell)$  is  $\hat{\Psi}^{1-\ell}(p_1^+(1))$ .

Analogously, we denote the curves in  $P_\kappa \cap \mathbf{R}_0$  by  $\kappa_0(\ell)$ , for  $\ell > 0$  and unbounded. Again, these are simple arcs whose endpoints lie on the vertical line  $\{r = 2\} \cap \mathbf{R}_0$ . The lower endpoint  $p_2^-(1)$  of  $\kappa_0(1)$  is the first intersection of the forward  $\mathcal{W}$ -orbit of  $q'_2$  with  $\mathbf{R}_0$ . Then for  $\ell > 1$ , the lower endpoint  $p_2^-(\ell)$  of  $\kappa_0(\ell)$  is  $\hat{\Psi}^{\ell-1}(p_2^-(1))$ . Likewise, the upper endpoint  $p_2^+(1)$  of  $\kappa_0(1)$  is the first intersection of the backward  $\mathcal{W}$ -orbit of  $\bar{q}'_2$  with  $\mathbf{R}_0$ , and for  $\ell > 1$  the upper endpoint of  $\kappa_0(\ell)$  is  $\hat{\Psi}^{1-\ell}(p_2^+(1))$ .

Note that these two infinite families of curves  $\{\gamma_0(\ell) \mid \ell \geq 1\}$  and  $\{\kappa_0(\ell) \mid \ell \geq 1\}$  are interlaced: between two  $\gamma_0$ -curves there is a  $\kappa_0$ -curve, and vice-versa. To be more precise, the geometry of the Wilson flow maps the lower endpoint  $q'_2$  of the “upper” curve  $\kappa$  in Figure 16 to the point  $p_2^-(1) \in \mathbf{R}_0$ , while the lower endpoint  $q'_1$  of the “lower” curve  $\gamma$  is mapped to  $p_1^-(1) \in \mathbf{R}_0$  which lies *above*  $p_2^-(1)$ . That is, we have  $z(p_1^-(1)) > z(p_2^-(1))$ . The return map of the Wilson flow then preserves this local order, so that we have

$$(30) \quad z(p_2^-(1)) < z(p_1^-(1)) < z(p_2^-(2)) < z(p_1^-(2)) < \cdots < z(p_2^-(\ell)) < z(p_1^-(\ell)) < \cdots < -1.$$

In order to complete the description of the curves in  $P_\Gamma \cap \mathbf{R}_0$  we must consider the  $\Psi_t$  flow of the third curve segment  $\tilde{\gamma}$ , and how the endpoints of the curves in its intersections with  $\mathbf{R}_0$  are attached to the endpoints of the curves  $\gamma_0(\ell)$  and  $\kappa_0(\ell)$  for  $\ell \geq 1$ .

The curve  $\tilde{\gamma}$  coincides with  $\Gamma \cap \{r \leq 2\}$  and its endpoints are  $q'_1, q'_2 \in \Gamma$ . These points are trapped in  $\mathbb{W}$  for the forward  $\Psi_t$  flow, hence the forward flow of  $\tilde{\gamma}$  under  $\Psi_t$  defines a non-compact surface  $P_{\tilde{\gamma}}$  in the region  $\{r \leq 2\} \subset \mathbb{W}$ .

We denote the curves in  $P_{\tilde{\gamma}} \cap \mathbf{R}_0$  by  $\tilde{\gamma}_0(\ell)$ , for  $\ell > 0$  and unbounded. Consider the point  $\Gamma(1) \in \tilde{\gamma}$ , whose radius coordinate is less than 2. It follows that the  $\mathcal{W}$ -orbit of  $\Gamma(1)$  is finite, thus intersects  $\mathbf{R}_0$  in a finite

number of points  $n$ . The integer  $n$  depends on the choice of the insertion map  $\sigma_1^\epsilon$ , but we omit this dependence from the notation, as it simplifies the presentation and does not impact the results below.

Moreover, without loss of generality, we may assume that the intersection of the  $\mathcal{W}$ -orbit of  $\Gamma(1)$  with the annulus  $\mathcal{A}$  is not contained in  $\mathbf{R}_0$ . The symmetry of the Wilson flow with respect to the annulus  $\mathcal{A}$  implies that the trace of the  $\mathcal{W}$ -orbit of  $\Gamma(1)$  on  $\mathbf{R}_0$  forms a symmetric pattern, where points of intersection are paired, each point below the center line  $\{z = 0\} \cap \mathbf{R}_0$  paired with a symmetric copy above this line. Hence,  $n$  is an even number.

The intersection  $P_{\tilde{\gamma}} \cap \mathbf{R}_0$  consists of an infinite collection of arcs, with endpoints in  $\{r = 2\} \cap \mathbf{R}_0$ . For  $1 \leq \ell \leq n/2$  label the curve containing with endpoints  $\{p_1^-(\ell), p_2^-(\ell)\}$  by  $\tilde{\gamma}_0(\ell)$ . Thus,  $\tilde{\gamma}_0(\ell)$  is a “parabolic curve” in the region  $\{z < 0\} \cap \mathbf{R}_0$ , as illustrated in Figure 17.

By the anti-symmetry of the flow  $\Psi_t$ , for each  $1 \leq \ell \leq n/2$  there is a corresponding “parabolic curve”  $\tilde{\tilde{\gamma}}_0(\ell)$  in the region  $\{z > 0\} \cap \mathbf{R}_0$  with endpoints  $\{p_1^+(\ell), p_2^+(\ell)\}$ . Let  $\Gamma_0(\ell) \subset \mathbf{R}_0$  denote the closed curve obtained by joining the endpoints of the curve  $\tilde{\gamma}_0(\ell)$  with the endpoints of the curve  $\tilde{\tilde{\gamma}}_0(\ell)$  via the curves  $\{\gamma_0(\ell), \kappa_0(\ell)\}$ . The curves  $\Gamma_0(\ell)$  for  $1 \leq \ell \leq n/2$  are illustrated in Figure 17 as the closed curves that *do not contain* the vertical arc  $\mathcal{R} \cap \mathbf{R}_0$  in their interiors.

The trace of  $P_{\tilde{\gamma}}$  on  $\mathbf{R}_0$  contains also an infinite number of connected arcs that do not contain points of the orbit of  $\Gamma(1)$ , and each of these arcs is again symmetric with respect to  $\{z = 0\}$ . For each point  $p_1^-(\ell)$  with  $\ell > n/2$  we obtain an arc in  $\mathbf{R}_0$  with  $p_1^-(\ell)$  as the lower endpoint, and  $p_1^+(\ell)$  as the upper endpoint. When joined with the arc  $\gamma_0(\ell)$  having the same endpoints, we obtain a closed curve  $\Gamma_0^\gamma(\ell)$  for  $\ell > n/2$ , that contains the vertical arc  $\mathcal{R} \cap \mathbf{R}_0$  in its interior.

Similarly, for each point  $p_2^-(\ell)$  with  $\ell > n/2$  we obtain an arc in  $\mathbf{R}_0$  with  $p_2^-(\ell)$  as the lower endpoint, and  $p_2^+(\ell)$  as the upper endpoint. When joined with the arc  $\kappa_0(\ell)$  having the same endpoints, we obtain a closed curve  $\Gamma_0^\kappa(\ell)$  for  $\ell > n/2$ , that also contains the vertical arc  $\mathcal{R} \cap \mathbf{R}_0$  in its interior. Moreover, the closed curves  $\Gamma_0^\gamma(\ell)$  and  $\Gamma_0^\kappa(\ell)$  are nested for  $\ell > n/2$ . These curves are illustrated in Figure 17 as the infinite sequence of nested closed curves that contain the vertical arc  $\mathcal{R} \cap \mathbf{R}_0$  in their interiors.

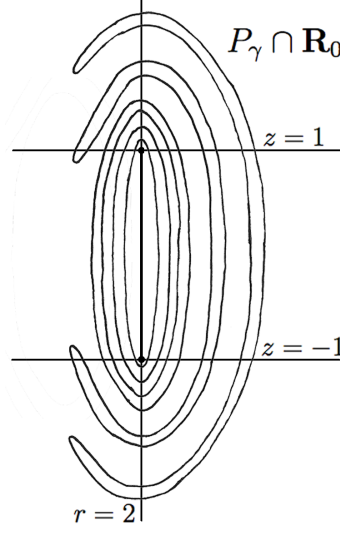
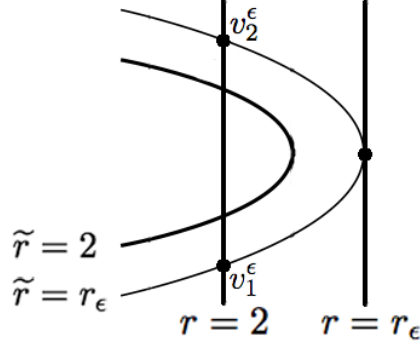
The curves  $\Gamma_0(\ell) \subset \mathbf{R}_0$  for  $1 \leq \ell \leq n/2$ , and  $\Gamma_0^\gamma(\ell), \Gamma_0^\kappa(\ell) \subset \mathbf{R}_0$  for  $\ell > n/2$ , can be visualized in terms of a modification of the illustration of a standard propeller in Figure 10. Since the curve  $\Gamma$  crosses the circle  $\{r = 2\} \cap \partial_h^- \mathbb{W}$ , the flow of the curves  $\gamma \cup \tilde{\gamma}$  and  $\tilde{\gamma} \cup \kappa$  each develops a singularity along this circle, which results in an infinite cylinder attached to the surface pictured in Figure 10. This infinite cylinder wraps around and is asymptotic to the Reeb cylinder  $\mathcal{R}$  in  $\mathbb{W}$ . Its intersections with  $\mathbf{R}_0$  yields the nested family  $\Gamma_0^\gamma(\ell)$  for  $\ell > n/2$ . A similar statement holds for the flow of the curve  $\kappa$ , yielding the nested curves  $\Gamma_0^\kappa(\ell)$  for  $\ell > n/2$ . The curves  $\Gamma_0(\ell)$  for  $1 \leq \ell \leq n/2$ , are obtained from the flow of the point  $\Gamma(1)$ , which now lies in the region  $r < 2$ .

**8.2. The transverse hypotheses.** We formulate the conditions on a Kuperberg plug  $\mathbb{K}_\epsilon$  for  $\epsilon > 0$  which will be assumed in the following sections of the text, where horseshoe dynamics are exhibited for the action of the pseudo-group  $\hat{\mathcal{G}}_\epsilon^*$  on  $\mathbf{R}_0$ .

Assume that the flow  $\Psi_t$  on the Wilson Plug satisfies Hypothesis 2.1, and that the construction of the flow  $\Phi_t^\epsilon$  on  $\mathbb{K}_\epsilon$  satisfies the conditions (K1) to (K8) in Section 2.3, and Hypotheses 6.2 and 6.3.

Observe that for a plug  $\mathbb{K}_\epsilon$  defined by the embeddings  $\sigma_i^\epsilon$  satisfying the Parametrized Radius Inequality (K8), the curve  $\theta' \mapsto \sigma_1^\epsilon(2, \theta', -2)$  in  $\mathcal{L}_1^{\epsilon-}$  contains two points with  $r = 2$ . In other words, the image under  $\sigma_i^\epsilon$  of the circle of radius  $r = 2$  intersects twice the cylinder  $\mathcal{C} \subset \mathbb{W}$  of points with radius  $r = 2$ . Thus the curve  $\tilde{r} = 2$  is  $\mathbf{R}_0$  intersects the vertical line  $r = 2$  in two points, as in Figure 18.

Hypothesis 6.2 and 6.3 imply that the parabolic curve of points in  $\mathbf{R}_0$  whose forward orbit hits  $E_1^\epsilon$  in points of radius  $r_\epsilon$  is tangent to the vertical line of radius equal to  $r_\epsilon$ . That is, the curve  $\tilde{r} = r_\epsilon$  is tangent to the vertical line  $r = r_\epsilon$ . Moreover, by the Parametrized Radius Inequality, the parabolic curve of points  $\tilde{r} = 2$  is tangent to the vertical line of radius equal to  $2 + \epsilon$ , and by Lemma 6.1, we have that  $r_\epsilon > 2 + \epsilon$ , as illustrated in Figure 18.

FIGURE 17. Trace of the surface  $P_\gamma$  on  $\mathbf{R}_0$ FIGURE 18. The points  $v_1^\epsilon$  and  $v_2^\epsilon$  in  $\mathbf{R}_0$ 

Next, assume that  $\epsilon > 0$  is sufficiently small so that  $2 + \epsilon < r_\epsilon < 2 + \epsilon_0/2$ . This implies that the parabolic curves  $\tilde{r} = 2$  and  $\tilde{r} = r_\epsilon$  in Figure 18 intersect the vertical line  $r = 2$  transversally. Recall that the orbits of the points  $\xi \in \mathbf{R}_0$  such that  $\tilde{r}(\xi) = r_\epsilon$  hit  $E_1^\epsilon$  in points of radius  $r_\epsilon$ .

Label the points of intersection of the curve  $\tilde{r} = r_\epsilon$  with the vertical line  $r = 2$  by

$$(31) \quad \{r = 2\} \cap \{\tilde{r} = r_\epsilon\} \cap \mathbf{R}_0 = \{v_1^\epsilon, v_2^\epsilon\},$$

where  $z(v_1^\epsilon) < z(v_2^\epsilon) < 0$  by the Hypothesis (K4). We will assume in addition that  $z(v_1^\epsilon) > -1$ , so that the curve  $\tilde{r} = r_\epsilon$  has a vertical offset. Note that for  $\epsilon = 0$ , the Radius Inequality implies that  $r_\epsilon = 2$  and  $v_1^\epsilon = v_2^\epsilon$  is the unique point  $\omega_1 \in \mathbf{R}_0$  defined by (25), so that  $z(v_1^\epsilon) + 1 = 0$ .

Observe that Hypothesis 6.2 implies that if  $r(\xi) \geq r_\epsilon$  then  $\tilde{r}(\xi) \geq r_\epsilon$ , while condition (K8) implies that if  $r(\xi) < r_\epsilon$  then  $\tilde{r}(\xi) \geq r(\xi) - \epsilon$ . Moreover, Hypothesis 6.3 implies that the curves  $\{\tilde{r} = cst\}$  are parabolic, that is the  $r$ -coordinate depends quadratically on the  $z$ -coordinate.

Finally, the domain  $U_{\phi_1^+}$  of the map  $\phi_1^+$  contains a neighborhood of the set  $\{\tilde{r} = 2\}$ , and thus we can assume that for  $\epsilon > 0$  sufficiently small we have that

$$(32) \quad V_0 = \{x \in \mathbf{R}_0 \mid r(x) \geq 2, \tilde{r}(x) \leq r_\epsilon\} \subset U_{\phi_1^+}.$$

That is, the set bounded by the vertical line of radius 2 and the parabolic curve of points whose forward orbit hit  $E_1^\epsilon$  in points of radius  $r_\epsilon$ , is contained in  $U_{\phi_1^+}$ .

**8.3. Invariant Cantor sets.** We assume that the conditions of Section 8.2 are satisfied.

Let  $\Gamma' \subset \mathcal{L}_1^{\epsilon-}$  be the intersection of the cylinder  $\{r = 2\} \in \mathbb{W}$  and  $\mathcal{L}_1^{\epsilon-}$ , and set  $\Gamma = (\sigma_1^\epsilon)^{-1}(\Gamma') \subset L_1^-$ . Observe that  $\Gamma$  is a traversing curve with parabolic shape, with its endpoints in the circle  $\{r = 3\}$ , and admits a parametrization as in Section 8.1. In particular, we can divide it in three parts,  $\Gamma = \gamma \cup \tilde{\gamma} \cup \kappa$  with  $\Gamma \cap \{r \geq 2\} = \gamma \cup \kappa$ , as in Figure 16.

Let  $V \subset L_1^-$  be the compact subset bounded by  $\Gamma$  and the circle  $\{r = r_\epsilon\}$ , as illustrated in Figure 19. Let  $V' = \tau(V) \subset E_1^\epsilon \subset \mathbb{K}$  be its image in the entry region  $E_1^\epsilon$ . Then the set  $V_0$  defined in (32) is identified with the set of points in  $\mathbf{R}_0$  for which the first transition point of their  $\Phi_t^\epsilon$ -flow lies in  $V' \subset E_1^\epsilon$ .

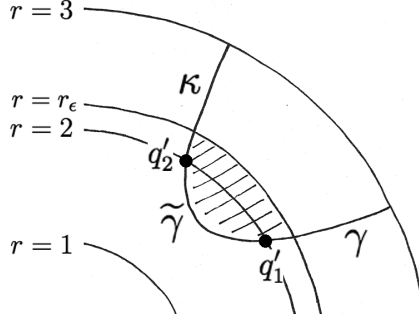


FIGURE 19. The shaded region  $V$  in  $L_1^-$

Recall that the *trace* of the Reeb cylinder in  $\mathbf{R}_0$  is the line segment  $\mathcal{R} \cap \mathbf{R}_0 = \{(r, z) \mid r = 2, -1 \leq z \leq 1\}$ .

Let  $P_\Gamma \subset \mathbb{W}$  be the propeller surface generated by the  $\Psi_t$  flow of the traversing curve  $\Gamma$ . Let  $n > 0$  denote the number of intersections of the flow of the point  $\Gamma(1)$  with the surface  $\mathbf{R}_0$ , which we assume is an even integer as discussed in Section 8.1. Then the trace  $P_\Gamma \cap \mathbf{R}_0$  consists of an infinite collection of closed curves, what we call the  $\Gamma_0$ -curves. Recall that these have two types: the closed curves that *do not contain* the trace of the Reeb cylinder in their interior, and are denoted by  $\Gamma_0(\ell) \subset \mathbf{R}_0$  for  $0 < \ell \leq n/2$ . We also have the two infinite families of closed curves  $\{\Gamma_0^\gamma(\ell) \mid \ell > n/2\}$  and  $\{\Gamma_0^\kappa(\ell) \mid \ell > n/2\}$  which contain the trace of the Reeb cylinder in their interior, as illustrated in Figure 17. For  $\ell > n/2$ , set  $\Gamma_0(\ell) = \Gamma_0^\gamma(\ell) \cup \Gamma_0^\kappa(\ell)$ .

By the symmetry of the Wilson flow, each  $\Gamma_0$  curve is symmetric with respect to  $\{z = 0\}$ , so that the observations for the forward  $\Psi_t$  flow of curves in  $\partial_h^- \mathbb{W}$  also apply to the reverse flow of curves in  $\partial_h^+ \mathbb{W}$ .

The traversing curve  $\Gamma = \gamma \cup \tilde{\gamma} \cup \kappa$  intersects the circle  $\{r = 2\} \cap L_1^-$  twice, in the points  $\{q'_1, q'_2\}$ , where  $q'_1$  is the inner endpoint of  $\gamma$ , and  $q'_2$  is the inner endpoint of  $\kappa$ . The  $\mathcal{W}$ -orbits of these points intersect the vertical segment  $\{r = 2, z < -1\}$  in an increasing sequence of interlaced points, as in (30), which limit to  $p_1^-$  as  $\ell \rightarrow \infty$ . For each  $\ell > 0$ , the lower intersection point  $p_2^-(\ell)$  is the lower endpoint of the curve  $\kappa_0(\ell)$ , and the upper intersection point  $p_1^-(\ell)$  is the lower endpoint of the curve  $\gamma_0(\ell)$ .

By Hypothesis 6.3, the curves  $\gamma_0(\ell)$  and  $\kappa_0(\ell)$  have parabolic shape near their intersection with the vertical line  $r = 2$ ; that is, the  $z$ -coordinate depends quadratically on the  $r$ -coordinate. As the points in the intersection  $\Gamma_0(\ell) \cap \{r = 2\}$  tend to  $p_1^-$ , the curves  $\gamma_0(\ell)$  and  $\kappa_0(\ell)$  accumulate on the trace of the Reeb cylinder,  $\mathcal{R} \cap \mathbf{R}_0$ , which is a vertical line segment, and these curves become increasingly vertical as they approach  $\mathcal{R} \cap \mathbf{R}_0$ .

We next require a technical result, that states that the curves  $\gamma_0(\ell)$  and  $\kappa_0(\ell)$  are in “general position” with respect to the curves  $\tilde{r} = 2$  and  $\tilde{r} = r_\epsilon$ . Recall that we assume the conditions of Section 8.2 are satisfied by the given map  $\sigma_1^\epsilon$ , and in particular, the vertical offset  $z(v_1^\epsilon) > -1$  for the points defined by (31).

**LEMMA 8.1.** *For  $\epsilon > 0$  sufficiently small, there exists  $\ell(\epsilon) > 0$  such that for  $\ell \geq \ell(\epsilon)$ , the curves  $\gamma_0(\ell)$  and  $\kappa_0(\ell)$  intersect the curves  $\tilde{r} = 2$  and  $\tilde{r} = r_\epsilon$  in four points, where the intersections are transverse.*

*Proof.* The assumption that the vertical coordinate  $z(v_1^\epsilon) > -1$  implies that for  $\ell$  sufficiently large, the curves  $\gamma_0(\ell)$  and  $\kappa_0(\ell)$  intersect the curve in  $\mathbf{R}_0$  defined by  $\tilde{r} = 2$  transversely. Let  $\ell(\epsilon)$  be the first index for which

this holds. Then by the nested properties of the curves  $\gamma_0(\ell)$  and  $\kappa_0(\ell)$ , the transversality property holds for all  $\ell \geq \ell(\epsilon)$  as well.  $\square$

The conclusion of Lemma 8.1 is illustrated in Figure 20. Note that the constant  $\ell(\epsilon)$  depends also on the choice of the embedding  $\sigma_1^\epsilon$  but for simplicity of notation we omit this dependence from the notation.

**PROPOSITION 8.2.** *Let  $\epsilon > 0$ , and let  $V_0$  and  $\ell(\epsilon) > 0$  be defined as above. Fix  $k \geq \ell(\epsilon)$ , and define  $\varphi_k = \widehat{\Psi}^k \circ \phi_1^+ \in \widehat{\mathcal{G}}_\epsilon^*$ . Then for  $V_0$  as defined in (32), the following results hold :*

- (1)  $U_k = \varphi_k(V_0) \cap V_0 \neq \emptyset$ ;
- (2)  $U_k$  intersects the curve  $\{\tilde{r} = 2\}$  along two disjoint arcs  $\alpha$  and  $\beta$ .

*Proof.* The image  $\phi_1^+(V_0) \subset \mathbf{R}_0$  is the set of first intercept points in  $\mathbf{R}_0$  for the  $\Psi_t$ -flow of the region  $V \subset L_1^-$ , where  $V$  is illustrated in Figure 19. Then the trace on  $\mathbf{R}_0 \subset \mathbb{W}$  of the  $\mathcal{W}$ -orbits of  $V$  is the union of the sets  $V_\ell = \widehat{\Psi}^\ell \circ \phi_1^+(V_0) \subset \mathbf{R}_0$  for  $\ell > 0$ . The region  $V_\ell$  is bounded by a segment in the vertical line  $\{r = r_\epsilon\} \cap \mathbf{R}_0$ , and by the curve  $\Gamma_0(\ell)$ , where we identify the rectangles  $\mathbf{R}_0$  in  $\mathbb{W}$  and  $\mathbb{K}_\epsilon$ .

For  $k \geq \ell(\epsilon)$ ,  $\Gamma_0(k)$  intersects the curves  $\{\tilde{r} = 2\}$  and  $\{\tilde{r} = r_\epsilon\}$  transversely, and each intersection consists of four points. Then  $V_k$  intersects the region bounded by the curve  $\{\tilde{r} = r_\epsilon\}$ , implying that  $U_k \neq \emptyset$  and that  $U_k \cap \{\tilde{r} = 2\}$  has two connected components, which are labeled  $\alpha$  for the lower one, and  $\beta$  for the upper one, as in Figure 20. Then  $U_k$  is bounded by  $\gamma_0(k)$ ,  $\kappa_0(k)$ , the vertical line  $\{r = 2\}$  and the curve  $\{\tilde{r} = r_\epsilon\}$ .

Observe that  $U_k$  is bounded by parts of the curves  $\gamma_0(k)$  and  $\kappa_0(k)$ . In Figure 20 we are assuming that  $k \leq n/2$ , and the case  $k > n/2$  is analogous since the shape of  $\gamma_0(k)$  and  $\kappa_0(k)$  near  $V_0$  is analogous for the two cases of  $k$ , as depicted in Figure 17.  $\square$

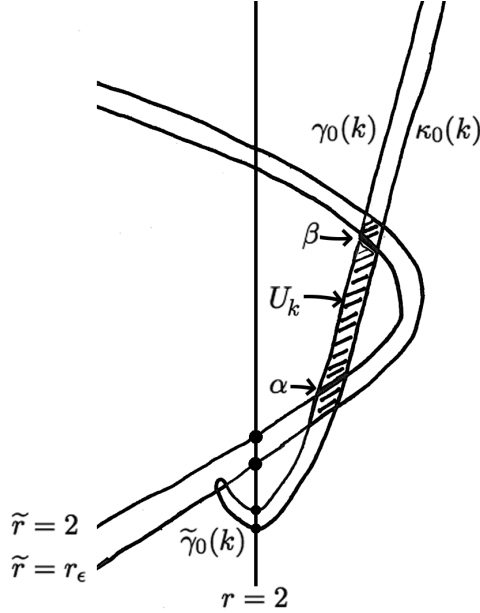


FIGURE 20. The region  $U_k$  and the curves  $\alpha$  and  $\beta$  in  $\mathbf{R}_0$

**REMARK 8.3.** *A priori, the boundary of  $U_k$  is contained in the union of  $\gamma_0(k)$ ,  $\kappa_0(k)$ , the curve  $\{\tilde{r} = r_\epsilon\}$  and the vertical line  $\{r = 2\}$ . The assumption that  $z(v_1^\epsilon) > -1$  implies that this region is disjoint from the vertical line  $\{r = 2\}$ .*

**8.4. The shift map.** Let  $\epsilon > 0$ , and let  $V_0$  and  $\ell(\epsilon) > 0$  be defined as in Section 8.3. Fix  $k \geq \ell(\epsilon)$  and define  $\varphi_k = \widehat{\Psi}^k \circ \phi_1^+$  and  $U_k = \varphi_k(V_0) \cap V_0$ , as in Proposition 8.2. We describe in detail the set  $U_k \cap \varphi_k(U_k)$  and show that it is composed of two connected components, and give some of the details of the description of the set  $U_k \cap \varphi_k(U_k \cap \varphi_k(U_k))$ . The recursive construction will then give us a collection of  $2^n$  disjoint compact regions in the image of  $\varphi_k^n$ , and their infinite intersection defines a Cantor set invariant under the action of  $\varphi_k$ , for which the restricted action is conjugate to the full shift.

Observe that  $U_k \subset V_0 \subset U_{\phi_1^+}$ . The forward  $\Phi_t^\epsilon$ -flow of  $U_k$  intersects the secondary entry region  $E_1^\epsilon$  in the subset  $U_k' \subset E_1^\epsilon$ . Then  $U_k'$  is bounded by the curve  $\{r = r_\epsilon\}$ , and the curves  $\gamma'(1, k)$  and  $\kappa'(1, k)$ , obtained by flowing forward to  $E_1^\epsilon$  the curves  $\gamma_0(k)$  and  $\kappa_0(k)$ , respectively. Set  $U_k'' = \tau^{-1}(U_k') \subset L_1^-$ , bounded by the circle  $\{r = r_\epsilon\}$  and the curves  $\gamma(1, k) = \tau^{-1}(\gamma'(1, k))$  and  $\kappa(1, k) = \tau^{-1}(\kappa'(1, k))$ . By construction,  $\gamma(1, k)$  intersects twice the circle  $\{r = 2\}$  and  $\kappa(1, k)$  also intersects twice  $\{r = 2\}$ , thus both  $\gamma(1, k)$  and  $\kappa(1, k)$  are traversing curves, as in Figure 21.

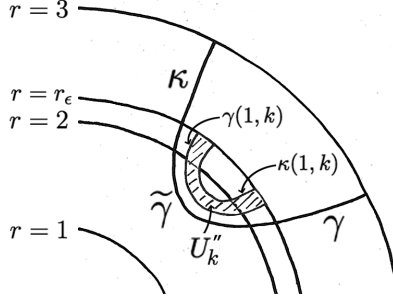


FIGURE 21. The region  $U_k''$  and parts of the curves  $\kappa(1, k)$  and  $\gamma(1, k)$  in  $L_1^-$

The surfaces  $P_{\gamma(1, k)}$  and  $P_{\kappa(1, k)}$  in  $\mathbb{W}$ , generated by the curves  $\gamma(1, k)$  and  $\kappa(1, k)$ , intersect the rectangle  $\mathbf{R}_0$  in a similar manner as  $P_\Gamma$ , as in Figure 17. Let  $\gamma_0(1, k; \ell)$  and  $\kappa_0(1, k; \ell)$  for  $\ell \geq 1$  and unbounded be the curves in the trace of the surfaces  $P_{\gamma(1, k)}$  and  $P_{\kappa(1, k)}$  on  $\mathbf{R}_0$ . The shape of these curves is analogous to the one of the curves  $\Gamma_0(\ell)$  in the trace of  $P_\Gamma$ . Observe that for each  $\ell > 0$ , the curves  $\gamma_0(1, k; \ell)$  and  $\kappa_0(1, k; \ell)$  are contained in the region bounded by  $\Gamma_0(\ell)$  and as  $\ell \rightarrow \infty$  these curves accumulate on  $\mathcal{R} \cap \mathbf{R}_0$ .

Since  $U_k'' \subset L_1^-$  is bounded by  $\gamma(1, k)$ ,  $\kappa(1, k)$  and the circle  $\{r = r_\epsilon\}$ , the region  $\widehat{\Psi}^\ell \circ \phi_1^+(U_k)$  is bounded by the curves  $\gamma_0(1, k; \ell)$ ,  $\kappa_0(1, k; \ell)$  and the vertical line  $\{r = r_\epsilon\}$ .

Consider now the case  $\ell = k \geq \ell(\epsilon)$ . Then  $\varphi_k(U_k) = \widehat{\Psi}^k \circ \phi_1^+(U_k)$  intersects the set  $\{r < 2\}$  along one connected component that is U-shaped and bounded by  $\gamma_0(1, k; k) \cap \{r < 2\}$  and  $\kappa_0(1, k; k) \cap \{r < 2\}$ . Also,  $\varphi_k(U_k)$  has two connected components in  $\{r \geq 2\}$ , each corresponding to one of the connected components in  $\gamma_0(1, k; k) \cap \{r \geq 2\}$ . Hence  $U_k \cap \varphi_k(U_k)$  has two connected components. Let  $W_0$  be the component on the left and  $W_1$  the component on the right as in Figure 22. The sets  $W_0$  and  $W_1$  depend on  $k$ , but we omit this dependence in the notation.

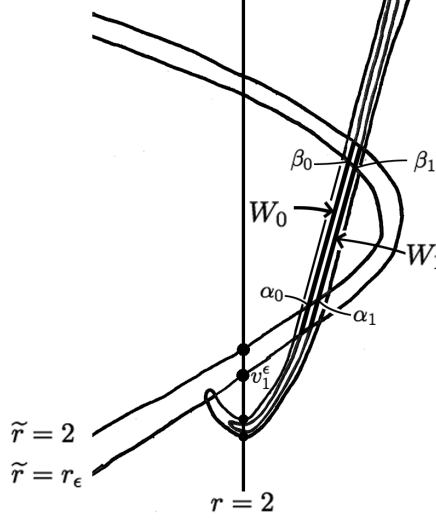
**LEMMA 8.4.** *For  $i = 0, 1$ , the sets  $W_i$  are non-empty and intersect the curve  $\{\tilde{r} = 2\}$  along two arcs  $\alpha_i \subset \alpha$  and  $\beta_i \subset \beta$ .*

*Proof.* The discussion above implies that the sets  $W_i$  are non-empty. Also, by construction  $W_i \cap \alpha$  and  $W_i \cap \beta$  are non-empty for  $i = 0, 1$ , set  $\alpha_i = W_i \cap \alpha$  and  $\beta_i = W_i \cap \beta$ , for  $i = 0, 1$ .  $\square$

We can now iterate the construction. For  $i_1 = 0, 1$ , consider the set  $\varphi_k(W_{i_1}) = \widehat{\Psi}^k \circ \phi_1^+(W_{i_1})$ . Since the curves bounding  $W_{i_1}$  cross the curve  $\{\tilde{r} = 2\}$ , the set  $\varphi_k(W_{i_1}) \subset \varphi_k(U_k)$  intersects the side  $\{r < 2\}$  in a U-shaped set and  $\varphi_k(W_{i_1}) \cap \{r \geq 2\}$  has two connected components one inside  $W_0$  and the other inside  $W_1$ . Thus we can define the four sets

$$W_{i_1, i_2} = \varphi_k(W_{i_1}) \cap W_{i_2} \subset W_{i_2} \quad \text{for} \quad i_1, i_2 = 0, 1.$$

In complete analogy with Lemma 8.4, we have that each  $W_{i_1, i_2}$  is non-empty and intersects  $\{\tilde{r} = 2\}$  along two arcs  $\alpha_{i_1, i_2} \subset \alpha_{i_2}$  and  $\beta_{i_1, i_2} \subset \beta_{i_2}$ . Observe that  $\varphi_k^{-1}(W_{i_1, i_2}) \subset W_{i_1}$ .

FIGURE 22. The regions  $W_0$  and  $W_1$  in  $\mathbf{R}_0$ 

Iterating this construction, we conclude that for any  $n > 0$  and for any sequence  $I = \{i_1, i_2, \dots, i_n\} \in \{0, 1\}^n$  the set  $W_I = W_{i_1, i_2, \dots, i_n}$  satisfies that:

- $W_I$  is non-empty;
- $W_I$  intersects the curve  $\{\tilde{r} = 2\}$  along two arcs  $\alpha_I$  and  $\beta_I$ .

We make two observations. For a sequence  $I \in \{0, 1\}^n$ ,  $I = \{i_1, i_2, \dots, i_n\}$  and a point  $\xi \in W_I$ , we have

$$(33) \quad \varphi_k^{-1}(\xi) \in W_{i_1, i_2, \dots, i_{n-1}}$$

$$(34) \quad \varphi_k^{-2}(\xi) = \varphi_k^{-1} \circ \varphi_k^{-1}(\xi) \in W_{i_1, i_2, \dots, i_{n-2}},$$

and so forth, so that by induction we have  $\varphi_k^{-(n-1)}(\xi) \in W_{i_1}$ . Also by construction,

$$W_I \subset W_{i_2, i_3, \dots, i_n} \subset W_{i_3, i_4, \dots, i_n} \subset \dots \subset W_{i_n}.$$

We can now define

$$(35) \quad W(\varphi_k) = \bigcap_{n \geq 1} \bigcap_{I = \{i_1, i_2, \dots, i_n\}} W_I$$

which is a Cantor set that is invariant under the map  $\varphi_k$ .

Observe that each  $\xi \in W(\varphi_k)$  is uniquely defined by an infinite string  $I_\xi = \{i_1, i_2, \dots, i_n, \dots\} \in \{0, 1\}^\mathbb{N}$ , which we call the shift coordinates on  $W(\varphi_k)$ . The identities (33), (34) and their generalization imply that under this identification, the map  $\varphi_k$  acts on the points of  $W(\varphi_k)$  via the right shift on the shift coordinates. We then have the standard observation about such maps:

**LEMMA 8.5.** *The periodic orbits for the restricted action  $\varphi_k: W(\varphi_k) \rightarrow W(\varphi_k)$  are dense in  $W(\varphi_k)$ .*

Finally, observe that for  $k' > k \geq \ell(\epsilon)$ , the regions bounded by the curves  $\Gamma_0(k')$  and  $\Gamma_0(k)$  are disjoint, hence we have that  $W(\varphi_{k'}) \cap W(\varphi_k) = \emptyset$ .

Combining the above results and observations, we have shown:

**THEOREM 8.6.** *For  $0 < \epsilon < \epsilon_0$  sufficiently small, let  $V_0$  and  $\ell(\epsilon) > 0$  be defined as above. Then for each  $k \geq \ell(\epsilon)$ , define  $\varphi_k = \hat{\Psi}^k \circ \phi_1^+ \in \hat{\mathcal{G}}_\epsilon^*$ , and let  $W(\varphi_k)$  be defined by (35). Then  $W(\varphi_k)$  is a Cantor set which is invariant under the action of  $\varphi_k$ , and the action admits a dynamical coding as a full-shift space. Thus, the action of the pseudo-group  $\hat{\mathcal{G}}_\epsilon^*$  on  $\mathbf{R}_0$  contains an infinite number of disjoint horseshoe dynamical systems, each with a dense set of periodic orbits.*

9. TOPOLOGICAL ENTROPY FOR  $\epsilon > 0$ 

The pseudogroup  $\widehat{\mathcal{G}}_\epsilon$  acting on  $\mathbf{R}_0$  was introduced in Definition 7.2, with generators obtained from the return maps  $\widehat{\Psi}$  and  $\widehat{\Phi}^\epsilon$ . Then in Section 8, for  $\epsilon > 0$  sufficiently small and after imposing a sequence of assumptions on the geometry of the construction of the flow  $\Phi_t^\epsilon$ , it was shown that the action of  $\widehat{\mathcal{G}}_\epsilon$  contains disjoint families of invariant Cantor sets. In this section, we impose one further condition on the construction of the flow  $\Phi_t^\epsilon$  which suffices to imply that each of these “horseshoe dynamical systems” is realized by the flow  $\Phi_t^\epsilon$ . It follows immediately from this that the flow  $\Phi_t^\epsilon$  has positive topological entropy and has infinite families of periodic orbits.

Recall that the map  $\varphi_k = \widehat{\Psi}^k \circ \phi_1^+$  was introduced in Proposition 8.2, and realizes a part of the dynamical properties of the action of the pseudo $\star$ group  $\widehat{\mathcal{G}}_\epsilon^*$  on  $\mathbf{R}_0$ . However, the map  $\varphi_k$  need not be realized by the return map of the flow  $\Phi_t^\epsilon$ . Recall that the map  $\phi_1^+ = \widehat{\Phi}^\epsilon|_{U_{\phi_1^+}}$ , where  $\phi_1^+$  is defined at  $\xi \in U_{\phi_1^+}$  with  $\eta = \phi_1^+(\xi)$ , if there is a  $\mathcal{K}_\epsilon$ -arc  $[\xi, \eta]_{\mathcal{K}_\epsilon}$  which contains a single transition point  $x \in E_1^\epsilon$ . On the other hand, we have that  $\zeta = \widehat{\Psi}^k(\eta)$  if there exists a  $\mathcal{W}$ -arc  $[\eta, \zeta]_{\mathcal{W}}$  in  $\mathbb{W}$ , which is independent of the return map  $\widehat{\Phi}^\epsilon$ .

The strategy in this section is to apply Corollary 7.5 to conclude that there is also a  $\mathcal{K}_\epsilon$ -arc  $[\eta, \zeta]_{\mathcal{K}_\epsilon}$  in  $\mathbb{K}_\epsilon$  between  $\eta$  and  $\zeta$ . When applied to points  $\xi \in W(\varphi_k)$ , this will imply that the map  $\varphi_k: W(\varphi_k) \rightarrow W(\varphi_k)$  represents a subsystem of the return map  $\widehat{\Phi}^\epsilon$ , and hence gives information about the dynamics of the flow  $\Phi_t^\epsilon$ . The difficulty is that Corollary 7.5 assumes that  $\eta \in U_{r_\epsilon}$  where  $U_{r_\epsilon}$  is defined by (29). We first obtain conditions on the map  $\sigma_1^\epsilon$  which will imply that this requirement is satisfied for  $\xi \in W(\varphi_k)$ , so that we can then use Theorem 8.6 to obtain a proof of Theorem 1.2.

**9.1. Wilson dynamics.** The orbits of the map  $\widehat{\Psi}$  on  $\mathbf{R}_0$  are simple to describe, in that for any point  $\xi \in \mathbf{R}_0$  with  $r(\xi) \neq 2$ , the orbit is finite in both forward and backward directions. However, as the value of  $r(\xi)$  tends to  $r = 2$ , the lengths of these finite orbits increase, as condition (2) implies that the vertical distance between the iterations  $\widehat{\Psi}^\ell(\xi)$  becomes arbitrarily small for  $r(\widehat{\Psi}^\ell(\xi))$  near to 2 and its vertical coordinate  $z(\widehat{\Psi}^\ell(\xi))$  near to either  $z = \pm 1$ . We give an approximation of the distance between points  $\widehat{\Psi}^\ell(\xi)$  and  $\widehat{\Psi}^{\ell+1}(\xi)$ , following the same approach as in Chapter 17 of [6]. These estimates are then used to impose restrictions on the insertion maps  $\sigma_1^\epsilon$  so that Corollary 7.5 can be applied.

Recall the functions  $f$  and  $g$  were chosen in Section 2.2, which are constant in the coordinate  $\theta$ , with

$$(36) \quad \mathcal{W} = g(r, \theta, z) \frac{\partial}{\partial z} + f(r, \theta, z) \frac{\partial}{\partial \theta} .$$

Hypothesis 2.1 and condition (2) imply there exists constants  $A_g, B_g, C_g$  such that the quadratic form  $Q_g(u, v) = A_g \cdot u^2 + 2B_g \cdot uv + C_g \cdot v^2$  defined by the Hessian of  $g$  at  $\omega_1$  is positive definite. Set

$$Q_0(r, z) = (d_{\mathbf{R}_0}((r-2), (z+1)))^2 = (r-2)^2 + (z+1)^2$$

then it follows that there exists  $D_g > 0$  such that

$$(37) \quad |g(r, \theta, z) - Q_g(r-2, z+1)| \leq D_g \cdot (|r-2|^3 + |z+1|^3) \quad \text{for } Q_0(r, z) \leq \epsilon_0^2$$

where  $\epsilon_0$  is the constant defined in (2). The condition (37) implies that for  $(r, z)$  sufficiently close to  $(2, -1)$ , the error term on the right-hand-side can be made arbitrarily small relative to the distance squared from the special point  $\omega_1 = (2, -1)$ . We also observe that (37) implies there exists constants  $0 < \lambda_1 \leq \lambda_2$  such that

$$(38) \quad \lambda_1 \cdot Q_0(r, z) \leq g(r, \theta, z) \leq \lambda_2 \cdot Q_0(r, z) \quad \text{for } Q_0(r, z) \leq \epsilon_0^2 .$$

Next, consider the action of the maps  $\widehat{\Psi}^\ell$  for  $\ell > 0$ . Let  $\xi \in \mathbf{R}_0$  with  $2 \leq r(\xi) \leq 2 + \epsilon_0$  and  $-7/4 \leq z(\xi) \leq -1/4$ , such that  $\widehat{\Psi}(\xi)$  is defined and  $z(\widehat{\Psi}(\xi)) < 0$ . Let  $T(\xi) > 0$  be defined by  $\widehat{\Psi}(\xi) = \Psi_{T(\xi)}(\xi)$ . Then the  $z$ -coordinate of  $\widehat{\Psi}(\xi)$  is given by

$$(39) \quad z(\widehat{\Psi}(\xi)) - z(\xi) = \int_0^{T(\xi)} g(\Psi_s(\xi)) ds \geq 0 .$$



If  $\xi \neq \omega_1$  then  $g(\Psi_s(\xi))$  is positive along the orbit segment for  $0 \leq s \leq T(\xi)$ , hence  $z(\widehat{\Psi}(\xi)) - z(\xi) > 0$ . Moreover, combining the estimates (38) and (39) and the estimate  $T(\xi) \geq 4\pi$  on the return time for the flow  $\Psi_t$  to  $\mathbf{R}_0$  for  $r(\xi) \geq 2$ , we obtain:

**LEMMA 9.1.** *For  $\delta > 0$ , suppose that  $\xi = (r, z) \in \mathbf{R}_0$  satisfies  $\delta < d_{\mathbf{R}_0}((r-2), (z+1)) < \epsilon_0$ . Then*

$$(40) \quad z(\widehat{\Psi}(\xi)) - z(\xi) \geq 4\pi \cdot \lambda_1 \delta^2 .$$

**9.2. Admissible deformations.** We assume that for  $0 < \epsilon < \epsilon_0$  the conditions of Section 8 are satisfied, so that the hypotheses of Proposition 8.2 and Theorem 8.6 are satisfied.

Recall that for the insertion map  $\sigma_1^\epsilon$  the points  $\{v_1^\epsilon, v_2^\epsilon\} \subset \mathbf{R}_0$  are defined by (31) and satisfy

$$(41) \quad r(v_1^\epsilon) = r(v_2^\epsilon) = 2 \quad , \quad -1 < z(v_1^\epsilon) < z(v_2^\epsilon) < 0 .$$

Define

$$(42) \quad \delta(\sigma_1^\epsilon) = z(\widehat{\Psi}^{-1}(v_1^\epsilon)) + 1 > 0 .$$

**HYPOTHESIS 9.2.** *Assume that  $\epsilon > 0$  is sufficiently small so that*

$$(43) \quad z(v_2^\epsilon) - z(v_1^\epsilon) < 4\pi \cdot \lambda_1 \cdot \delta(\sigma_1^\epsilon)^2 .$$

Hypothesis 6.3 implies that the boundary curve  $\{\tilde{r} = r_\epsilon\} \subset \mathbf{R}_0$  of the region  $V_0$  is parabolic, as illustrated in Figure 18, which implies that for a fixed  $v_1^\epsilon \in \mathbf{R}_0$  then for  $\epsilon > 0$  sufficiently small, the condition (43) will be satisfied.

Let  $V_0$  and  $\ell(\epsilon) > 0$  be as defined as in Theorem 8.6. Fix  $k \geq \ell(\epsilon)$ , and define  $\varphi_k = \widehat{\Psi}^k \circ \phi_1^+$ . Set  $U_k = \varphi_k(V_0) \cap V_0$  as defined in Proposition 8.2. Then let  $W(\varphi_k)$  be defined by (35). By Theorem 8.6 we have that  $\varphi_k: W(\varphi_k) \rightarrow W(\varphi_k)$ .

**PROPOSITION 9.3.** *Assume that Hypothesis 9.2 holds for the insertion map  $\sigma_1^\epsilon$ . Then for each  $\xi \in W(\varphi_k)$  with  $\eta = \varphi_k(\xi)$ , there exists a  $\mathcal{K}_\epsilon$ -arc  $[\xi, \eta]_{\mathcal{K}_\epsilon}$  in  $\mathbb{K}_\epsilon$ . Thus, there exists  $\ell_\xi \geq 1$  such that  $\eta = \widehat{\Phi}^{\ell_\xi}(\xi)$ .*

*Proof.* Let  $(r, z) \in \mathbf{R}_0$  satisfy  $Q_0(r, z) \leq \epsilon_0^2$  and  $z \geq z(\widehat{\Psi}^{-1}(v_1^\epsilon))$ . Then  $Q_0(r, z) \geq Q_0(2, z) \geq \delta(\sigma_1^\epsilon)^2$ , so that by (40) we have

$$(44) \quad z(\widehat{\Psi}(r, z)) - z \geq 4\pi \cdot \lambda_1 \cdot \delta(\sigma_1^\epsilon)^2 > z(v_2^\epsilon) - z(v_1^\epsilon) .$$

Now let  $\eta \in V_0$ , for  $V_0$  defined by (32). Then  $z(v_1^\epsilon) \leq z(\eta) \leq z(v_2^\epsilon)$  by the convexity of the region  $V_0$ . It then follows from (40) applied to  $(r, z) = \eta$  that

$$(45) \quad z(\widehat{\Psi}^{-1}(\eta)) = z + \left( z(\widehat{\Psi}^{-1}(\eta)) - z \right) \leq z - 4\pi \cdot \lambda_1 \cdot \delta(\sigma_1^\epsilon)^2 < z(v_2^\epsilon) - (z(v_2^\epsilon) - z(v_1^\epsilon)) = z(v_1^\epsilon) .$$

That is, the image  $\widehat{\Psi}^{-1}(V_0)$  lies below the line  $\{z = z(v_1^\epsilon)\}$ , and hence lies outside the region bounded by the curve  $\tilde{r} = r_\epsilon$  whose lower edge lies on this line by the choice of  $v_1^\epsilon$  in (31) and the convexity of the region  $V_0$ . That is, for all  $\eta \in V_0$  we have  $\tilde{r}(\widehat{\Psi}^{-1}(\eta)) > r_\epsilon$ .

Let  $\xi \in W(\varphi_k)$  and set  $\eta = \varphi_k(\xi) = \widehat{\Psi}^k \circ \phi_1^+(\xi) \in W(\varphi_k) \subset V_0$ . Then for the point  $\zeta = \widehat{\Psi}^{-1}(\eta)$  we have  $\tilde{r}(\zeta) > r_\epsilon$  by the above estimates.

Following the  $\mathcal{K}_\epsilon$ -orbit of  $\zeta$  backwards and applying Proposition 7.4 and Corollary 7.5 we obtain that  $\xi$  and  $\zeta$  are in the same  $\mathcal{K}_\epsilon$ -orbit.

Now consider the  $\mathcal{W}$ -orbit segment  $[\zeta, \eta]_{\mathcal{W}}$ . If  $[\zeta, \eta]_{\mathcal{W}}$  does not contain any transition points, then  $\eta$  is in the  $\mathcal{K}_\epsilon$ -orbit of  $\zeta$  and thus in the  $\mathcal{K}_\epsilon$ -orbit of  $\xi$ . If  $[\zeta, \eta]_{\mathcal{W}}$  contains transition points, let  $x_1$  be the first transition point. Then  $x_1$  is a secondary entry point in  $E_1^\epsilon$  with  $r(x_1) > r_\epsilon$  and Corollary 7.5 implies that its  $\mathcal{K}_\epsilon$ -orbit contains the facing point  $y_1 \in S_1^\epsilon$ . The  $\mathcal{K}_\epsilon$ -orbit of  $y_1$  continues to the first intersection with  $\mathbf{R}_0$  which is the point  $\eta$ . Hence  $\eta$  is in the  $\mathcal{K}_\epsilon$ -orbit of  $\xi$ .  $\square$

We next deduce an important consequence of Proposition 9.3. Observe that for every  $\xi \in W(\varphi_k)$  we have  $z(\xi) < 0$  and thus the flows  $\Psi_t$  and  $\Phi_t^\epsilon$  intersect the set  $W(\varphi_k) \subset \mathbf{R}_0$  transversally. Let  $\ell_\xi \geq 1$  be the integer defined in Proposition 9.3 so that  $\varphi_k(\xi) = \widehat{\Phi}^{\epsilon^{\ell_\xi}}(\xi)$ . Then both maps are continuous at  $\xi$  and there is an open neighborhood  $U_\xi \subset V_0$  for which the identity  $\varphi_k(\xi') = \widehat{\Phi}^{\epsilon^{\ell_\xi}}(\xi')$  holds for all  $\xi' \in U_\xi$ . The set  $W(\varphi_k)$  is compact, so there exists a finite collection of such open sets which cover  $W(\varphi_k)$ . Hence, there exists  $N_k$  so that for all  $\xi \in W(\varphi_k)$  there exists  $1 \leq \ell_\xi \leq N_k$  for which  $\varphi_k(\xi) = \widehat{\Phi}^{\epsilon^{\ell_\xi}}(\xi)$ . As a consequence, we have:

**COROLLARY 9.4.** *Assume that Hypothesis 9.2 holds for the insertion map  $\sigma_1^\epsilon$ . Then there exists  $T_k > 0$  such that for each  $\xi \in W(\varphi_k)$  there exists  $0 < t_\xi \leq T_k$  such that  $\varphi_k(\xi) = \Phi_{t_\xi}^\epsilon(\xi)$ .*

**9.3. Topological entropy.** We define the entropy of a flow  $\varphi_t$  on a compact metric space  $(X, d_X)$  using a variation of the Bowen formulation of topological entropy [1, 18]. The definition we adopt is symmetric in the role of the time variable  $t$ . For  $T > 0$ , define a metric on  $X$  by

$$(46) \quad d_X^T(x, y) = \max \{d_X(\varphi_t(x), \varphi_t(y)) \mid -T \leq t \leq T\} \quad , \quad \text{for } x, y \in X \quad .$$

Two points  $x, y \in X$  are said to be  $(\varphi_t, T, \delta)$ -separated if  $d_X^T(x, y) > \delta$ . A set  $E \subset X$  is  $(\varphi_t, T, \delta)$ -separated if all pairs of distinct points in  $E$  are  $(\varphi_t, T, \delta)$ -separated. Let  $s(\varphi_t, T, \delta)$  be the maximal cardinality of a  $(\varphi_t, T, \delta)$ -separated set in  $X$ . Then the topological entropy is defined by

$$(47) \quad h_{top}(\varphi_t) = \frac{1}{2} \cdot \lim_{\delta \rightarrow 0} \left\{ \limsup_{T \rightarrow \infty} \frac{1}{T} \log(s(\varphi_t, T, \delta)) \right\} .$$

It is a standard fact that for a compact space  $X$ , the entropy  $h_{top}(\varphi_t)$  is independent of the choice of the metric  $d_X$  on  $X$ .

Given a  $\varphi_t$ -invariant subset  $K \subset X$ , we can define the restricted topological entropy  $h_{top}(\varphi_t, K)$  by the same formula (47), where we now require that the  $(\varphi_t, T, \delta)$ -separated sets in the definition must be subsets of  $K$ . It follows immediately that we have the estimate

$$(48) \quad h_{top}(\varphi_t) \geq h_{top}(\varphi_t, K) \quad .$$

Let  $\epsilon > 0$  be given, and assume that  $\Phi_t^\epsilon$  is a Kuperberg flow as constructed above which satisfies the *generic hypotheses* of Section 6, the *geometric hypotheses* of Section 8, and the Hypothesis 9.2 above. Then we have:

**THEOREM 9.5.** *The topological entropy  $h_{top}(\Phi_t^\epsilon) > 0$ .*

*Proof.* Let  $V_0$  and  $\ell(\epsilon) > 0$  be defined as in Theorem 8.6. Choose  $k \geq \ell(\epsilon)$ , and define  $\varphi_k = \widehat{\Psi}^k \circ \phi_1^+ \in \widehat{\mathcal{G}}_\epsilon^*$ . Then let  $W(\varphi_k) \subset \mathbf{R}_0$  be the  $\varphi_k$ -invariant Cantor set defined by (35). By Proposition 9.3, the set  $W(\varphi_k)$  is invariant under the return map  $\widehat{\Phi}^\epsilon$  for the flow  $\Phi_t^\epsilon$ . Let  $\widehat{W}(\varphi_k)$  denote the flow saturation of  $W(\varphi_k)$  which is then a compact invariant set for  $\Phi_t^\epsilon$ . By (48) it will suffice to show that  $h_{top}(\Phi_t^\epsilon, \widehat{W}(\varphi_k)) > 0$ .

Note that  $W(\varphi_k) \subset \widehat{W}(\varphi_k)$  is a transverse section for the flow  $\Phi_t^\epsilon$  restricted to  $\widehat{W}(\varphi_k)$ , and by Corollary 9.4 the flow has bounded return times to the section  $W(\varphi_k)$ .

**LEMMA 9.6.** *The map  $\varphi_k: W(\varphi_k) \rightarrow W(\varphi_k)$  is the first return map for the flow  $\Phi_t^\epsilon$  restricted to  $\widehat{W}(\varphi_k)$ .*

*Proof.* Note that  $\widehat{\Phi}^\epsilon$  is the first return map of the flow  $\Phi_t^\epsilon$  to the section  $\mathbf{R}_0$ . Given  $\xi \in W(\varphi_k)$ , Proposition 9.3 states that there is some least  $\ell_\xi$  such that  $\varphi_k(\xi) = \widehat{\Phi}^{\epsilon^{\ell_\xi}}(\xi) \in W(\varphi_k)$ . Thus, it suffices to show the  $\mathcal{K}_\epsilon$ -orbit segment  $[\xi, \varphi_k(\xi)]_{\mathcal{K}_\epsilon}$  is disjoint from  $\widehat{W}(\varphi_k) \subset U_k$  except at the endpoints. In fact, we prove that for any  $\xi \in U_k$  such that  $\varphi_k(\xi) \in U_k$ , the  $\mathcal{K}_\epsilon$ -orbit segment  $[\xi, \varphi_k(\xi)]_{\mathcal{K}_\epsilon}$  does not intersect  $U_k$ .

Since  $\xi \in W(\varphi_k) \subset U_k \subset U_{\phi_1^+}$ , we have that  $\widehat{\Phi}^\epsilon(\xi) = \phi_1^+(\xi) = \eta$  and thus  $r(\eta) \leq r_\epsilon$  since  $U_k \subset V_0$  and the points in  $V_0$  have  $\tilde{r}$ -coordinate smaller or equal to  $r_\epsilon$ . Consider the  $\mathcal{K}_\epsilon$ -orbit segment  $[\eta, \widehat{\Psi}(\eta)]_{\mathcal{K}_\epsilon}$ . If  $[\eta, \widehat{\Psi}(\eta)]_{\mathcal{K}_\epsilon}$  does not contain transition points, then it does not intersect  $\mathbf{R}_0$  in its interior. If not, let  $x_1$

be the first transition point that is a secondary entry point in  $E_1^\epsilon$ . Since  $z(\eta) < z(\widehat{\Phi}^{k-1}(\eta))$ , then by the arguments in the proof of Proposition 9.3, we have

$$z(\eta) < z(\widehat{\Phi}^{k-1}(\eta)) < z(v_1^\epsilon),$$

thus  $x_1$  is a secondary entry point outside the region  $U' \subset E_1^\epsilon$ . In particular,  $r(x_1) > r_\epsilon$ . Let  $y_1 \in S_1^\epsilon$  be the secondary exit point such that  $x_1 \equiv y_1$ , then by construction  $y_1$  is the last transition point in  $[\eta, \widehat{\Psi}(\eta)]_{\mathcal{K}_\epsilon}$ . By Proposition 7.4 and Hypothesis 6.2 all the  $\mathcal{W}$ -arcs in the  $\mathcal{K}_\epsilon$ -orbit segment  $[\eta, \widehat{\Psi}(\eta)]_{\mathcal{K}_\epsilon}$  have radius greater than  $r_\epsilon$ . Hence any point in the intersection of the interior of the orbit segment  $[\eta, \widehat{\Psi}(\eta)]_{\mathcal{K}_\epsilon}$  with  $\mathbf{R}_0$  has radius greater than  $r_\epsilon$  and thus does not belongs to  $U_k$ , in particular does not belongs to  $\widehat{W}(\varphi_k)$ .

Repeating the argument, consider the  $\mathcal{K}_\epsilon$ -orbit segment  $[\widehat{\Psi}^\ell(\eta), \widehat{\Psi}^{\ell+1}(\eta)]_{\mathcal{K}_\epsilon}$  for any  $1 \leq \ell \leq k-1$ . If  $[\widehat{\Psi}^\ell(\eta), \widehat{\Psi}^{\ell+1}(\eta)]_{\mathcal{K}_\epsilon}$  does not contains transition points, then it does not intersects  $\mathbf{R}_0$  in its interior. If not, let  $x_1$  be the first transition point that is a secondary entry point in  $E_1^\epsilon$ . Since  $z(\widehat{\Psi}^\ell(\eta)) \leq z(\widehat{\Phi}^{k-1}(\eta))$ , then we have

$$z(\widehat{\Psi}^\ell(\eta)) \leq z(\widehat{\Phi}^{k-1}(\eta)) < z(v_1^\epsilon),$$

thus  $x_1$  is a secondary entry point outside the region  $U' \subset E_1^\epsilon$ . In particular,  $r(x_1) > r_\epsilon$ . Let  $y_1 \in S_1^\epsilon$  be the secondary exit point such that  $x_1 \equiv y_1$ , then by construction  $y_1$  is the last transition point in  $[\widehat{\Psi}^\ell(\eta), \widehat{\Psi}^{\ell+1}(\eta)]_{\mathcal{K}_\epsilon}$ . Then all the  $\mathcal{W}$ -arcs in the  $\mathcal{K}_\epsilon$ -orbit segment  $[\widehat{\Psi}^\ell(\eta), \widehat{\Psi}^{\ell+1}(\eta)]_{\mathcal{K}_\epsilon}$  have radius greater than  $r_\epsilon$ . Hence any point in the intersection of the interior of the orbit segment  $[\widehat{\Psi}^\ell(\eta), \widehat{\Psi}^{\ell+1}(\eta)]_{\mathcal{K}_\epsilon}$  with  $\mathbf{R}_0$  has radius greater than  $r_\epsilon$  and thus does not belongs to  $U_k$ , in particular does not belongs to  $\widehat{W}(\varphi_k)$ .  $\square$

We claim that the restricted map  $\varphi_k: W(\varphi_k) \rightarrow W(\varphi_k)$  has positive entropy, and it then follows by standard techniques that  $h_{top}(\Phi_t^\epsilon, \widehat{W}(\varphi_k)) > 0$ .

In the following, we use Proposition 8.2 and the labeling system in Section 8.4. In particular, let  $W_0, W_1 \subset \mathbf{R}_0$  be the disjoint sets introduced in Lemma 8.4. Let  $\delta > 0$  be such that the  $d_{\mathbf{R}_0}$ -distance between the sets  $W_0$  and  $W_1$  is greater than  $\delta$ . We obtain a lower bound estimate on the maximum number  $s(\varphi_k, n, \delta)$  of points in an  $(\varphi_k, n, \delta)$ -separated subset of  $W(\varphi_k)$  as a function of  $n$ .

For a sequence  $I \in \{0, 1\}^n$ , recall that  $W_I = W_{i_1, i_2, \dots, i_n}$  is a closed and open cylinder set in the Cantor set  $W(\varphi_k)$ . For any pair of distinct sequences  $I, J \in \{0, 1\}^n$ , choose points

$$(49) \quad \xi \in W_I \cap W(\varphi_k) \quad , \quad \eta \in W_J \cap W(\varphi_k) .$$

Let  $1 \leq m \leq n$  be the largest index such that  $i_m \neq j_m$ . Then

$$\begin{aligned} \varphi_k^{-(n-m)}(\xi) &\in W_{i_1, i_2, \dots, i_m} \subset W_{i_m} \\ \varphi_k^{-(n-m)}(\eta) &\in W_{j_1, j_2, \dots, j_m} \subset W_{j_m} . \end{aligned}$$

Fix  $n \geq 1$  and let  $E_n \subset U_k \subset \mathbf{R}_0$  be a collection of  $2^n$  points obtained by choosing one point from each of the sets  $W_I \cap W(\varphi_k) = W_{i_1, i_2, \dots, i_n} \cap W(\varphi_k)$  where  $I \in \{0, 1\}^n$ . Then  $E_n$  is a  $(\varphi_k, n, \delta)$ -separated set, and so  $s(\varphi_k, n, \delta) \geq 2^n$ . It follows that  $s(\varphi_k, n, \delta) \geq 2^n$ , and thus  $h_{top}(\varphi_k, W(\varphi_k)) \geq \ln(2) > 0$ .  $\square$

We point out another consequence of Theorem 8.6 and Proposition 9.3.

**COROLLARY 9.7.** *The restriction of the flow  $\Phi_t^\epsilon$  to  $\widehat{W}(\varphi_k)$  has a countably dense set of periodic orbits.*

*Proof.* The restriction of the map  $\varphi_k$  to  $\widehat{W}(\varphi_k)$  has horseshoe dynamics by Theorem 8.6, and hence has a dense set of periodic orbits. Each of these orbits for  $\varphi_k$  is also a periodic orbit for the return map  $\widehat{\Phi}^\epsilon$  by Proposition 9.3.  $\square$

Note that the conclusions of Theorem 8.6 apply to the map  $\varphi_k$  for any choice of  $k \geq \ell(\epsilon)$ , and for each such flow the set  $W(\varphi_k) \subset U_k$  as illustrated in Figure 20. See also Remark 8.3. In particular, the set  $W(\varphi_k)$  is contained in the region between the curves  $\gamma_0(k), \kappa_0(k) \subset \mathbf{R}_0$ . As remarked in Section 8.3, these curves are asymptotic to the trace  $\mathcal{R} \cap \mathbf{R}_0$  of the Reeb cylinder as  $k$  increases, so the Cantor sets  $W(\varphi_k)$  also limit to subsets of  $\mathcal{R}$ .

Now assume that the flow  $\Phi_t^\epsilon$  also satisfies the offset Hypothesis 9.2, and let  $\mathcal{P}_\epsilon$  denote the union of all periodic orbits of  $\Phi_t^\epsilon$  and let  $\overline{\mathcal{P}}_\epsilon$  denote the closure of  $\mathcal{P}_\epsilon$  in  $\mathbb{K}_\epsilon$ . It then follows from Corollary 9.7 that the intersection  $\overline{\mathcal{P}}_\epsilon \cap \mathcal{R}$  is non-empty. It would be interesting to be able to describe the closure  $\overline{\mathcal{P}}_\epsilon$ , or at least the trace  $\overline{\mathcal{P}}_\epsilon \cap \mathcal{R}$  of this closure on  $\mathcal{R}$ , as some sort of analog of the *bad set* for compact flows as discussed in [2, 3], though that seems like a rather difficult task.

**9.4. Smooth admissible deformations.** Suppose that we are given a standard Kuperberg flow  $\Phi_t = \Phi_t^0$  on  $\mathbb{K}$  constructed starting with a Wilson flow  $\Psi_t$  on the Wilson Plug  $\mathbb{W}$  which satisfies Hypothesis 2.1, and that the construction of the flow  $\Phi_t$  on  $\mathbb{K}$  satisfies the conditions (K1) to (K8) in Section 2.3, and the *Strong Radius Inequality* in Hypotheses 6.3 for  $\epsilon = 0$ . We construct a family of flows  $\Phi_t^\epsilon$  for  $0 < \epsilon < \epsilon_0$  sufficiently small, which give a smooth deformation of  $\Phi_t$  such that for each  $\epsilon > 0$ , the flow  $\Phi_t^\epsilon$  satisfies the hypotheses of Theorem 9.5.

The construction of the flows  $\Phi_t^\epsilon$  uses a two-step process. In the first step, we introduce a small vertical offset to the insertion map  $\sigma_1^\epsilon: D_1 \rightarrow \mathbb{W}$ . After this, we modify the insertion by increasing the radius of the insertion of the vertex of the parabola as in Figure 7(C).

Recall that  $(2, \overline{\theta}_1, -1) \in \mathcal{R}$  is the special point on the Reeb cylinder defined in Hypotheses 6.3, for the case  $\epsilon = 0$ . Let  $0 < \epsilon' < \epsilon_0$  and choose a point  $v_1(\epsilon') \in \mathcal{R}$  which satisfies  $z(v_1(\epsilon')) = -1 + \epsilon'$  and  $\theta(v_1(\epsilon')) = \overline{\theta}_1$ . That is,  $v_1(\epsilon')$  is a perturbation of the special point  $(2, \overline{\theta}_1, -1)$  in the vertical direction along  $\mathcal{R}$ . Let  $\widetilde{\sigma}_1^{\epsilon'}: D_1 \rightarrow \mathbb{W}$  denote the vertical translate of  $\sigma_1$  so that the vertex of the image curve  $\widetilde{\sigma}_1^{\epsilon'}(\{r = 2\} \cap L_1^-)$  is the point  $v_1(\epsilon')$ .

Next, slide the map  $\widetilde{\sigma}_1^{\epsilon'}$  along the parabolic curve  $\widetilde{\sigma}_1^{\epsilon'}(\{r = 2\} \cap L_1^-)$  so that the vertex now lies on the cylinder  $\{r = 2 + \epsilon\}$  where  $\epsilon$  is sufficiently small so that the offset Hypothesis 9.2 is satisfied for the given Wilson flow  $\Psi_t$  on  $\mathbb{W}$ . This yields the embedding  $\sigma_1^\epsilon: D_1 \rightarrow \mathbb{W}$  for which  $v_1(\epsilon')$  is  $\mathcal{W}$ -flow of the lower intersection point defined in (31). Intuitively, the value of  $\epsilon$  is proportional to  $(\epsilon')^2$  as the graph of  $\widetilde{\sigma}_1^{\epsilon'}(\{r = 2\} \cap L_1^-)$  as illustrated in Figure 7(C) is quadratic. This yields our family of insertion maps  $\sigma_1^\epsilon$ .

The smooth family of second insertion maps  $\sigma_2^\epsilon: D_2 \rightarrow \mathbb{W}$  can then be defined similarly. However, we now point out that in the proof of Theorem 9.5, and its preparatory results, the role of the second insertion only arises in one manner. We require that the entry/exit condition for orbits of  $\mathcal{K}_\epsilon$  entering a face of the second insertion be satisfied for points  $\xi \in E_2^\epsilon$  when  $r(\xi) > r_\epsilon$ . In particular, this condition will be satisfied if the insertion  $\sigma_2^\epsilon = \sigma_2$  is the given map for the construction of the flow  $\Phi_t^0$ , which satisfies the original radius inequality, and thus as noted previously, has corresponding value of  $r_\epsilon = 2$ . Thus, in order to obtain the claim of Theorem 9.5, it is not even necessary to modify the upper insertion.

Thus, we obtain a smooth family of deformations of  $\Phi_t$  where each map  $\Phi_t^\epsilon$  satisfies the hypotheses of Theorem 9.5, and hence has positive entropy with infinitely many periodic orbits, as asserted in Theorem 1.2.

## REFERENCES

- [1] R. Bowen, *Entropy for group endomorphisms and homogeneous spaces*, **Trans. Amer. Math. Soc.**, 153:401–414, 1971.
- [2] R. Edwards, K. Millett, and D. Sullivan, *Foliations with all leaves compact*, **Topology**, 16:13–32, 1977.
- [3] D.B.A. Epstein and E. Vogt, *A counterexample to the periodic orbit conjecture in codimension 3*, **Ann. of Math. (2)**, 108:539–552, 1978.
- [4] É. Ghys, *Construction de champs de vecteurs sans orbite périodique (d’après Krystyna Kuperberg)*, Séminaire Bourbaki, Vol. 1993/94, Exp. No. 785, **Astérisque**, Vol. 227: 283–307, 1995.
- [5] J.C. Harrison,  *$C^2$  counterexamples to the Seifert conjecture*, **Topology**, 27:249–278, 1988.
- [6] S. Hurder and A. Rechtman, *The dynamics of generic Kuperberg flows*, **Astérisque**, Vol. 377:1–250, 2016.
- [7] S. Hurder and A. Rechtman, *Perspectives on Kuperberg flows*, **submitted**, 2016; arXiv:1607.00731.
- [8] A. Katok, *Lyapunov exponents, entropy and periodic orbits for diffeomorphisms*, **Inst. Hautes Études Sci. Publ. Math.**, 51:137–173, 1980.
- [9] K. Kuperberg, *A smooth counterexample to the Seifert conjecture*, **Ann. of Math. (2)**, 140:723–732, 1994.
- [10] G. Kuperberg and K. Kuperberg, *Generalized counterexamples to the Seifert conjecture*, **Ann. of Math. (2)**, 144:239–268, 1996.
- [11] S. Matsumoto, *K.M. Kuperberg’s  $C^\infty$  counterexample to the Seifert conjecture*, **Sūgaku**, Mathematical Society of Japan, 47:38–45, 1995. Translation: **Sugaku Expositions**, 11:39–49, 1998, Amer. Math. Soc.
- [12] S. Matsumoto, *The unique ergodicity of equicontinuous laminations*, **Hokkaido Math. J.**, 39:389–403, 2010.

- [13] P.B. Percell and F.W. Wilson, Jr., *Plugging flows*, **Trans. Amer. Math. Soc.**, 233:93–103, 1977.
- [14] A. Rechtman, *Pièges dans la théorie des feuilletages: exemples et contre-exemples*, **Thèse**, l'Université de Lyon – École Normale Supérieure de Lyon, 2009.
- [15] P.A. Schweitzer, *Counterexamples to the Seifert conjecture and opening closed leaves of foliations*, **Ann. of Math. (2)**, 100:386–400, 1974.
- [16] H. Seifert, *Closed integral curves in 3-space and isotopic two-dimensional deformations*, **Proc. Amer. Math. Soc.**, 1:287–302, 1950.
- [17] D. Sullivan, *A counterexample to the periodic orbit conjecture*, **Inst. Hautes Études Sci. Publ. Math.**, 46:5–14, 1976.
- [18] P. Walters, **An Introduction to Ergodic Theory**, Graduate Texts in Math. Vol. 79, Springer-Verlag, New York, 1982.
- [19] F.W. Wilson, Jr., *On the minimal sets of non-singular vector fields*, **Ann. of Math. (2)**, 84:529–536, 1966.

STEVEN HURDER, DEPARTMENT OF MATHEMATICS, UNIVERSITY OF ILLINOIS AT CHICAGO, 322 SEO (M/C 249), 851 S. MORGAN STREET, CHICAGO, IL 60607-7045

*E-mail address:* hurder@uic.edu

ANA RECHTMAN, INSTITUTO DE MATEMÁTICAS, UNIVERSIDAD NACIONAL AUTÓNOMA DE MÉXICO, CIUDAD UNIVERSITARIA, 04510 CIUDAD DE MÉXICO, MEXICO

*E-mail address:* rechtman@im.unam.mx